Self/Co-Assembling Peptide-based Nanocarriers for Anticancer Drug Delivery

by

Parisa Sadatmousavi

A thesis

presented to the University of Waterloo

in fulfillment of the

thesis requirement for the degree of

Doctor of Philosophy

in

Chemical Engineering - Nanotechnology

Waterloo, Ontario, Canada, 2014

AUTHOR'S DECLARATION

I hereby declare that I am the sole author of this thesis. This is a true copy of the thesis, including any required final revisions, as accepted by my examiners.

I understand that my thesis may be made electronically available to the public.

Abstract

Current diagnostic and therapeutic nanocarriers, including liposomes, micelles, and polymeric- and protein-based nanoparticles, are designed to have key functional properties such as: (i) longevity in the bloodstream, leading to accumulation of therapeutic cargos in neoplastic areas with leaky vasculatures; (ii) targeting of specific pathological sites through surface modification with targeting ligands; (iii) stimuli-responsive characteristics for controlled drug release under specific conditions. While some of these drug delivery systems have advanced into clinical stages, other nanocarriers remain under development to overcome issues with effective delivery such as lack of target-ability and fast clearance from circulation. Self-assembling peptides have recently shown great potential as nanocarrier materials for drug and gene delivery, owing to their safety, efficiency, and targeting capabilities. An amino acid pairing strategy enables us to design self/co-assembling peptides with multiple functionalities to fulfill drug delivery requirements.

This thesis focuses on functionalization and characterization of self/co-assembling peptides as nanocarriers for hydrophobic anticancer drug delivery. Diethylene glycol (DEG) conjugation and protein binding are the two modification strategies used in this thesis to impart longevity and target-ability upon the peptide-based delivery system. The studies include: (i) characterization of self-assembling properties of the diethylene glycol (DEG)-conjugated amino acid pairing peptide AAP8, (ii) investigation of the self/co-assembling features of a model ionic-complementary peptide (EAR8-II) in complex with the hydrophobic drug pirarubicin, and the anticancer activity of the complex, (iii) the interactions between peptide-drug complexes and serum proteins from the thermodynamic viewpoint, (iv) quantification of the effect of protein binding to the peptide-based delivery system on immune responses and biocompatibility, and (v) exploration of the targeting capability of albumin-bound peptide-drug complexes towards lung cancer cells.

Uncontrollable aggregation of AAP8 was the first issue to address in order to develop a promising platform for the peptide-based delivery system. Diethylene glycol (DEG), a short segment of polyethylene glycol (PEG), was conjugated to AAP8 either at one or both terminals, and then self-assembling and drug encapsulation properties of both functionalized AAP8s were characterized to evaluate the effect of DEG-modification. The results illustrated a significant reduction in uncontrollable aggregation, and the formation of uniform fibular nanostructures. In addition, DEG

conjugation provided the peptide with safer features towards immune cells by reducing cellular toxicity to macrophages. Moreover, DEG-functionalization improved hydrophobic drug stabilization, as demonstrated by sustained cytotoxic efficacy against lung carcinoma cells over a relatively long time compared to the non-functionalized AAP8.

Protein binding strategy was the second approach to utilize the peptide-based delivery system with more biocompatibility and target-ability features. EAR8-II was studied as a model ionic-complementary peptide with high capability of pirarubicin encapsulation and anticancer activities against different cancer cells. Albumin as a most abundant protein in serum was selected to assess its binding affinity to the delivery system, and evaluate its binding effect on immune responses and anticancer activities.

The results showed a central role of albumin in the *in vitro* delivery of peptide-drug complexes to target lung cancer cells based on the following characteristics: (a) Non-covalent binding of albumin to the complex through hydrogen bonding and Van der Waals interactions. The interaction was confirmed by physicochemical methods such as fluorescence quenching and isothermal titration calorimeter (ITC). (b) Shielding properties of albumin for the complex against macrophages and blood components (erythrocytes and complement protein C5b-9). In the presence of albumin, phagocytosis and cytokine expression level of macrophages and hemolytic activity of the peptide-drug complex reduced significantly due to the smaller particle size of the albumin-bound complexes compared to unprotected ones. (c) Targeting the lung cancer cells, possibly because of the inhibition of the albumin-binding protein SPARC (secreted protein, acidic and rich in cysteine). SPARC is a glycoprotein over expressed in lung cancer cells with high affinity to albumin. The results from *in vitro* SPARC expression in A549 cells, a type of human non-small cell lung carcinoma (NSCLC), showed a significant drop by the albumin-bound complex at the mRNA level evaluated by qRT-PCR. This effect can be explained by transporting the albumin-bound complex into the cell surface, binding to the SPARC proteins, and so inhibiting the SPARC expressions.

This work lays out a foundation for modification and characterization of the self/co-assembly peptide-based nanocarriers for hydrophobic anticancer drug delivery, especially to improve longevity and target-ability properties.

Acknowledgements

I would first and foremost like to express my heartfelt thanks to my supervisor, Dr. Pu Chen, for his encouragement and guidance throughout my research. He has provided me with infinite support through difficulties in the research and helped me learn the abilities to become an independent open-minded critical thinker and creative biomedical researcher. I am also very appreciative of his generosity by providing me such a great lab and research environment in a cutting-edge research area.

Next, I would like to acknowledge my advisory committee members, Dr. Jean Duhamel, Dr. Michael C. Tam, Dr. Frank Gu, and Dr. Neil McManus for their interest and critical advice during my PhD research program. I also thank my external committee member Dr. Todd Hoare for his participation in my defense and valuable comments.

I am so thankful for the financial support I received during my graduate studies including: National Science and Engineering Research Canada (NSERC PGS-D), Ontario Graduate Scholarship (OGS), Waterloo Institute of Nanotechnology Fellowship (WIN), Murray Moo-Young Biotechnology Scholarship, Merit scholarship from the Faculty of Engineering, President's Graduate Scholarship of University of Waterloo, and Women in Engineering Entrance Scholarship.

I also want to extend my special thanks to the many individuals and research groups that contributed to the experimental work during my research at the University of Waterloo. I truly acknowledge Jasper Huang's effort and contribution in immune studies discussions, suggestions and performing complement activation experiments. Thanks to Dr. David Spafford and his research associates Adrienne Boone and Adriano Senatore, who assisted me with fluorescence microscopy techniques; Dale Weber and Mishi Savulescu for their help with TEM and flow cytometry at the Biology department. My special thanks goes to César Brinatti for the critical advice on ITC and its data analysis. Thanks to Dr. Yuan and her laboratory researchers at the Shanghai hospital for the in *vivo* studies. I appreciate Jennifer Coggan for her generosity in letting me use the fluorescence plate reader in her laboratory.

My next acknowledgements go to the researchers and students in our laboratory: Dr. Shan Yu Fung, Dr. Mousa Jafari, Dr. Abdolhamid Firooz, Tatiana Sheinin, Dr. Denise Gosselink, Nita Modi, Dr. Xiao xia Han, Baoling Chen, Frank Yong Ding, Mohammad Ali Sheikholeslam, and Kaveh Sarikhani for their unlimited support, training the experimental techniques, and scientific advice

during my PhD program. I would also like to thank the undergraduate and co-op students working with me in past few years: Edgar Cao, Vanessa Ng, Daniele Bacinello, Tewodros Mamo, Sam Sohn, and Eugene Kovalenko for their hard work and assistance in the experimental performance and contributing to some of my publications.

Finally, I would like to thank my friends and family for their continued support and belief in me. A special thank you to my parents, and two sisters Parastou and Peivand for encouraging me all the way in my research career.

Most importantly, I would like to dedicate this thesis to my husband Jordan Hamilton who never stopped believing in me to pursue my ambitions.

Table of Contents

List of Figures

List of Tables

Nomenclature

Acronym	Full name
AAP	Amino Acid Pairing
AFM	Atomic Force Microscopy
ANS	1-anilino-8-Naphthalene Sulfonate
APP	All paring peptide
BSA	Bovine Serum Albumin
CAC	Critical assembly concentration
CD	Circular Dischroism
CMC	critical micelle concentration
CPP	Cell-penetrating peptides
CTP	Cell-targeting peptides
DDS	Drug Delivery System
DEG	Diethylene Glycol
DOX	Doxorubicin
ECM	extracellular matrix
EPC	eggphosphatidylcholine
EPR	Enhanced Permeability and Retention effect
EPT	Ellipticine
FDA	US Food and Drug Administration
FT-IR	Fourier Transform Infrared
gP60	Glycoprotein 60
HB	Hydrogen bonding
HPMA	N-(2-Hydroxypropyl) methacrylamide
i.p	Intraperitoneal
kDa	Kilo Dalton
mAb	Monoclonal antibodies
MPS	Mononuclear phagocyte system
nab^{TM}	Nanometer albumin-bound
NP	Nanoparticle

Acronym	Full Name
NSCLC	Non-small cell lung carcinoma
PAMAM	Poly(amino amine)
PBLA	b-benzyl-L-aspartate
PEG	Polyethylene Glycol
PGA-PTX	polyglutamate-paclitaxel
PIHCA	polyisohexylcyanoacrylate
PIHCA	Polyisohexylcyanoacrylate
PK	Pharmacokinetics
PLGA	Poly)lactic-co-glycolic) acid
RES	reticuloendothelial system
SEDDS	Self-emulsifying drug delivery systems
SEDDS	Self-emulsifying drug delivery systems
sHsp	small Heat shock protein
siRNA	small interfering RNA
SPARC	Secreted Protein, Acidic and Rich in Cysteine
THP	Pirarubicin

Chapter 1

Introduction

1.1 Overview

Cancer is one of the most devastating diseases with more than 10 million new cases every year worldwide. Cancer prognosis, diagnosis, and therapy have been topical research concepts of the past few decades. The design and synthesis of efficient drug delivery systems that will increase the therapeutic efficiency of drugs while minimizing their side effects are highly important in medicine research. Paul Ehrlich in 1906 coined the idea of the "magic bullet" drug by introducing the targeting concept, in which one part of a drug should consist of a recognizing ligand to bind to the target, and the second part provide the therapeutic action at the disease site [1]. Material chemistry and nanotechnology are now revolutionizing the generation of multifunctional systems, to reach to the idea of the "magic bullet". Conventional pharmaceutical agents suffer from their lack of target-ability, deleterious side effects, and fast clearance from circulation. Thanks to nanotechnology, the controlled size, shape and multi-functionality of particles, self-assembly, and controlled release of drugs are emerging to resolve the limitations of conventional drugs [2].

In the past few decades, many delivery systems have made great advances in improved solubility, transport, safety, and targeting as nanocarriers in cancer therapy. Liposomes, polymers, and proteins are the pioneer devices in encapsulating therapeutic agents for safer delivery [3]. All these drug delivery systems are designed to possess many advantages over free drugs, such as protecting drugs from degradations; preventing drugs from interacting with their biological environment, enhancing the attraction of drugs to the pathological areas, controlling drugs release and their biodistribution, and improving intracellular penetration. Biodegradability, biocompatibility, environmental sensitivity, extended circulation half-life, and distinct uptake efficiency in the target tissues but not in normal ones are the main features in designing any viable drug delivery system [2,4].

Nanocarriers without surface modifications are usually recognized as foreign particles by the body's defense system, targeted by macrophages, and readily removed from the circulation before reaching their targeted sites. Hence, the first step in modifying the nanocarriers is surface decoration for longevity [4]. Long-circulating pharmaceutical agents have the advantage of slowly accumulating in pathological sites with leaky vasculatures, due to their large particle size, which is known as

passive targeting through enhanced permeability and retention (EPR) effect [5]. Polymer-drug conjugates have a long history of contributing to the EPR effect by providing a prolonged circulation half-life, stealth properties and reduced antigenicity. Hydrophilic polymers such as poly (styrene-co-maleic acid) (SMA) [6] and poly (ethylene glycol) (PEG) [7,8] have been shown to protect drug carriers from reiculoendothelial system (RES) or macrophages, and consequently impart the *in vivo* longevity. One of the main advantages of polymeric drugs is patient compliance and improved quality of life, as less-frequent drug administration is needed owing to their longer plasma half-life. However, some limitations affect the use of polymer conjugates, including their molecular weight, solubility, biocompatibility, biodegradability, and clearance from the body. On the other hand, many natural polymers such as peptides can be used as drug carriers for extra precaution [9].

In the past two decades, albumin, as the most-abundant protein among serum proteins, has attracted great interest as an exogenous or endogenous carrier for long circulating drug delivery systems [10]. Drugs or active molecules for diagnostic applications can bind covalently or non-covalently to serum albumin for treating various diseases, primarily cancers, arthritis, hepatitis, and diabetes [11,12]. Several delivery systems have taken advantage of drug albumin-binding characteristic and have been advanced in clinical trials or approved as marketed products. For instance, Levemir® is an approved insulin detemir controlling glucose levels in diabetes patients by binding to circulating albumin [13]. Abraxane® is another approved albumin-based therapeutic, in which the anticancer drug Paclitaxel is bound to albumin forming 130 nm nanoparticles (*nab*™-technology) for intravenous administration against solid tumors [14]. In principle, this technology relies on albumin's major role in the delivery of hydrophobic drugs to target tissues, based on the following features: (i) albumin's non-covalent binding affinity to many hydrophobic molecules, utilizing their transport in the body to release them at the cell surface; (ii) albumin's binding to endothelial cell surface receptor called glycoprotein (gp60), initiating transcytosis of plasma components; (iii) albumin's accumulation in tumor areas through Secreted Protein Acidic and Rich in Cysteine (SPARC) binding, increasing the concentration of albumin-bound drugs inside tumors. SPARC is over expressed glycoprotein in tumor tissues responsible for tumor metastasis, and it has a high affinity for albumin; therefore, albumin uptake has shown to be higher in tumor cells than normal cells [15,16].

In addition to liposomes, polymers, micelles and other biomaterials applied in drug delivery, self/co-assembling peptides, have emerged as an important class of biomaterials with a wide range of applications in drug and gene delivery, vaccines, tissue engineering and regenerative medicine [17–19]. Peptides can be rationally designed to form functional nanostructures with multiple properties involving controlled stable structures, incorporation with active molecules (DNA, siRNA,

hydrophobic molecules, etc.), enhanced cell penetration [20] and targeting ability [21], some inherited antimicrobial features [22], improved cell attachments [23], and many more. Therefore, these self-assembling peptides could be major candidates for designing universal multifunctional nanocarriers for nanomedicine development.

A class of self/co-assembling ionic-complementary peptides (EAK16s) has been developed as nanocarriers for drug delivery systems. These peptides are amphiphilic, meaning they can encapsulate and stabilize hydrophobic compounds in aqueous solution [24]. EAK16-II has demonstrated great promise in both *in vitro* and *in vivo* delivery of hydrophobic drugs by inhibiting tumor growth significantly compared to free drug [25]. Owing to the unique structure of amphiphilic peptides and their potential, a *de novo* design principle, amino acid pairing (AAP), has been suggested to establish a platform for designing functional self-assembling peptides. Amino acid pairing strategy focuses on the side chain complementarity and compatibility in the structural engineering point of view. The design principle of amino acid pairing self/co-assembling peptides is guided by three major side chain interactions: hydrophobic interaction, electrostatic interaction and hydrogen bonding. In addition, the side chain would achieve to certain physiochemical stability to maximize pair affinity and minimize free energy [26]. While these newly designed systems and other self/co-assembling peptides have shown immense potential, issues remain in optimizing the self-assembled structures and making them more robust for *in vivo* applications. Uncontrollable aggregation, enzymatic degradation, and lack of stability of such peptides limit their *in vivo* applications, therefore, in this research, two main strategies- diethylene glycol (DEG) conjugation and serum albumin protein binding- are applied to stabilize self/co-assembling peptide-based drug delivery systems in physiological conditions. The detailed objectives of this research project and outline of the thesis are presented next.

1.2 Research Objectives

The goal of this research is to develop self/co-assembling peptide-based delivery of hydrophobic anticancer drugs, to improve longevity, target-ability, and highly efficient therapeutic properties. To achieve this goal diethylene glycol (DEG) conjugation and albumin binding strategies are incorporated to improve the above features. The specific objectives of the thesis are listed below:

1) Characterize the physiochemical properties of the amino acid pairing peptide (AAP8) functionalized with diethylene glycol (DEG)

- To determine the effect of DEG-conjugation on peptide self/co-assembly properties such as uncontrollable aggregation, critical self-assembly concentration, secondary structure, and nanostructure formation.
- To investigate the effect of DEG-conjugation on peptide and hydrophobic drug complexation and *in vitro* anticancer activity

2) Evaluate self/co-assembly properties of an ionic-complementary peptide, EAR8-II, and its potential in *in vitro* delivery of the hydrophobic drug Pirarubicin (THP)
   - To demonstrate the advantages of EAR8-II as a model ionic-complementary peptide over the previously introduced EAK16-II and AAP8
   - To evaluate the optimum ratio between the peptide and the drug in order to form stable structures and achieve effective anticancer activity *in vitro*
3) Explore the binding affinity between serum proteins (i.e., BSA and IgG) and the EAR8-II-THP complex
   - To determine the stability of the complex in a serum environment
   - To explore the nature of binding between serum albumin and peptide-drug complexes
4) Study the effect of serum albumin binding to the EAR8-II-THP complex on immune responses
   - To investigate macrophage responses, including cytotoxicity, uptake and cytokine expression against the albumin-bound EAR8-II-THP complex
   - To examine the hemolytic activity and complement activation induced by the complex in the presence and absence of serum albumin
5) Determine the target-ability of the albumin-bound peptide-based drug delivery system
   - To measure anticancer activity and cellular uptake of the complex
   - To show SPARC inhibition in non-small cell lung carcinoma (A549)

1.3 Outline of the Thesis

This thesis consists of five main research-based chapters preceded by the introduction and literature review chapters and followed by the conclusions and recommendations chapter. Chapter 1 introduces the overview of the thesis and points out the detailed objectives of the research. Chapter 2 provides a

comprehensive background on current drug delivery systems, their advantages and limitations. It also reviews the background of self-assembling peptides and their drug delivery applications.

Chapter 3 focuses on the first strategy for modifying peptide-drug complexes to promote longevity. Diethylene glycol (DEG), a short segment of polyethylene glycol (PEG), was selected to attach to the short-sequence amino acid pairing peptide (AAP8). Even though this peptide has shown promise in the design of novel functional biomaterials, it has a propensity to initiate uncontrollable aggregations. DEG-functionalization showed subsequent advantages in conquering this aggregation issue. The physiochemical properties, such as nanostructure, secondary structure, and critical aggregation concentration, are analyzed by atomic force microscopy, FT-IR spectroscopy, and steady-state fluorescence measurements, respectively, to evaluate the effect of DEG-conjugation on peptide aggregation. The functionalized AAP8s are tested for their hydrophobic drug encapsulation and *in vitro* delivery characteristics.

Chapter 4 introduces a model ionic-complementary peptide EAR8-II for hydrophobic drug encapsulation and *in vitro* delivery. EAR8-II inherits advantages from two formerly developed self/co-assembling peptides EAK16-II and AAP8. The effects of the peptide-to-drug ratio in the complexes are evaluated on the particle size, pH, charge, and stabilized THP in the solution, as well as *in vitro* anticancer activity and uptake against two cancer cell lines (A549 and HeLa).

Chapter 5 studies the interaction between serum proteins such as albumin and immunoglobulin G (IgG) from a thermodynamic point of view. First, the molecular and secondary structures of the peptide-drug complex in the presence of albumin are analyzed by TEM, DLS, and FT-IR spectroscopy methods, respectively. Second, fluorescence quenching technique and isothermal titration calorimetery (ITC) are employed to determine the binding properties.

Chapter 6 investigates the effect of serum albumin binding on immune responses. Macrophages, one of the primary immune cells, are treated with the complexes, and immune response analysis is conducted to evaluate the cytotoxicity, drug uptake and expression level of cytokines (e.g., iNOs, COX-2, TNF-α, IL-2, IL-1β). In addition, the complexes are tested on pooled human serum and red blood cells to examine the complement activation and hemolytic activity induced by the complexes.

Chapter 7 evaluates the anticancer activity mechanism of the EAR8-II-THP complexes in the presence of BSA, by exploring the expression level of secreted protein acidic and rich in cysteine (SPARC) in cancer cell line (A549). SPARC is overexpressed in cancer cells with high albumin affinity; therefore, a drug delivery system with SPARC inhibition capability is considered to be a targeted delivery system.

Chapter 8 summarizes the overall outcomes of the thesis in respect to the objectives. It states this thesis's original contribution to the research, and finally recommends the future work for this research and the areas for expansion.

Chapter 2

Literature Review

2.1 Current Advances in Multifunctional Nanocarriers for Anticancer Drugs

More than fifty years ago, Richard Feynman coined the concept of nanosurgeons and nanodevices in his revolutionary talk "There is Plenty of Room at the Bottom", where he encouraged researchers and specialists to develop devices capable of interacting with the body at the cellular level [27]. Following those initiations, nanoparticles have revolutionized the administration of medicines in the past few decades. Before 1970s, administration of pharmaceutical suspensions intravenously as well as poorly soluble drugs was almost impossible [28]. Recent advances in nanomedicine address these issues by improving solubility, and sustainability to further improve the pharmacokinetics and lower the side effects [29]. Table 2.1 summarizes the deficiencies of free drugs and highlights the advantages of drug delivery systems in pharmaceutical applications [30]. The progressive timeline of nanomedicine is also presented in Figure 2.1 (adapted from [31,32]) showing progress in drug delivery systems in the past sixty years. Technologies involved in the development of drug carriers are divided into four main categories: liposomes and micelles, polymer-drug conjugates, biodegradable polymeric nanoparticles, and peptide/protein-based materials [33].

Smart drug delivery systems can provide a very bright future for pharmaceutical research, due to several reasons. Passive targeting or enhanced permeability and retention (EPR) effect of drug delivery systems (DDS) enhance the accumulation of the drug in pathological areas. DDS technologies improve therapeutic index of established drugs by controlling release profile. In addition, recently the therapeutic effects of nucleic acids, peptides, and plasmids are growing. However, without drug delivery systems, administration of these compounds is impossible. In general, nanocarriers improve the pharmacokinetics and pharmacodynamics properties of therapeutic agents by increasing plasma half-life (which improves patient compliance due to less frequent required dose), protecting the drug from proteolytic enzymes, reducing in immunogenicity, enhancing stability of proteins, improving solubility of low Mw drugs, and increasing potential for targeted delivery [34]. In this section, I review the current delivery systems indicating their advantages and limitations.

Table 2.1 Non-ideal properties of drugs and their therapeutic implications. Adapted from reference [30]. Reprinted with permission from AAAS.

Problem	Implication	Effect of DDS
Poor solubility	A convenient pharmaceutical format is difficult to achieve, as hydrophobic drugs may precipitate in aqueous media. Toxicities are associated with the use of excipients such as Cremphor® EL (the solubilizer for paclitaxel in Taxol).	DDS such as lipid micelles or liposomes provide both hydrophilic and hydrophobic environments, enhancing drug solubility.
Tissue damage on extravasation	Inadvertent extravasation of cytotoxic drugs leads to tissue damage, e.g., tissue necrosis with free doxorubicin.	Regulated drug release from the DDS can reduce or eliminate tissue damage on accidental extravasation.
Rapid breakdown of the drug in vivo	Loss of activity of the drug follows administration, e.g., loss of activity of Camptothecins at physiological pH.	DDS protects the drug from premature degradation and functions as a sustained release system. Lower doses of drug are required.
Unfavorable pharmacokinetics	Drug is cleared too rapidly by the kidney. For example, requiring high doses or continuous infusion.	DDS can substantially alter the PK of the drug and reduce clearance. Rapid renal clearance of small molecules is avoided.
Poor biodistribution	Drugs that have widespread distribution in the body can affect normal tissues, resulting in dose limiting side effects, such as the cardiac toxicity of doxorubicin.	The particulate nature of DDS lowers the volume of distribution and helps to reduce side effects in sensitive, Non-target tissues.
Lack of selectivity for target tissues	Distribution of the drug to normal tissues leads to side effects that restrict the amount of drug that can be administered. Low concentrations of drugs in target tissues will result in suboptimal therapeutic effects.	DDS can increase drug concentrations in diseased tissues such as tumors by the EPR effect. Ligand-mediated targeting of the DDS can further improve drug specificity.

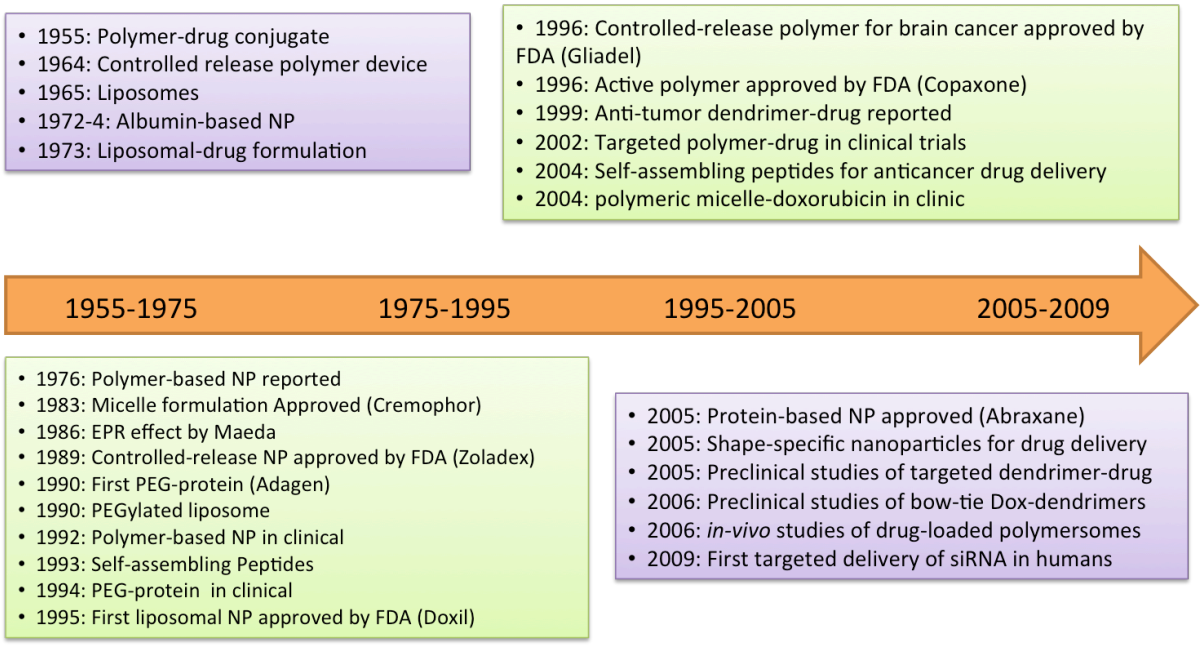

Figure 2.1. Timeline of the development of nanoparticle therapeutics adapted from reference [31].

2.1.1 Liposome-based Drug Delivery Systems

Liposomes are known as frontier nanomaterials for cancer therapy. In 1964, Bangham *et.al* first introduced liposomes and proposed their lamellae structure for bilayer phospholipids [35,36]. Liposomes were further improved and became more popular for drug delivery applications. Ten years after introduction of liposomes, G. Gregoriadis initiated the entrapment of Penicillin and Actinomycin D in liposomes in order to decrease their deleterious side effects on non-diseased tissues in cancer chemotherapy [37]. In 1980, first examples of targeted nanoparticle using ligand-conjugated liposomes were introduced and showed some promising preclinical and clinical results in the treatment of various diseases [38,39]. Doxil was the first FDA-approved liposomal-based drug (1995), in which doxorubicin was encapsulated into a liposome carrier to increase its half-life and reduce its cardiotoxicity compared with free doxorubicin [31,40]. Many liposomal delivery systems either Polyethylene glycol (PEG)-conjugated or non-PEG conjugated, encapsulating various drugs, are currently in clinical stages. So far only Doxil is approved by the FDA, and Genexol-PM is only approved in South Korea [41] as cancer therapeutics. There are few more liposomal-based FDA approved drugs for other applications such as fungi infections, lymphomatous meningitis, etc. [33]. Despite the progress in liposomal delivery, liposomes tend to be eliminated rapidly from the blood and captured by RES, primarily in the liver. Several techniques including modification by long-

circulating polymers and antibodies, attachment of diagnostic labels and stimuli-sensitive ligands, incorporation of cell-penetrating peptides, viral components, and magnetic targeting components, have aimed to overcome the problems [42]. The trend of liposome evolution is shown in Figure 2.2.

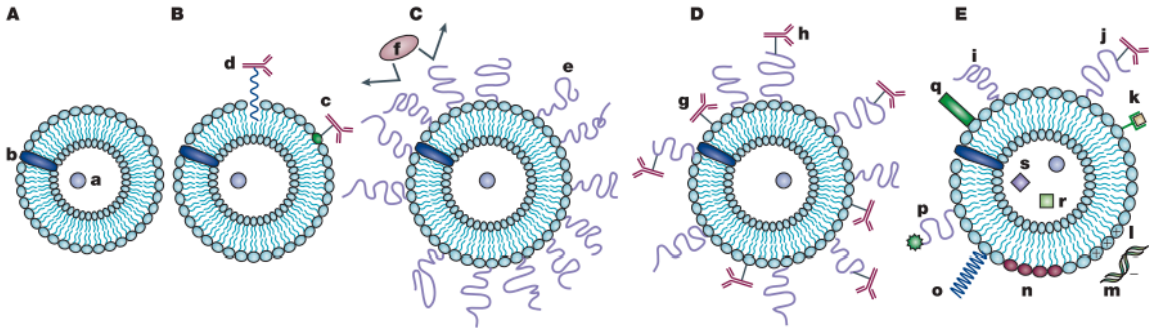

Figure 2.2. **(A)** Plain phospholipid with (a) water-soluble drug, and (b) water-insoluble drug, **(B)** Antibody (c) directly and (d) hydrophobically attached, **(C)** (e) PEG-grafted for long circulating and shields from the interaction with opsonizing proteins (f), **(D)** long circulating immunoliposome, (g) antibody attached to liposome, (h) or grafted to the polymeric chain, **(E)** new generation of liposome with incorporation of (i) protective protein, (j) targeting ligand, (k) diagnostic label, (l) positively charged lipid for (m) DNA complexation, (n) stimuli-responsive lipid, (o) stimuli-responsive polymer, (p) cell-penetrating peptide, (q) viral component, (r) targeting magnetic particle, (s) gold particles for electron microscopy. Adapted from reference [42]. Reprinted with permission from Rights Link.

2.1.2 Polymer-based Drug Delivery Systems

Polymeric nanoparticles are also important materials that progressed significantly during drug delivery evolution. Linear or branched polymer chains are mainly used as inert carriers for therapeutic agents. In 1976, Judah Folkman and Robert Langer published a Nature article regarding sustained release of proteins and other macromolecules from polymeric nanomaterials, as one of the premier innovations in polymeric delivery systems [43]. In 1992, a phase I clinical trial of doxorubicin carried by polyisohexylcyanoacrylate (PIHCA) nanoparticles was reported increasing doxorubicin cytotoxicity and reducing cardiotoxicity compared with unprotected doxorubicin [44]. In 1994, Robert Langer *et al.* developed PLGA-PEG, an amphiphilic copolymer composed of two biocompatible blocks, where exhibited considerably increase in blood circulation time and decreased liver accumulation [45]. The FDA approved two polymeric drug delivery systems in 1996, including controlled-release polymer for brain cancer (Gliadel) and biologically active polymer (Copaxone)

[31,40]. In 2011, peptide-conjugated PLGA-PEG encapsulating Docetaxel entered clinical trial phase I [32]. In general, polymeric nanocarriers can be mainly categorized into the following types including polymer-drug conjugates, polymer-protein conjugates, polymeric micelles, and multicomponent polyplexes (Figure 2.3) [34].

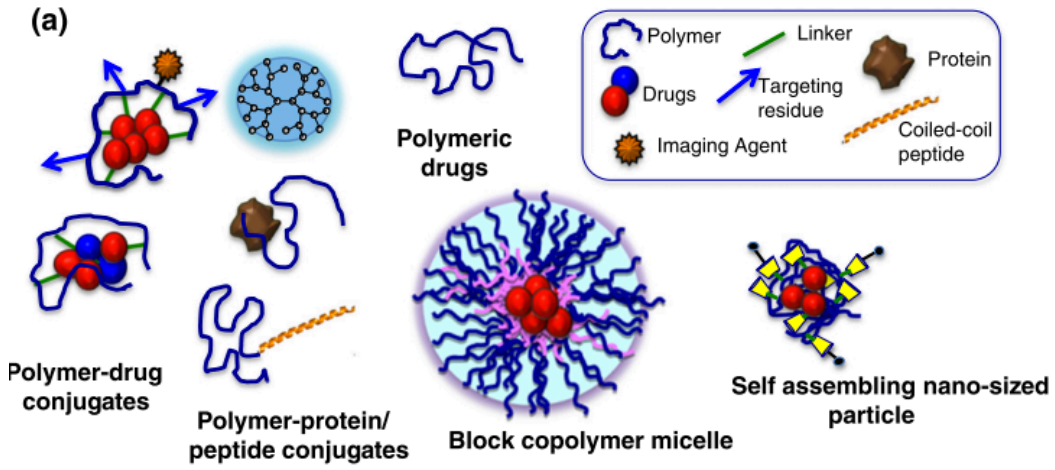

Figure 2.3. Schematic of the sub-classes of polymer therapeutics. Adapted from Reference [46].

2.1.2.1 Polymer-Drug Conjugates

The strategy of polymer-drug conjugate, at its early development stages, had mainly focused on the delivery of commercialized anticancer drugs such as paclitaxel, doxorubicin, Platinates, and Camptothecin. Those drugs were suffering from their insolubility, deleterious side effects, cardiotoxicity, and poor pharmacokinetics [47]. Ringsdorf first coined the idea of polymer-anticancer drug conjugates in 1975 [48], followed by succeeding research by Kopecek *et al.,* in late 1970s designing the first synthetic polymer-drug conjugate (HPMA-DOX) [49]. The rationale behind designing polymer-drug conjugates was to control the distribution of low-molecular weight anticancer agents throughout body and consequently lower side effects. Most of the low molecular weight drugs leave the circulation stream within few minutes, whereas polymer conjugates ideally produce long-circulating compounds that circulate for several hours and further assist passive targeting through enhanced permeability and retention effect (EPR) [47]. Ringsdorf proposed a model for pharmacologically active polymers including three main compartments in polymer backbone: 1) Solubilizer (co-monomer or blocks of nontoxic water- or lipid soluble), 2) Pharmacon (Drug fixation

and release, and response to living systems), 3) Transport System (homing device for targeting and receptor reaction, and non-specific resorption enhancer for improving biodistribution) [48]. This model provides a guideline for designing a systematic polymer-drug conjugate system. The detailed mechanism of action of polymer-drug conjugates is presented in Figure 2.4. This mechanism shows the low renal elimination rate, EPR effect, biodegradability of polymer, and release of drug to enhance therapeutic index [47].

It is worth noting that the only approved polymer-drug conjugate for cancer therapy is OnCaspar (PEGylated L-asparaginase), which was approved in 1994 and being used for acute lymphoblastic leukemia [33]. There are few more FDA approved polymer-cytokine / enzyme / growth factor / antibody conjugates available in the market for other types of therapies [50]. Polyethylene glycol is one of the most common polymers used for drug conjugates proving the long circulation lifetime for drugs. There are several chemistries involved in PEG-drug conjugation that utilize FDA approval including amidation, reductive amination, and Michael addition. Nonetheless, nowadays up to sixteen of these compounds are being tested in advanced clinical trials. The most reliable one is Opaxio (or also known as Xyatax CT-2013), which is a conjugation of polyglutamate-paclitaxel (PGA-PTX). This compound targets various cancers, particularly non-small-cell lung cancer; ovarian cancer as a single agent or combination chemotherapy, and so far showed gender-dependent promises in clinical trial phase III [47,51]. Research also showed that due to the complexity of the nature of cancer, combination therapy results better improvement in cancer patients. Recently, Duncan *et al.* established a combination therapy for breast cancer containing HPMA copolymer conjugating both aromatase inhibitor aminoglutethimide (a hormone therapy) and doxorubicin (a chemotherapy). This combination therapy illustrated greater activity against breast cancer cells than individual conjugates *in vitro* showing treatment of hormone-dependent cancers. The combination therapy provides opportunities for treating multi-drug resistant (MDR) metastatic cancers [47,52].

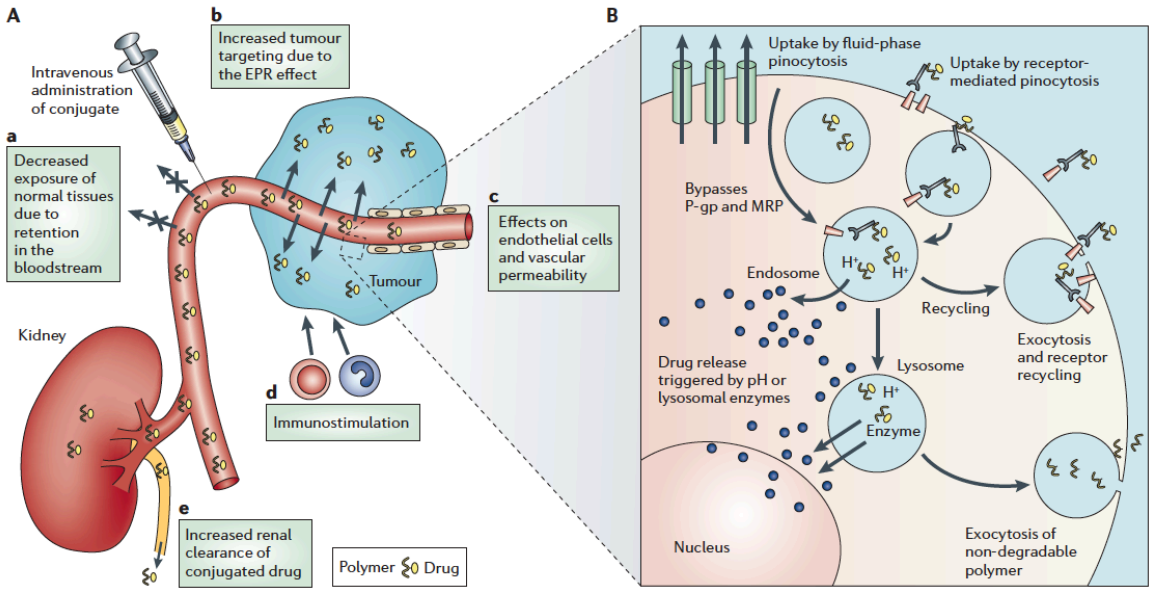

Figure 2.4. Current understanding of the mechanism of action of polymer-drug conjugates. **(A)** Hydrophilic polymer-drug conjugates administrated intravenously can be deigned to remain in the circulation. **(B)** On arrival to the tumour interstitium, polymer-conjugated drug is internalized by tumour cells through either fluid-phase pinocytosis (in solution), receptor-mediated pinocytosis following non-specific membrane binding (due to hydrophobic or charge interactions) or ligand–receptor docking. Adapted from Reference [47]. Reprinted with permission from Rights Link.

2.1.2.2 Polymer-Protein Conjugates

The history of polymer-protein conjugates started with the pioneer research by Frank F. Davis and colleagues in the late 1970s. They introduced the first PEGylation technique by covalently binding Polyethylene glycol (PEG) to bovine liver catalase and bovine serum albumin in order to reduce immunogenicity and enhance circulating life of proteins [53,54]. Since then, PEGylation has become the standard method for improving pharmacokinetics and pharmacodynamics properties of therapeutic agents due to PEG's lack of immunogenicity, antigenicity, and toxicity. PEG is highly hydrophilic and protecting proteins from immune response and degradation, as well as providing conjugation without cross-linking to the proteins that helps the easy release [34]. In 1990, the first PEG-enzyme conjugate (ADAGEN) was approved by the FDA for treatment of combined immunodeficiency disease [50]. Regardless of the advantages associated with PEG, there are some drawbacks limiting its application including lack of biodegradability and reducing protein activity due to conjugation.

2.1.2.3 Polymeric Micelles

Polymers are also used in drug delivery systems while encapsulating hydrophobic drugs either through micellization or microemulsification. Micelles, in general, are amphiphilic linear or branched polymers that spontaneously self-assemble in aqueous solution, and they can encapsulate hydrophobic drugs in their hydrophobic core [55]. The core/shell structure forms at above threshold concentration referred to as the "critical micelle concentration" (CMC). The core/shell structure provides the hydrophobic core as a reservoir for entrapping insoluble compounds as well as the hydrophilic corona for solubilizing the micelles in aqueous environment. In 1976, Peter Speiser, a pioneer in development of nanoparticles published the first journal article focused on polymerized micelles for vaccination purposes with controlled release of the antigen and consequently improved immune responses. He introduced new terms of "nanoparts" representing solidified micelles containing drugs used as immunological adjuvants [56]. There are many advantages regarding using micelles in drug delivery applications including easy conjugation for active targeting, high drug loading capacity in the hydrophobic core and rapid cellular uptake due to their nano-range size properties. Micelles protect drugs from degradation before reaching the target, and consequently, increase the plasma half-life and lower the cytotoxicity to the unaffected tissues. However, there are some limitations toward using surfactant-like micelles in drug delivery such as toxicity and lack of biocompatibility.

Polymeric micelles are usually block copolymers consisting of hydrophilic (A) and hydrophobic (B) blocks arranged in di-block (AB) or tri-block (ABA). These micelles form from self-assembling of block- or grafted copolymers containing polymer segments of different structure and functionality such as ionic and nonionic block, or hydrophilic and hydrophobic block. One of the recent examples of polymeric micelles is functionalized PEG-poly (b-benzyl-L-aspartate) (PBLA) block copolymer with adriamycin facilitated with pH-cleavable hydrazone bond. Hydrazone is stable at pH 7.4, whereas in acidic pH is instable and let the encapsulated drug be released in tumor environment [57].

Among many explored polymeric cases in the research stage, only five passively targeted micelle products have been advanced to clinical trials including NK012 (PEG-PGlu-(campothecin)), NK105 (PEG-P(aspartate)), SP1049C (Pluronic L61-F127-(Doxorubicin)), NC-6004 (PEG-PGlu-(cisplatin)), and Genexol-PM (PEG-P(D,L-lactide)-(Paclitaxel)). For example, NK012 is a polymeric micelle containing a block copolymer of PEG and polyglutamate conjugated with anticancer drug campothecin (SN-28) is being tested in clinical phase II to target breast cancer [58]. Among all these

polymeric micelles only Genexol received the FDA approval to be used in patients with breast cancer [59].

Dendirimers are other branch of therapeutic polymers that recently being developed for drug delivery application. For example, dendrimer-platinate is a conjugation of Poly(amido amine) PAMAM and Cisplatin, which was highly water-soluble and showed a slow release of drug *in vitro* and great anticancer activity against melanoma, where Cisplatin did not have similar activity on its own [60]. Vogtle *et al*., initially invented dendrimers in the 1970s and studied the controlled synthesis of dendrimers producing branched polymers with large molecular activities. Dendrimers contain individual "wedges" called dendrons that initiate from the core and each layer of concentric branching added up to form treelike architecture with a large number of surface groups. Each layer of branches is called by G#, starting with G0 which is the first branch after core. The higher the G level goes the higher branched dendrimers creates. The base of dendrimers can be polymers (e.g. PAMAM), amino acids (e.g. tryptophan, glutamic acid, alanine, etc.), and glycodendrimers (e.g. glycosides). Dendrimers either encapsulate hydrophobic drug molecules in their voids to further controlled release of the drugs or drug being covalently conjugated to dendrimers through pH-sensitive ligands. Considerable advances were reported about dendrimers capabilities in both hydrophobic and hydrophilic drugs delivery in *in vitro* and *in vivo* [60,61].

2.1.3 Protein-based Drug Delivery Systems

Naturally self-assembled proteins such as ferritin/apoferrintin protein cage [62], plant-derived viral capsids, the small Heat shock protein (sHsp) cage, albumin, soy, and whey protein have been used for drug delivery systems. Their biocompatibility, biodegradability, and low toxicity properties make them ideal candidates for drug delivery systems. Based on proteins' shape in a drug delivery system they categorized into microspheres, nanoparticles, protein cages, nanoparticles, hydrogels, and film structures. Table 2.2 summarizes the protein-based drug delivery systems and their pharmaceutical uses [63].

Protein cages are uniformly sized shell structures from virus or virus-like materials where the nucleic acids of the virus are replaced by therapeutics compounds. The uniform cage size in protein cages is an advantage of this type of drug delivery systems due to even drug loading and drug release, as well as avoidance of uncontrollable macromolecular aggregations. Protein cages can incorporate multifunction properties including attachment of fluorophores for imaging and diagnosis purposes, and attachment of carbohydrates, peptides, and nucleic acids for targeting and therapeutic objectives.

Figure 2.5 illustrates the schematic of folic acid conjugated protein cage loaded with doxorubicin. This protein cage is made of a model plant virus, Hibiscus chlorotic ringspot virus (HCRSV) conjugated with folic acid to impart cancer-targeting functionality and loaded with polyprotic acid and doxorubicin used against ovarian cancer cells. Results showed significant improvement of uptake and cytotoxicity of doxorubicin in the ovarian cancer cells [64].

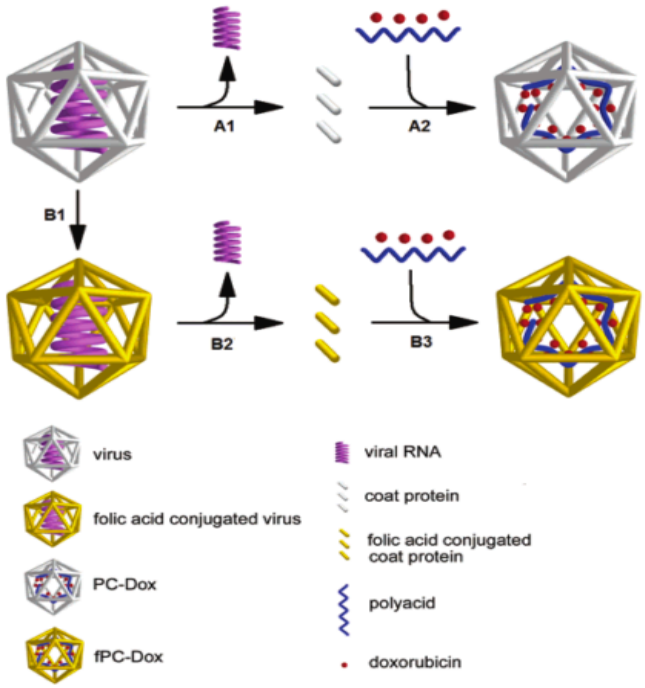

Figure 2.5. Schematic illustration of doxorubicin loaded viral protein cage. Step A1 and B2 are indicative of the removal of viral RNA from the virus. Step A2 and B3 involve the encapsulation of polyacid and doxorubicin during assembly of protein cage. Step B1 refers to the conjugation of folic acid onto the viral protein coat. Adapted from reference [64]. Reprinted with permission from Rights Link.

Small heat shock proteins (sHsp) are another example of protein cages. These cages are composed of exterior, interior and interface surfaces compartments. The stability of these cages is significantly high in large temperature (max. 70°C) and pH (5-11) ranges [65]. The existence of unique cysteine residues on the interior surface of the cage provides functional thiol group binding of small molecules such as doxorubicin. The pH and temperature sensitivity properties of sHsp offer controlled release of doxorubicin in pH and temperature dependent manner.

Soy proteins are inexpensive and accessible source used in drug delivery systems. Soy protein isolates (SPI) are purified from soy plant consisting dry soy globulin proteins. In a two-step process

soy protein films are produced. These steps are protein denaturation by preheating and then crosslinking of disulfide bonds and hydrophobic attractions. Soy films have been used in delivering of two different drugs such as methylene blue and rifampicin for treatment of gastric intestinal tract [63,66].

Table 2.2. List of protein-based drug delivery systems (DDS), the primary protein used, characteristics of the DDS, and the pharmaceuticals involved. Adapted from Ref [63]. Reprinted with permission from Rights Link.

Protein	**Delivery system**	**Description**	**Drugs**
Albumin	Nanoparticles	**1.** Bioconjugate hydrophilic drug **2.** Extremely robust to various conditions **3.** Bind to many drugs such as indole compound, penicillin benzodiazepins **4.** Non-toxicity, biodegradability and immunogenicity **5.** The most abundant plasma protein	6-coumarin, DOX, Abraxane
Casein	Microsphere	**1.** Easy to incorporate hydrophobic drug **2.** Very tolerable to robust conditions **3.** Nontoxic of the degradable end product **4.** No disulfide bridge	Progesterone, DOX, theophylline
Collagen	Microparticles, minirods	**1.** Low toxicity, biodegradability, and immunogenicity **2.** Structral protein with high content of glycine, hydroxyproline and hydroxylysine **3.** Contain carboxyl group and secondary amino groups with possible cross-linking function	Glucocorticosteroids, FITC-dextran, all-trans retinol
Elastin polypeptide (ELP)	ELPs-DOX nanoparticles, hydrogel	**1.** Thermally reversible protein self- assembling into aggregate at phase transition for therapeutic application **2.** Elastin-like polypeptide has a pentapeptide repeatable unit as Val-Pro-Gly-Xaa-Gly **3.** MW of ELP can be made by recombinant technology as precisely as possible **4.** Genetic and chemical modification of ESP for versatile functionalities as well as control of biopolymer properties	DOX, plasmid DNA
Ferritin/apoferritin	Protein cage	**1.** Assembled and disassembled size- container at different pH **2.** The first protein cage to be used **3.** Three distinct features: exterior, interface, interior for different functionalities **4.** Genetic and chemical modification for possible combination of biology and material science	RGD4C peptide, FITC
Gelatin	Microsphere, hydrogel	**1.** Low toxicity, biodregradability of end pro- ducts, and biocompatility **2.** Denatured form of collagen **3.** Use as ingredient in drug formulations Possess many carboxyl functional groups for cross-linking	Colchicine, thrombocidin (rTC-1), lysozyme
Gliadin	Nanoparticles	**1.** Plant protein derived from wheat **2.** Non-toxicity, biocompatible and biodegradable **3.** Protect carrier from breaking down by stomach acid **4.** Easy to entrap hydrophilic drugs due to its water solubility	Vitamine E, Linaloo and linalyl acetat (LLA), benzalkonium

			chloride (BZC), all-trans-retinoic acid
Small heat shock protein (sHsp)	Protein cage	**1.** Uniform cage size with 12 nm exterior and 6.5nm interior **2.** Genetically, chemically modified interior and exterior for multifunctionalities as well as controlling of the protein properties **3.** Large pores (3 nm) between interior and exterior for easy cargo exchange **4.** Use as scaffold for chemical reactions and material synthesis	Fluorescein, RGD 4C peptide, anti-CD4 antibody, DOX
Soy protein	Film	**1.** Abundant and inexpensive plant protein **2.** Highly soluble in water and easy to incorporate hydrophilic drug **3.** Non-toxicity and reusable end products	Methylene blue, rifampicin
Viral capsid	Protein cage	**1.** Modification of specific amino acid residues resulting in multifunctionalities **2.** Viral diversity providing different size and shape as well as catalyst functions **3.** Three distinct features: interior, interface and exterior for possible therapeutic applications **4.** Assembled and dissembled biological container at different conditions	DOX, poly-anethole-sulphonic, antibody 19G2
Whey protein	Hydrogel, whey protein beads, microspheres	**1.** Independent of pH change, easy to entrap hydrophilic drugs **2.** Possibly form gel, foam and emulsion Biocompatible and biodegradable end product **3.** Protect drugs from digestive enzymes	Riboflavin, caffeine, retinol
Zein	Microspheres	**1.** Use to entrap hydrophobic drug, **2.** Has antibacterial activity, **3.** Protect ivermecin from photodegradation **4.** Low toxicity of degradable end products, biocompatible, **5.** Less expensive	ivermectin

Albumin is one of the most common proteins used in drug delivery systems. It plays an important role in encapsulating of hydrophobic drugs and targeting specific tissues. 130-nanometer albumin-bound (*nab*^{TM}) technology was the first new class of protein-based drug delivery technology approved by FDA in 2005 [67]. This technology exploits the transport properties of albumin including: (i) albumin binds non-covalently to many molecules including fatty acids, vitamins, bilirubin, hormones, and acidic and hydrophobic drugs, (ii) albumin initiates translocation of drug in cytoplasm through receptor binding. Gp60 is 60 kDa glycoprotein existed dominantly on the endothelial cell surface that can bind to albumin with high affinity, (iii) albumin accumulate in tumor sites dominantly due to the secretion of the albumin-binding protein SPARC (Secreted Protein, Acidic and Rich in Cysteine). It has been reported many cancer cells have over expression of SPARC. Albumin has high binding affinity with SPARC, which can cause concentrating albumin in tumor sites. Albumin is also known

as source of nutrition and energy for cancer cells that can be an advantage for drug delivery system containing albumin as a drug carrier. The detailed mechanism of albumin contained drug uptake by cancer cells is explained by Neil Desai *et al*. and illustrated in Figure 2.6 reprinted from reference [68]. The transport of albumin-bound drug across the endothelial cell membrane in the area of tumors is facilitated by Gp60 receptor and caveolin-1 mediated transcytosis. Albumin-drug molecules accumulation enhance significantly in tumor sites due to the presence of albumin-binding protein SPARC in the tumor interstitium [15,16,67–69].

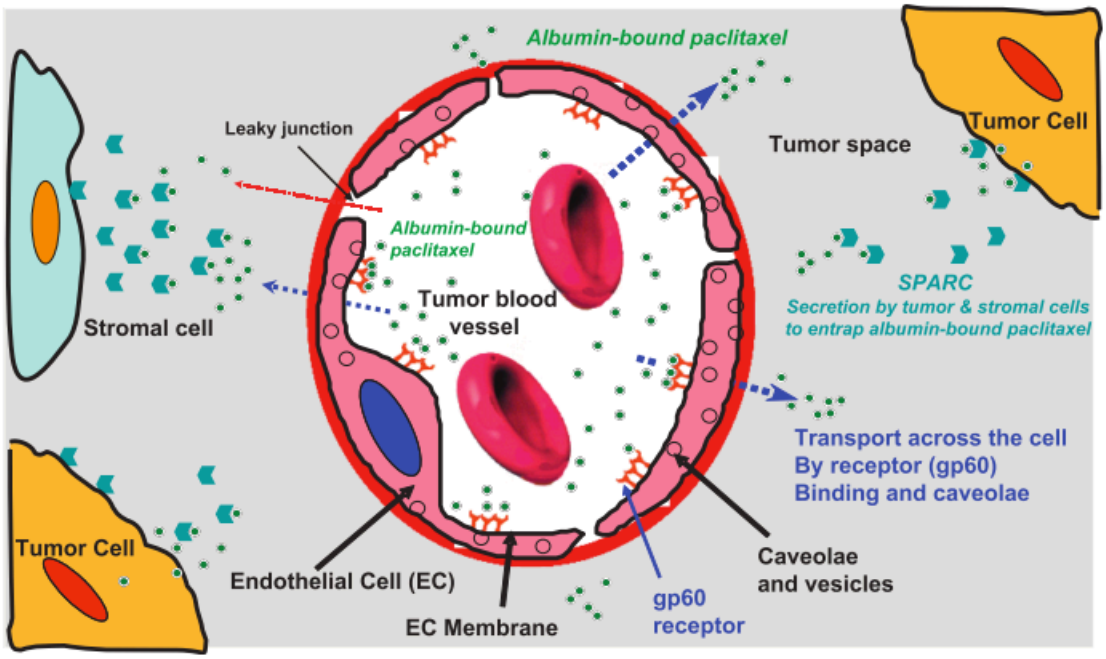

Figure 2.6. Mechanisms for the transport and accumulation of albumin-bound paclitaxel in tumors. Adapted from reference [68].

2.2 Modification of Nanocarriers Enhancing Functionalities

Application of nanocarriers in pharmaceuticals has shown enhanced the *in vitro* and *in vivo* efficiency of many established drugs, however many of these nanocarriers without further modifications are suffering from their low selectivity, low circulation life, and uncontrolled release profile. Therefore, over the past decades several surface modification strategies have been established in order to control biological properties of nanocarriers. The most common strategies comprise increasing stability and half-life of nanocarriers, implementing passive and active targeting moieties, incorporating responsiveness to the local physiological-associated stimuli such as pH and temperature, utilizing

with imaging/contrast ligands for therapy and diagnostic purposes [4]. The following sections summarize the basic surface modifications of nanocarriers and the current advances made.

2.2.1 Longevity in Blood

The essential property of pharmaceutical nanocarriers is longevity in blood. Since human's immune system shows defense against any foreign particle, nanoparticles can be easily recognized by macrophages (also called opsonization) and removed from circulation before performing their function. Therefore, modifying nanocarriers so they cannot be recognized by macrophages is a crucial consideration in pharmaceuticals. The important reasons for making long-circulating drugs and nanocarriers are as followings: (i) maintaining a required level of a therapeutic agent in blood for extended time intervals; (ii) slow accumulation of drug-containing nanocarriers in pathological sites or enhanced permeability and retention (EPR) effect also called a 'passive targeting'; (iii) prolonged circulation of nanocarrier can help to achieve a better 'active targeting' for targeted nanocarriers and more time for interaction between nanoparticles and pathological sites [5,70,71]. Polyethylene glycol (PEG), an FDA approved polymer for use as vehicle or base in foods, cosmetics and pharmaceuticals, has shown a great potential in increasing longevity of nanoparticles such as liposomes, polymers, peptides and proteins [8,72–76].

2.2.1.1 Poly(ethylene glycol), PEG- modification

Frank Davis pioneered PEGylation of a protein in 1977 at University of California, Berkeley. He had studied the immunogenic properties of the poly ethyleneglycol (PEG) and also developed the method for covalent attachment of PEG to proteins [77]. His observations show that the PEGylated protein has greatly reduced immunogenicities and enhanced circulation time in rabbits and mice. PEG is known as a candidate to be conjugated to protein/peptide for a number of reasons: (1) hydrophilicity, (three water molecules bond per one oxyethylene unit) that is by increasing the molecular mass of PEG, the solubility in water will increase, (2) linearity, (3) lack of charge (4) easy detection in mass spectroscopy spectrum (5) approved by the FDA for use as a vehicle or base in food, cosmetics, and pharmaceuticals including injectable, topical, nasal and rectal formulations [8].

The surface functionalization of nanoparticle (NP) systems with PEG has become a standard strategy to increase NP circulation half-life. By reducing nonspecific interactions with proteins through its hydrophilicity and steric repulsion effects, PEG provides long circulating drug delivery systems with reduced opsonization and complement activation. PEG was approved by the FDA for clinical use due to its low toxicity and lack of immunogenicity. There are numbers of clinically

approved therapeutics that rely on PEG properties for improved *in vivo* profiles, including liposomes (Doxil), PEG–drug conjugates (Oncaspar) and polymeric NPs (Genexol-PM) [78–80].

PEGylation of β-sheet forming self-assembling peptides has also been studied through various work ever since the first report by Lynn *et al.* of the conjugation of PEG to the amyloid peptide (10-35 Aβ) [81,82]. This early work showed that the PEGylation prevented lateral association of the fibrils inhibiting the irreversible step of fibrilogenesis. Elastin like polypeptides based on (VPGVG)4 and (VPAVG)4 were also conjugated with PEG which enhanced their self-assembling properties [83]. Moreover, PEGylation of the GAGA peptide, which is based on the Bombyx mori silk, enhanced peptide self-assembly through formation of both parallel and anti-parallel β-sheets [84]. Collier *et al.* introduced an interesting self-assembling peptide Q11 (Ac-QQKFQFQFEQQ-Am) and elegantly studied the effect of PEGylation on the self-assembling procedure through conjugation of different PEG chains either on one side or two sides of the peptide. Their results showed that PEG conjugation strongly prevented lateral aggregation of the fibril-forming peptides. Further on they showed a great promise of Q11 as an immune adjuvant [18,85].

PEG is formed in the process of linking more than one repeating chain of ethylene glycol to form linear or branched polymers. To enhance the pharmacokinetics and pharmacodynamics properties of peptides or proteins, a stable bond connecting PEG polymer to the peptide of choice is generated. Contributing factors that affect properties of PEGylated peptide are: (1) the number of PEG chains, (2) the molecular weight of PEG, (3) the location of the PEG conjugated to the peptide sequence, and (4) the chemistry applied to bind PEG to the peptide. The important characteristic of first generation of PEGylation was utilization of low molecular weight of linear PEGs (< 12 KDa) with side reactions or weak linkages upon conjugation with peptides. However, the second generation of PEGylation was designed to avoid the limitations present in the first generation such as restriction of low molecular weight, unstable linkage, and lack of selectivity in substitution [7,8,74]. The molecular weight of PEG plays an important role in protein activity: high molecular weight of PEG causes reduced activity *in vitro* and elevated activity *in vivo* by improving pharmacokinetic profile. The rapid decrease in systemic clearance was observed by increasing Mw of PEG from 21 to 70 kDa [86]. To couple PEG to peptides or proteins it is necessary to activate the functional group and one or both terminals. The selection of the functional group in PEG is based on the type of available reactive groups in the peptide/protein molecules. For peptides, typical reactive amino acids are lysine, cysteine, histidine, arginine, aspartic acid, glutamic acid, serine, threonine, and tyrosine, as well as N-terminal amino group and C-terminal carboxylic acid [7,74].

2.2.1.2 Protein-Nanoparticle Interactions

Nanomaterials and their unique properties have attracted the attention of many areas of science including physics, chemistry, engineering, and medicine. The interesting fact about nanomaterials is the very distinct mechanical, physical, and chemical properties of nanoparticles from those of their bulk counterparts, due to the significantly smaller particle size and high surface area. In a biological and medical point of view, nanoparticles are small enough to interact with physiological components and potentially reach the target tissues. Interaction between nanoparticles and biomolecules is an important subject that has been studied extensively. In the biological environments, the surface of nanoparticles is immediately covered by biomolecules (e.g., proteins) resulting in the formation of "protein corona" on the nanoparticles' surface. The nanoparticles covered with biomolecules or protein corona are the surfaces can be "seen" by biological entity such as cells and tissues, which is dramatically different from the surface of intact nanoparticles. Therefore, a deep understanding of the fundamental interactions of nanomaterials with biological components plays a key role in nanomedicine research [87,88]. The surface properties and protein corona of nanoparticles suggested an important effect on their circulation time and clearance rate, which are governed by phagocytosis (i.e., mononuclear phagocytes uptake) [89]. The intrinsic characteristics of nanoparticles such as composition, size, shape, charge, coatings, surface modifications, crystallinity, hydrophobicity, and wettability highly affect the formation of the protein coronas [90,91].

Albumin as the most abundant protein in plasma, which is highly soluble, and stable in the pH range of 4-9 and high temperature (60°C). Albumin is also known for its biodegradability, availability, and lack of toxicity as well as its favored uptake by tumor cells and inflamed areas. All these properties make albumin a potential candidate for drug delivery systems. Numerous studies have shown improvement in pharmacokinetics of active drugs and peptides while bound with albumin as well as high accumulation of albumin in inflamed joints in arthritic disease and solid tumors [92].

Abraxane (ABI-007 or *nab-paclitaxel*) is a trademark name for Albumin-Paclitaxel conjugate utilizing *nab*^{TM} technology was the first product approved by FDA for treating metastases breast cancer and meanwhile it has been approved in 41 countries. Compared to Paclitaxel (Taxol), Abraxane demonstrated 14% higher antitumor activity among breast cancer patients after failure of combination of chemotherapy for metastatic breast cancer. In addition, Abraxane increased the maximum tolerated dose (MTD) of the paclitaxel from 175 to 260 mg/m^2 [67]. Previously used paclitaxel also known as Taxol had a drawback of containing synthetic solvent for parental administration (Cremophor EL) as a pre-medication that caused hypersensitivity. Abraxane overcame

the issues involving with Taxol, which avoided the use of cremophor and was well tolerated by the patients for 30 min intravenous infusion. So far, *nab*-paclitaxel has been applied to different types of cancers besides breast cancer, including lung, melanoma, and pancreatic cancers. For all the listed named cancer, ABI-007 is advanced up to clinical phase III and is in process of approval based on the latest results reported in 2012. *Nab* technology has been employed for various anticancer drugs such as *nab*-*D*ocetaxel (ABI-008) against prostate cancer, *nab*-Rapamycin (ABI-009) mTOR inhibitor in solid tumors, *nab*-17AAG (ABI-010) Hsp90 inhibitor, *nab*-VDA (ABI-011) vascular disrupting agent, and Novel Taxane (ABI-013) that have advances in different clinical stages [11].

Besides albumin-bound drugs, albumin has shown the great capability of binding other therapeutic or diagnostic molecules. B. Elsadek and F. Kratz reported a comprehensive summary of application of albumin in their review article in 2012 [12]. Albumin-binding pro-drug (DOXO-EMCH, or INNO-206) for breast and lung cancer and sarcoma, albumin-modified exendin-4 conjugate for treating type 2 diabetes, Albuferon (fusion of albumin and interferon-a-2b) for treating hepatitis C [93], fluorescein-labeled albumin for detecting brain tumor during surgery and diagnosis applications (e.g., AFL-HSA) [94,95], albumin-binding antibodies for antibody receptor-mediated cancer therapy (e.g., MM-111)[96], albumin conjugate antiviral C34 peptide for inhibiting HIV-1 (e.g., PC-1505) [97], and etc.

Despite the functionality of the nanoparticles, depends on their size and compositions they can be harmful to the human body and cause protein-misfolding related diseases, and here is where nanotoxicology comes to play in order to design safer nanoparticles for biological applications [98]. The affinities of protein bindings are highly dependent on nanoparticles' composition. For instance, Linse *et al.* focused on the potential of nanoparticles in promoting protein assembly into amyloid fibrils (β2-m protein) by assisting the nucleation process for potentially preventing human diseases such as Alzheimer's, Creutzfeld-Jacob disease, and dialysis-related amyloidosis. They have shown the role of nanoparticles (e.g., copolymers, cerium oxide particles, quantum dots, and carbon nanotubes) in enhancing the rate of protein fibrillation by increasing the lag time of nucleation due to their enormous surface areas. The results showed that surface hydrophobicity of the nanoparticles affected the NP-induced fibrillation more than the particle sizes. In Figure 2.7, authors presented the artistic rendering of amyloid protein fibrillation in the presence of nanoparticles emphasizing the role of nanoparticles in increasing risk of amyloidosis and other protein-misfolding diseases [99–101].

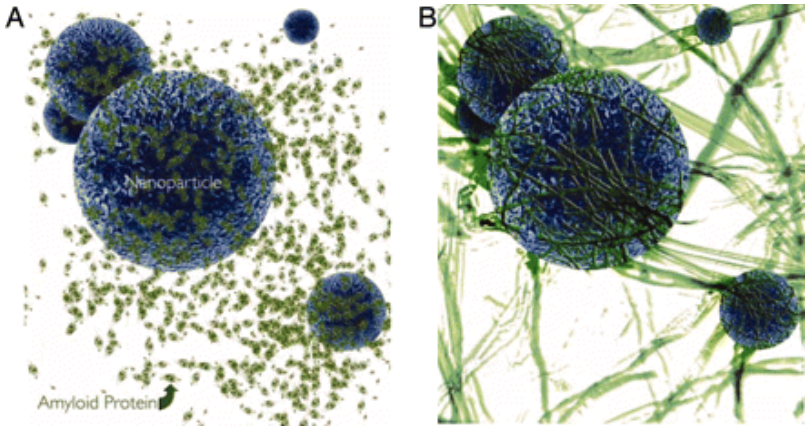

Figure 2.7. **(A)** Depicted here are large NPs (blue) and an amyloid protein (green) in its monomeric and folded state. **(B)** This artistic rendering shows the association of the amyloid protein with the NP surfaces, perhaps with the generation of small oligomers, which are the precursors to fibrils. In solution, larger protein fibrils appear as the surface association of proteins enhances their growth. Adapted from reference[101]. Reprinted with permission from PNAS.

2.2.2 Targeting

The further development of the concept of multifunctional nanocarrier involves the attempt to add the specific target recognition functionality to the long-circulated nanocarrier. As noted above, most existing anticancer therapeutic agents do not differentiate between cancerous and normal cells, leading to systemic toxicity and adverse effects. Severe side effects in bone marrow suspension; cardiomyopathy and neurotoxicity greatly limit the maximal allowable dose of drug. Nanotechnology offers great-targeted approaches that can provide significant benefits for cancer therapy. There are two main targeting strategies for nano-scale drug delivery systems, including passive targeting and active targeting [2,4,102].

The selective targeting based on permeability of the delivery system into tumor vasculature is considered to be a ‘passive targeting’. When tumor cells are growing, rapid vascularization occurs around cancerous cells to nourish growing tumors with oxygen and nutrients. This leads to leaky, defective architecture and impaired lymphatic drainage, which leads to the EPR effect and results in accumulation of nanoparticles at the tumor site. To pursue the passive targeting, the size and surface properties of drug delivery system should be controlled. The optimal size should not be less than 100 nm in diameter and the surface should be hydrophilic to avoid clearance by macrophages. EPR effect can exploit through surface modification of the nanocarriers. The anatomical factors responsible for EPR effect of macromolecules in solid tumors are extensive angiogenesis with high vascular density,

leaky vasculatures due to lack of smooth muscles, lymphatic clearance and slow venous return that promote retention and accumulation of macromolecules in the interstitium [5].

An ‘active targeting’, achieved by conjugating nanoparticles with a targeting motif, provides a specific binding and subsequent accumulation of nanoparticle at the tumor site or intracellular organelles of cancer cells [2]. Figure 2.8 offers a schematic presentation of the combination of passive and active targeting.

The active targeting agents are generally classified as proteins (mainly antibodies and their fragments [103–106]), nucleic acids (aptamers [107]), and other receptor ligands (peptides [21,108], vitamins and carbohydrates [109]). Monoclonal antibodies (mAb) are the conventional targeting conjugates for cancerous cells, approved by the FDA, but have two main limitations in their application: their large size and non-specific binding to the reticuloendothelial system (RES) [21]. Peptides present excellent alternatives to antibodies for cancer targeting due to their small size and lack of uptake by RES, high specificity to target cells, flexibility in design, synthesis and screening. Cell-targeting peptides (CTPs) are short sequences, usually composed of three to ten amino acids, which can interact and bind to a specific over-expressed receptor on the targeted cell line with high affinity and specificity [110,111]. This feature of CTPs enables them to be applied as a targeting agent in nanocarrier complexes to promote their selective uptake for therapeutic or imaging purposes. In addition to the cell surface targeting peptides, significant numbers of other peptides with an ability to target tumor vasculatures have already been identified [112,113]. It is suspected that free peptides are cleared very rapidly, whereas the conjugated peptides have a longer circulation lifetime. There are many examples using cell-targeting peptides for delivery *in vitro* and *in vivo,* including liposome [114,115], polymer nanoparticles [116–118], and albumin [119].

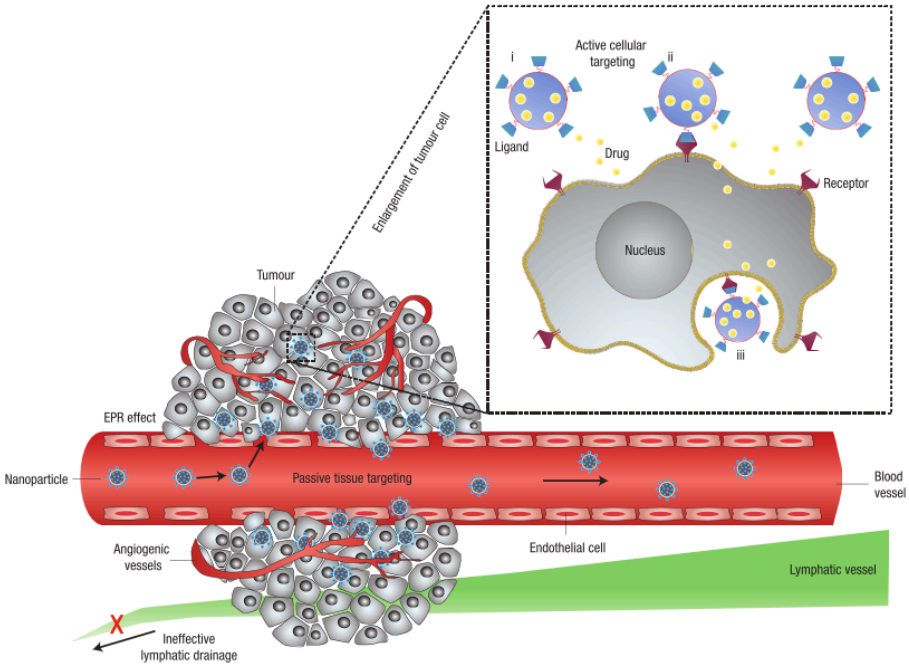

Figure 2.8. Schematic representation of different mechanisms by which nanocarriers can deliver to tumors. Polymeric nanoparticles are shown as representative nanocarriers (circles). Passive tissue targeting is achieved by extravasation of nanoparticles through increased permeability of the tumour vasculature and ineffective lymphatic drainage (EPR effect). Active cellular targeting (inset) can be achieved by functionalizing the surface of nanoparticles with ligands that promote cell-specific recognition and binding. The nanoparticles can (i) release their contents in close proximity to the target cells; (ii) attach to the membrane of the cell and act as an extracellular sustained-release drug depot; or (iii) internalize into the cell. Adapted from reference [2]. Reprinted with permission from Nature Nanotechnology.

2.2.3 Stimuli-responsive

The stability of a PEGylated nanocarrier does not always benefit a drug delivery system. The drug entrapped in a nanocarrier should be specifically released into the tumor avoiding normal cells. Therefore, an additional functional group, allowing detachment of PEGs when exposed to certain local stimuli in a pathological condition, can be utilized in a multifunctional nanocarrier. One of such stimuli is lower pH that has been noticed in inflamed and tumor areas. Releasable PEGylation (rPEG) has been developed chemically to tether drug and controls its release in low pH environments. The most frequently employed chemical bonds for this purpose are esters, carbonates, carbamates, hydrazones or amides [86]. Figure 2.9 illustrates the schematic of “smart” pH-sensitive immune-liposome and its function in tumor site, in which in low pH area the protective PEG is “de-shielding” and cell-penetrating function enables carrier penetration of tumor cells [1,120]. Other stimulus

conditions playing role in drug or gene delivery are redox potential, temperature, magnetic fields and ultrasound. Change in temperature can present both internal and external stimuli factor for drug release. Hyperthermia, usually associated with inflammation, is considered an internal effect of temperature. Therefore high temperature can be locally applied on target tissue allowing nanoparticle to release the therapeutic agent [121–123]. Magnetic field of different gradient applied to the body can concentrate magneto-sensitive DDS in target area [124].

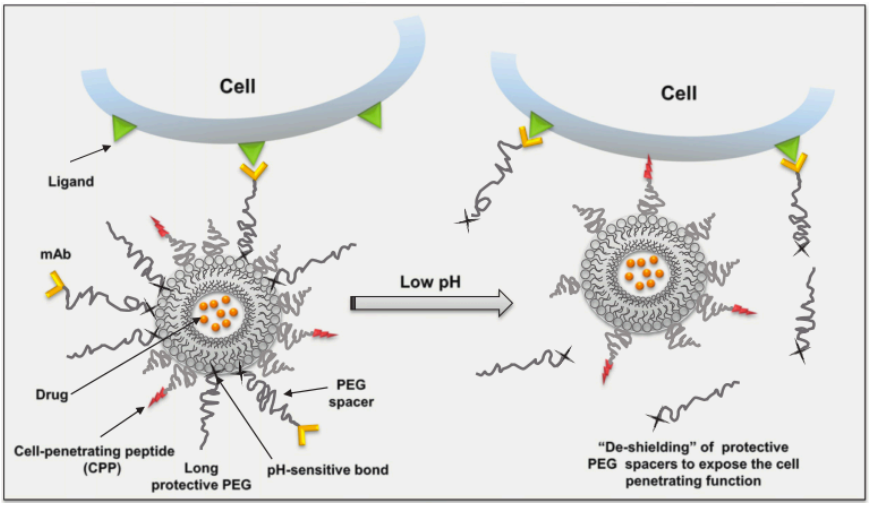

Figure 2.9. Schematic presentation of "smart" stimulus-sensitive long-circulating immunoliposome. Adapted from reference [1]. Reprinted with permission from Elsevier.

2.3 Self-Assembling Peptides: Emerging Biological Nanomaterial

Molecular self-assembly by the definition is spontaneous association of molecules under thermodynamic equilibrium conditions into stable and ordered structures due to the formation of non-covalent interactions [125]. In the past two decades, self-assembling peptide nanostructures have been advanced tremendously in generation of new nanomaterials and nanodevices. The origin of self-assembling peptide research is attributed to Shuguang Zhang *et al.* in 1992 by discovering a 16-residue peptide EAK16-II in a region of alternating hydrophobic and hydrophilic residues in Zuotin, a yeast protein [126]. EAK16 spontaneously forms to β-sheet structure due to hydrophobic alanine side chains on one side and ionic-complementary pairs of positively charged lysine and negatively charged glutamic acid side chains on the other surface. This structure is unusually stable in extreme conditions such as high temperatures, various pH changes, denaturation reagents such as SDS, guanidine. HCl

and urea [127]. A number of self-assembling peptides have been systematically designed and developed inspired by EAK16 self-assembly properties. So far, self-assembling peptide have been categorized into three distinct types applicable for various applications including scaffolding for tissue repair, tissue engineering, drug delivery, molecular medicine, and nanofabrication.

2.3.1 Type I Self-assembling Peptides- Molecular Lego

The first category of self-assembling peptides consists of the peptides with block structure and distinct hydrophilic and hydrophobic surfaces. Because of this amiphilicity they form β-sheet structures in aqueous solution and similar to Lego components the pegs and holes complement each other on the hydrophilic surface. The hydrophilic surface contains complementary ions in different patterns. For example modulus I have alternating negative and positive charge (- + - + - + - +), modulus II has - - + + - - + +, and modulus IV has - - - - + + + + charge distribution pattern [125,128]. EAK16-II, EAK16-IV, DAR16-IV, RAD16-I, RAD16-II, *etc.* are examples of Type I self-assembling peptides that have been studied and developed as matrices for mammalian cell attachment and drug delivery purposes [129–132].

Zhang *et al.* have proposed the class of complementary ionic pairing peptides that undergo spontaneous assembly in physiological conditions to form microscopic and macroscopic structures into different geometric shapes. The alternative charge distribution play the important role in β-sheet self-assembling process, *i.e.* substituting positive charge Lys by positive charge Arg and the negative charge Glu with Asp does not change the self-assembly process drastically. However, if the positive charge residues are replaced by negative charge residue the peptide can no longer undergo self-assembly process or form β-sheet structures in physiological solutions. In addition, if more hydrophobic residues such as Leu, Ile, Phe or Tyr replace the alanine residues, tendency of the molecules to self-associate to form matrices will enhance.

RAD16 and EAK16 were tested extensively for cell attachment and scaffold applications. A stable attachment of a number of mammalian cell types such as mouse fibroblast (NIH-3T3), human cervical carcinoma (HeLa), rat neuronal cells (PC12), human ovary carcinoma (OVAR-5), *etc.*, with the peptide materials have been observed [129,130]. The presence of 50% charged residues and β-sheet structures of these peptides facilitates the formation of a hydrogel scaffold as a template for cell proliferation. RAD16-I has been commercialized with a trade name of PuraMaterix^{TM} by 3DM Inc. (Cambridge, MA, USA) for tissue cells encapsulation and growth in three-dimensional peptide scaffold and exhibited significant cellular behaviors such as proliferation, functional differentiation,

active migration, and extensive production of extracellular matrices (ECM). One of the advances of PuraMatrix^{TM} involved extensive neurite outgrowth and active synapse formation [130,133]. Advantages associated with these peptides are negligible immune response and tissue inflammation when introduced into animals. Exploiting their biocompatibility and self-assembly properties, application of these peptides in animal models for hemostasis [134], bone and cartilage regeneration [135], cardiovascular [136], and neurosurgical [137] are under extensive research. The Type I self-assembling peptides also showed a great potential in drug and gene delivery systems that will be discussed in detail in the following sections.

2.3.2 Type II Self-assembling Peptides- Molecular Switches

There are several peptides that have shown drastic changes in molecular structure at different pH and temperature conditions. EAK12 and DAR16-IV are the examples of molecular switch peptides. At room temperature DAR16-IV has a β-sheet structure with 5 nm in length, however, at high temperature peptide goes under transition to form α-helical structure with 10 nm in length. EAK12 can go under three distinct conformational states at various pH. β-sheet structure is the dominant secondary structure of EAK12 in pH 1-3, and at pH 4 the β-sheet content is reduced and backbone conformation is changed. At pH 5 and over the transition to α-helix is noticeable, where in pH between 6 and 10 a stable α-helix conformation forms [128].

2.3.3 Type III Self-assembling Peptides- Molecular Paint

Type III peptides self-assemble on the surface and form monolayers for specific surface interactions or binding. These peptides are known for their unique features; the first feature is the functional group at the terminal segment for recognition by other molecules, receptors, or cells. The second feature is the central linker, which provides rigidity and flexibility. The third feature is the surface anchor, which facilitates the covalent bond between the peptide and the surface. This surface functional peptide series were mainly designed to study cell-to-cell communication, and cell behavior [125].

S. Zhang *et al.* have developed a biologically active surface using two oligopeptides including a cell adhesion segment $(RADS)_n$ (n= 2 or 3) at the N-terminus, connected to oligo(alanine) linker and a cysteine residue at the C-terminus as an anchor to attach the peptide covalently onto gold-coated surfaces and forming a monolayer. RADSC-14 and RADSC-16 with sequences of (RADSRADAAAAAAC, and RADSRADSRADSAAAC) are the two examples used in their study. They fabricated a variety of surfaces and formed patterns that areas either supporting or inhibiting cell

adhesion. These engineered surfaces were mainly capable of aligning cells in a well-defined pattern, leading to formation of the cell array for biomedical applications [138].

2.3.4 Type IV Self-assembling Peptides- Surfactant-like

Surfactant-like peptides are known for the formation of either nanotube or nano-vesicle structures through hydrophilic head and hydrophobic tail. Developments of these structures have significant consequences in design of non-lipid biological surfactants to provide an enclosure for the RNA-based or peptide enzymes. The basic molecular structure of these surfactant-like peptides is hydrophilic head containing aspartic acid and hydrophobic tail containing one of the amino acids such as glycine, alanine, valine or leucine. Each peptide is approximately 2 nm long, similar to the biological phospholipids. There is a packing difference between lipids and peptides due to the intermolecular hydrogen bonds along the backbone among amino acids in peptide sequence. Whereas, in lipid structures the hydrophobic tails pack tightly to fully displace water, preventing the formation of hydrogen bonds. The examples of Type IV self-assembling peptides are G_xD_2 (x= 4 to 10), A_6D, V_6D, V_6D_2, and L_6D_2, *etc*. These peptides are self-assembled into a fibular dense network with several microns in length. In the proposed molecular models, hydrophobic tails (e.g. glycine) are hidden from the aqueous environment and hydrophilic heads expose to the aqueous environment in both interior and exterior surfaces forming the bilayer structure in the shape of nanotube or nano-vesicle [125,139,140].

2.3.5 Other Self-assembling Peptides

The other self-assembling peptides in biological applications are peptide-amphiphile nanofibers for resembling extracellular matrix (ECM), cell-penetrating peptides for delivering nucleic acids and therapeutics facilitating membrane trafficking applications. Hartgerink *et al.* first introduced a self-assembling peptide-amphiphile mineralized with five distinct regions including (1) alkyl chain (hydrophobic tail), (2) four consecutive cysteine residues (disulfide bonds promote polymerization), (3) three glycine residues (hydrophilic head), (4) phosphorylated serine residue (calcium ion interaction), and (5) RGD peptide (cell adhesion ligand) [141]. Cell-penetrating peptides (CPP) and peptide transduction domains (PTD) are also very well known for enhancing translocation of therapeutics into cells. These peptides are conjugated to the delivery systems and so far they have shown safety features, efficient transit *in vivo*, no size constrains on cargo, biodegradable, and non-immunogenicity. There are several examples of PTD and CPP motifs such as TAT, ANTp, NLS, RGD, and *etc.* [20,142,143].

(A) Molecular Lego

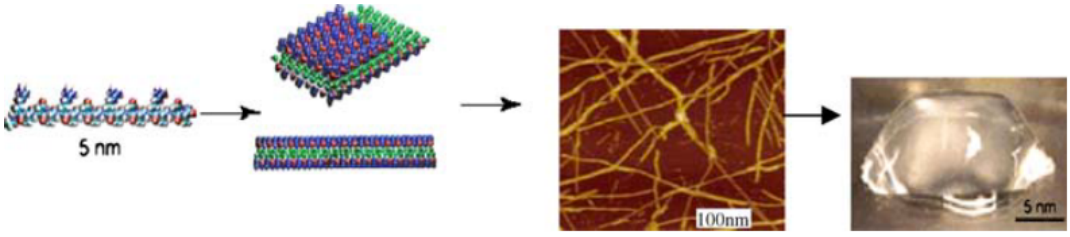

(B) Molecular Switch

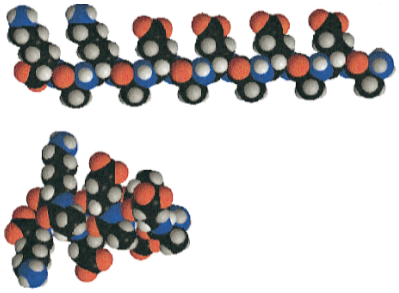

(C) Molecular Paint

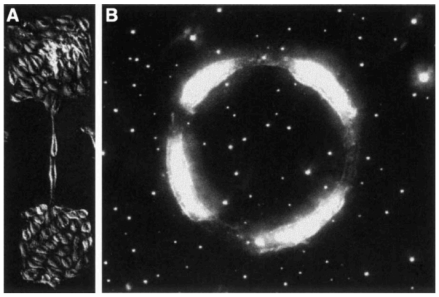

(D) Surfactant-Like

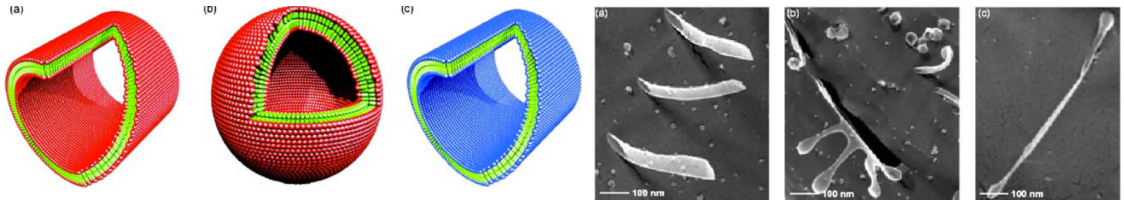

Figure 2.10. **(A)** Molecular Lego – Ionic complementary peptide with alternating polar and non-polar pattern self-assemble into β-sheet structure forming scaffold hydrogel, **(B)** Molecular switch – conformational change of self-assembling peptide from β-sheets to α-helix structure exposing different pH or temperature, **(C)** Molecular paint – Endothelial cells formed a pattern assisted by self-assembling peptide, **(D)** Surfactant-like - Molecular models of surfactant peptides V6D and K2V6 forming nanotubes and nano-vesicles. Adapted from references [125,144].

2.4 Self-assembling Peptides as Potential Carriers for Anticancer Drug Delivery

Over the past two decades, a new class of self-assembling peptides such as ionic-complementary, amphiphilic peptides and recently amino acid paring peptides has been systematically studied for different applications including drug, gene delivery, and tissue engineering [24,126,129,145,146].

Amongst many emerging drug carriers, peptides carry a great potential in overcoming many challenges in delivery and increasing drug biocompatibility, efficiency, and potency to conjugate with targeting and long circulating moieties. The natural properties of peptides, such as ability to penetrate cells, targeting, and therapeutic characteristics make them attractive candidates for drug delivery systems. Research on peptide-mediated delivery systems has shown very promising capabilities to deliver therapeutic agents such as hydrophobic anticancer drugs, small molecules, and oligonucleotides [24,147]. Self-assembling peptides can be rationally manipulated to form a variety of stable nanostructures, such as fibers [148,149], nanorods [150] , nanotubes [151] , nano-vesicles [140] and globules [152], as well as incorporate naturally binding motifs with an affinity to inorganic materials. Various interactions are involved in peptide formation, including hydrogen bonding, ionic interaction, van der Waals and hydrophobic interactions. Based on the application, in fact, millions of peptides with a desirable structure and function can be constructed [153].

As discussed above, Zhang *et al*. and Chen *et al*. have extensively studied the self-assembling ionic-complementary peptide, EAK16-II, for various applications including drug delivery [25,126,146,154]. EAK16-II has sixteen amino acids creating both hydrophobic and hydrophilic side, the negative and positive charges also altered along the sequence (Figure 2.11). This peptide can spontaneously organize itself into a β-sheet structure by electrostatic interaction between ionic-complementary residues. Fung *et al.* investigated the capability of the self-assembling peptide EAK16-II to deliver a hydrophobic anticancer drug. They discovered that the EAK16-II peptide could stabilize the hydrophobic compound, Ellipticine, in an aqueous solution. They also showed that the molecular state of Ellipticine (protonated or crystalline) in solution is EAK16-II concentration dependent. As a consequence, the release kinetics of ellipticine from a peptide-ellipticine complex into eggphosphatidylcholine (EPC) vesicles, which are used as a cell membrane mimic, depends significantly on concentration and as a result on molecular state of Ellipticine. In addition, the *in vitro* anticancer activity results of peptide-Ellipticine complexes towards two cancer cell lines, A549 and MCF-7 suggested a promising potential of EAK16-II as a carrier for a hydrophobic compounds [24,146]. Their study has initiated the future development of self-assembling peptide-based delivery of chemotherapeutics.

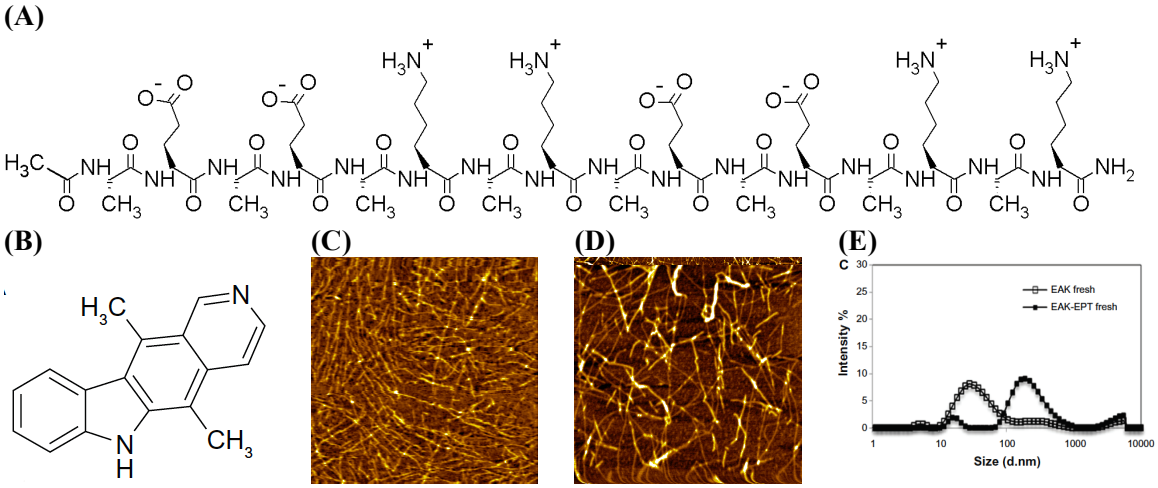

Figure 2.11. Molecular structure **(A)** of EAK16-II (Ac-AEAEAKAKAEAEAKAK-NH_s), **(B)** Ellipticine, Nanostructure of **(C)** EAK16-II, and **(D)** EAK16-II-EPT complex on mica surface observed by AFM. **(E)** Particle size distribution of EAK16-II and the EAK-EPT complex in aqueous solution by DLS. Adapted from reference [25].

Recent advances* in EAK16-based anticancer drug delivery system illustrated a successful delivery of the ellipticine to the tumor site *in vivo*. In summary cellular uptake, toxicity, and apoptosis results in an A549 human lung carcinoma cell line indicate that EAK16-II-EPT complexes were significantly more effective than treatment with EAK16-II or ellipticine alone. This is due to the ability of EAK16-II to stabilize ellipticine in a protonated state in well-formed nanostructures approximately 200 nm in size. *In vivo* observations in an A549 nude mouse tumor model showed a higher antitumor activity and lower cytotoxicity of EAK16-II-EPT complexes than in the control group treated with ellipticine alone after 14 days intraperitoneal (i.p) injection (Figure 2.12). Tumor growth in animals was significantly inhibited after treatment with EAK16-II-EPT complexes, and without any significant side effects such as weight loss [25].

* This study was based on my collaborative research with Dr. Yong-fang Yuan at People's Hospital affiliated to Shanghai Jiao Tong University and published as "Sadatmousavi, P.; Wu, Y.; Wang R.; Lu, S.; Yuan, Y.; Chen, P. "Self-assembly Peptide-based Nanoparticles Enhance Anticancer Effect of Ellipticine *in vitro* and *in vivo*", International Journal of Nanomedicine, 2012:7 3221-3233"

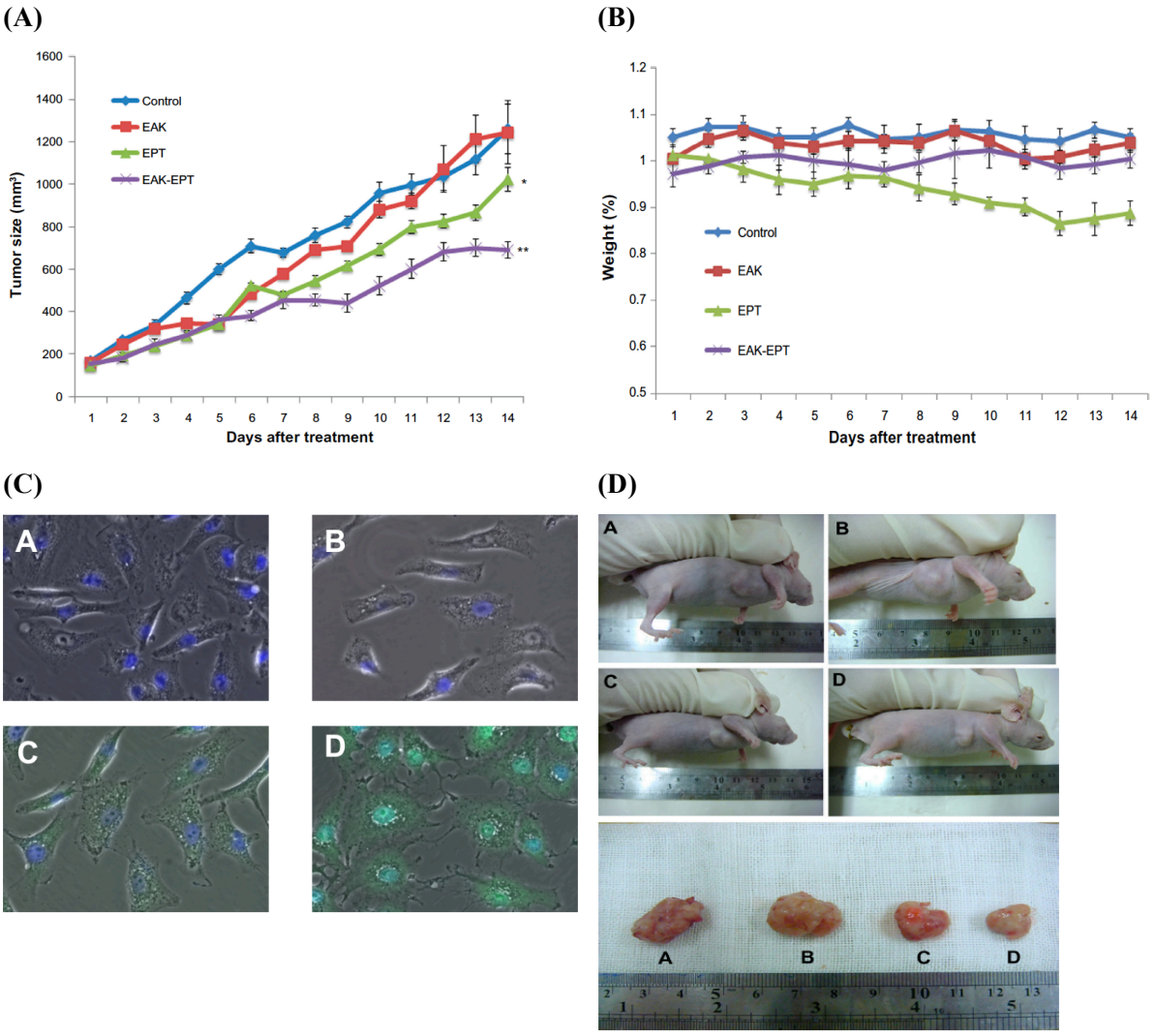

Figure 2.12. **(A)** Size of tumors in the four groups after treatment with 11.25 mg/kg EPT and 22.5 mg/kg EAK16-II in complex once a day for a total 14 days. **(B)** Mouse body weight in four groups during 14 days, **(C)** *in vitro* cellular uptake of EPT by A549 cells, overlap (DAPI and green) images for A-Untreated, B- EAK16-II control, C- EPT control, D-EAK16-II-EPT complex. High uptake of EPT in complex treated cells where cyan color visible for D. **(D)** Representative example of tumors from four groups after treatment on day 14. A-D represents the same ordered treatment as (C). Adapted from reference [25].

2.4.1 Amino Acid Pairing Design for Self-assembling Peptides

A novel strategy to design self-assembling peptides called "amino acid pairing" (AAP) strategy has been patented and developed in Dr. Chen's research group in 2010-11 [155]. The amino acid side

chains of self- assembling peptide can provide major interactions with adjacent peptide molecules including ionic interaction, hydrogen bonding, and hydrophobic interaction. AAP-based peptide design provides complementary interactions that achieve certain stereo-chemical and physicochemical stability, resulting in pair affinity and minimum pairing free energy. Figure 2.13 shows an AAP strategy for designing different self-assembling peptide systems. The ionic-complementary peptides are characterized by alternating positively and negatively charged residues; hydrogen bonding peptides are characterized by alternating hydrogen bonding pairs consisting of proton donors and acceptors; and all pairing in a peptide contains all of hydrogen bonding, electrostatic, and hydrophobic bonding amino acid pairs [26,155] .

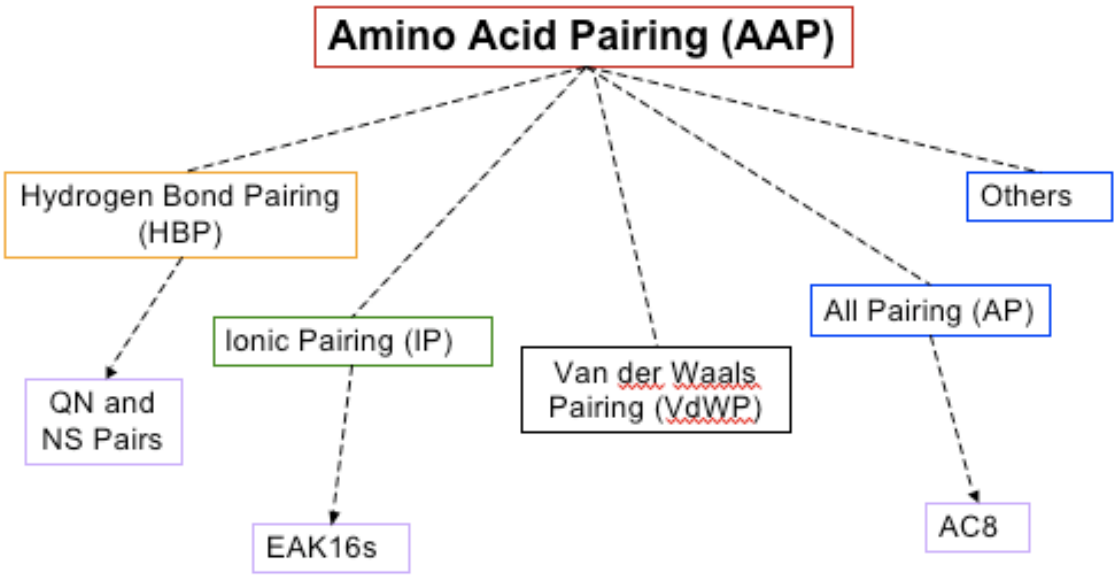

Figure 2.13. Amino acid pairing strategy [155].

The *de novo* all pairing peptide (APP8) was designed recently based on amino acid pairing strategy. This peptide contains eight amino acids including four hydrophobic phenylalanine (F) side chains, which are inserted among hydrogen bonding pair (QN) and an ionic pair (EK) with the side-to-side amphiphilic design. The four (F) residues provide strong hydrophobic interactions utilized by aromatic ring stacking; they also impart hydrophobic region that can stabilize hydrophobic compounds for drug delivery purposes. The ionic pair (EK) and hydrogen bonding pair (QN) expected to enhance solubility and stability of self-assembly structure of the peptide. The former two pairs (QN) and (EK) increase overall hydrophilicity to be in balance with hydrophobic residues (F) to

provide good solubility in water. It has been shown previously the dominant β-sheet rich nanofibers by FT-IR for this peptide (Figure 2.14).

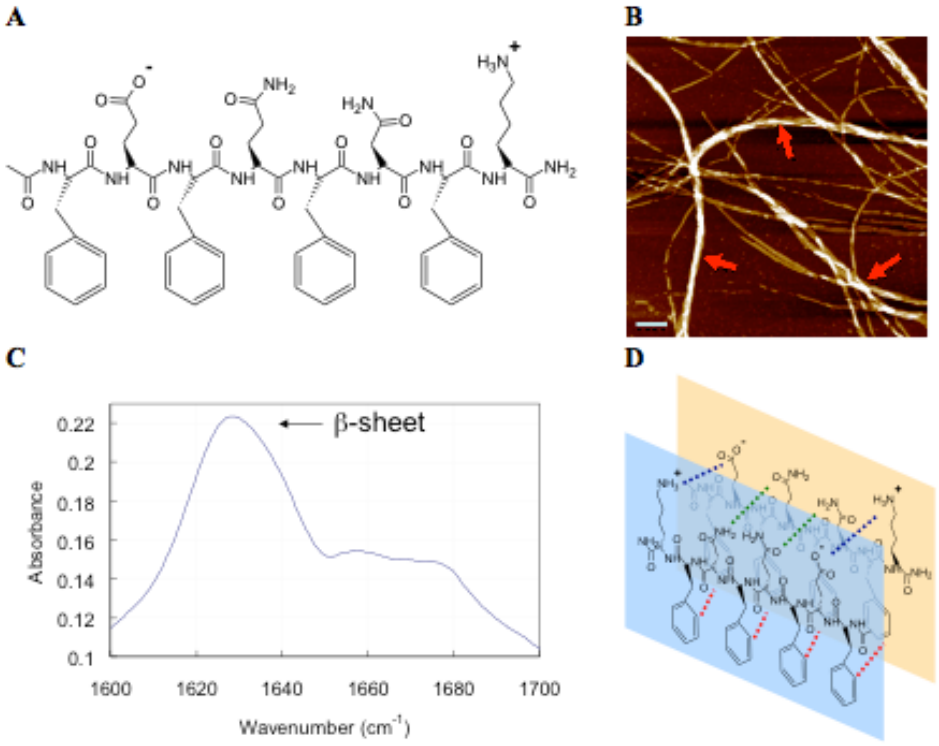

Figure 2.14. De novo design of the all-pairing peptide APP8 and the self-assembly. **(A)** Molecular structure of APP8. **(B)** APP8 can self-assemble into nanofibers at a peptide concentration of 0.1 mg ml^{-1} (87 μM); the scale bar represents 200 nm. **(C)** AAP8 has a predominant secondary structure of β-sheets by FT-IR. **(D)** A proposed model shows that AAP8 forms anti-parallel β-sheets with the assistance of amino acid pairing: red, blue and green dotted lines represent hydrophobic amino acid pairing (π-π stacking), ionic pairing and hydrogen bond pairing, respectively. Adapted from reference [26]. Reprinted with permission from Rights Link.

The nano-structure assembly of APP8 peptide is concentration dependent as shown in Figure 2.15. Critical assembly concentration (CAC) of this peptide is 10 μM, in which the bundles of fibers form beyond this concentration. APP8 peptide has shown capability for encapsulating hydrophobic compound and stabilizing it in aqueous solution and the peptide-drug complexes exhibited good anticancer activity against two cancer cell lines, A549 and MCF-7, and were stable upon serial dilution in water [26].

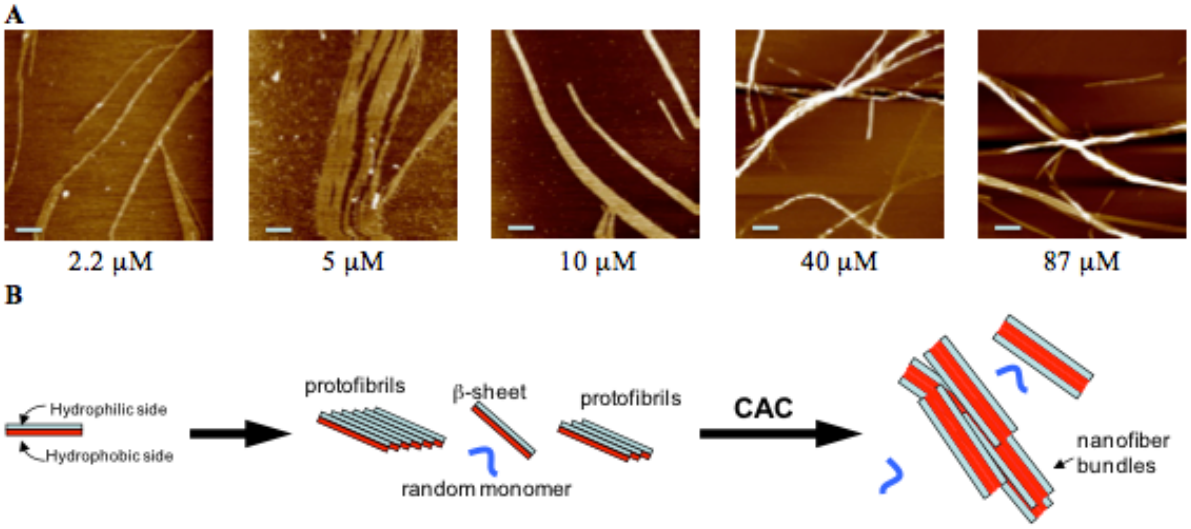

Figure 2.15. Nanostructure formation of APP8 in relation to the "CAC". **(A)** AFM images of the self-assembled nanostructures as a function of APP8 concentration (2.2–87 μM). The scale bar represents 250 nm. **(B)** A proposed self-assembly mechanism in relation to the "CAC". Adapted from reference [26]. Reprinted with permission from Rights Link.

The current research is focusing on the self-assembling peptides and their modifications to improve their functionalities towards longevity and low immunogenicity. The details of modifications are discussed in the following chapters. First, all pairing peptide (APP8) also called amino acid pairing peptide (AAP8) was modified with a short segment of polyethylene glycol to enhance stability, avoid uncontrollable aggregations and lower immune responses. Second, a short ionic-complementary peptide (EAR8-II) was employed as a carrier for anticancer drug, Pirarubicin, where the protein binding strategy was used to advance the delivery efficiency and hinder phagocytosis.

Chapter 3[†]

Diethylene Glycol (DEG) Functionalized Self-Assembling Peptide Nanofibers and their Hydrophobic Drug Delivery Potential

Abstract

Self-assembling peptide nanofibers have emerged as important nano-biomaterials, with such applications as delivery of therapeutic agents and vaccines, nanofabrication and biomineralization, tissue engineering and regenerative medicine. Recently, a new class of self-assembling peptides has been introduced, which considers amino acid pairing (AAP) strategies in the peptide sequence design. Even though these peptides have shown promising potential in the design of novel functional biomaterials, they have a propensity to initiate uncontrollable aggregations and be degraded by proteolytic enzymes. These present the most significant challenge in advancing self-assembling peptides for *in vitro* and *in vivo* applications. Functionalizing biomaterials with polyethylene glycol (PEG) has been shown to surmount such problems. Here, the results of conjugating diethylene glycol (DEG), a short segment of PEG, to one of the AAP peptides, AAP8, with eight amino acids in sequence, are reported. The results indicate that incorporation of DEG into the peptide sequence modulates fiber self-assembly through creating more aligned and uniform nanostructures. This is associated with increasing solubility, stability, and β-sheet content in secondary structure in the peptide. The DEG conjugation of AAP8 also shows reduced cellular cytotoxicity. The functionalized AAP8 improves the peptide capability of stabilizing and delivering a hydrophobic anticancer compound, ellipticine, in aqueous solution, consequently inducing more cytotoxicity towards lung carcinoma cells over a relatively long time, compared to the non-functionalized AAP8. The presented functionalized peptide and its drug delivery application indicate a potentially useful design strategy for novel self-assembling peptide biomaterials for biotechnology and nanomedicine.

Key Words

[†] This chapter is based on a paper " P. Sadatmousavi, T. Mamo, P. Chen, Diethylene Glycol (DEG) Functionalized Self-Assembling Peptide Nanofibers and their Hydrophobic Drug Delivery Potential, *Acta Biomaterialia* 8 (2012) 3241–3250".

Drug delivery, self-assembling peptide (SAP), amino acid pairing (AAP), Diethylene glycol (DEG), functionalization

3.1 Introduction

Self-assembling peptides are a class of biomaterials showing promising results for various biomedical applications, including delivery of therapeutic agents and vaccines, nanofabrication, biomineralization, tissue engineering, and regenerative medicine [17–19]. Recently, a new class of self-assembling peptides based on the design principle of amino acid pairing (AAP) has been introduced, with the model peptide AAP8 showing great promise in creating β-sheet-rich nanofibers, stabilizing and delivering a hydrophobic anticancer agent [156]. The design of AAP self-assembling peptides is unique as it is based on the combination of several side chain interactions, including hydrophobic interaction, electrostatic interaction, and hydrogen bonding. While these newly designed systems and other self-assembling peptides have shown immense potential, issues remain in optimizing the self-assembled structures and making them more robust for *in vivo* applications [79]. A major issue to be addressed in improving the self-assembled fibril nanostructures is avoiding the uncontrollable aggregation of the β-sheet structures while improving the fibers' capability to form predictable nanostructures [9,85]. The surface of the nanofibers must be modified for effective biomedical applications *in vivo*. To address these issues, conjugating the peptide units with a short segment of polyethylene glycol (PEG) polymer is here proposed.

Surface functionalization of nanoparticles (NPs) with polyethylene glycol, PEG, has become a standard strategy for increasing the NP circulation half-life in the bloodstream, as the functionalization reduces protein opsonization and macrophage uptake [78,79,157]. By reducing non-specific interactions with proteins through its hydrophilicity and steric repulsion effects, PEG results in long circulating drug delivery systems with reduced opsonization and complement activation [79]. PEG has been approved by the U.S. Food and Drug Administration (FDA) for clinical use due to its low toxicity and lack of immunogenicity. A number of clinically approved therapeutics rely on PEG for improved *in vivo* profiles, including liposomes (Doxil), PEG–drug conjugates (Oncaspar) and polymeric NPs (Genexol-PM) [80]. Various researchers have also shown the PEGylation effect on iron oxide nanoparticles for *in vivo* cancer imaging through the enhanced permeability and retention (EPR) effect [158]. Liu *et al*. reported properties of synthesized PEGylated nanoparticles with low cytotoxicity and high resistance to phagocytosis by macrophages *in vitro*, as well as low accumulation of them in liver and spleen *in vivo* biodistribution tests. These results make the nanoparticles highly preferable in tumor imaging. The authors claimed that these outstanding characteristics are dependent

on the significant shielding effect of PEG coating, providing neutral surface charge under physiological conditions [158].

The exceptional properties of PEG make this polymer a potential candidate for resolving issues involved in nanoparticle formation. Nanoparticles can have the problems of insolubility, toxicity, bio-incompatibility and a low circulation half-life in the bloodstream for *in vitro*, *in vivo*, and preclinical applications. The PEGylation of β-sheet forming self-assembling peptides has been studied since the first report by Lynn *et al.* on conjugation of PEG to the amyloid peptide (10-35 Aβ) [81,82]. This early work showed that PEGylation prevented lateral association of fibrils, inhibiting irreversible steps of fibrillogenesis. Elastin-like polypeptides based on $(VPGVG)_4$ and $(VPAVG)_4$ were also conjugated with PEG enhancing self-assembly properties [83]. Moreover, PEGylation of the GAGA peptide, which is based on Bombyx mori silk, enhanced the peptide self-assembly through formation of both parallel and anti-parallel β-sheets [84]. Another interesting work studied the effect of PEGylation on the Q11 self-assembling peptide through conjugation of different PEG chains at various points in the backbone of the peptide [85]. The work showed that PEG conjugation strongly prevented lateral aggregation of fibril-forming peptide, resulting in well-ordered peptide matrices.

In the current work, we focus on an amino acid pairing peptide, AAP8, with eight amino acids in its sequence. AAP8 contains four hydrophobic phenylalanine (F) side chains, a hydrogen bonding pair (QN), and an ionic pair (EK), in the sequence FEFQFNFK. This peptide previously showed great promise for various applications because of its unique self-assembly properties [156]. However, lack of solubility and the possibility of uncontrollable aggregation have led to formation of non-uniform nanostructures, making this peptide unsuitable for further applications. To overcome this issue and enhance nanostructure configuration, diethylene glycol (DEG), a short segment of a PEG chain, was conjugated to the model peptide AAP8. Since AAP8 is a short eight amino acid peptide, it is hypothesized that conjugating a shorter segment of a PEG molecule should be enough to obtain the desired effects. We believe that the longer the PEG chain, the more likely it interferes with the self-assembly of the peptide. To investigate the various configurations of DEG conjugation, AAP8 was conjugated with DEG on one or both terminals of the molecule, forming AAP8-DEG and DEG-AAP8-DEG. We utilized spectroscopy and microscopy techniques to determine the effect of DEG conjugation on peptide self-assembly, the β-sheet content in secondary structure, and the formation of peptide nanostructures. To further investigate the drug delivery potential of the modified AAP8 with diethylene glycol, we used an anticancer agent, ellipticine (EPT), as the model hydrophobic drug. Non-small cell lung carcinoma (A549) were used to evaluate anticancer activity of ellipticine

encapsulated with either AAP8 or modified AAP8s. In addition, the effect of DEG-conjugated on macrophage (RAW 264.7) cytotoxicity as one of the innate immune responses was evaluated.

3.2 Experimental

3.2.1 Materials

The peptide AAP8 (Ac-FEFQFNFK-NH_2) and the two diethylene glycol (DEG) (-NH-CH_2-CH_2-O-CH_2-CH_2-O-CH_2-CO-) conjugated amino acid pairing (AAP8) peptides: Ac-FEFQFNFK-DEG-NH_2 and Ac-DEG-FEFQFNFK-DEG-NH_2 were purchased from CanPeptide Inc (Quebec, Canada). The synthesis method for all three peptides was based on solid-phase peptide synthesis (SPPS). The diethylene glycol was treated as one of the amino acids in the synthesis of the whole sequence. Matrix-assisted laser desorption ionization time-of-flight mass spectroscopy (MALDI-TOF-MS) showed the molecular weight of 1147.31 g/mol for AAP8, 1293 g/mol for Ac-AAP8-DEG-NH2, and 1437 g/mol for Ac-DEG-AAP8-DEG-NH2. The purity of peptides were verified by CanPeptide as >95% by LC-MS characterization. The peptide aqueous solutions were prepared with pure water (Milli-Q: 18.2 MΩ). The anticancer agent ellipticine (99.8% pure) and fluorescence marker, 1-anilino-8-Naphthalene Sulfonate (ANS, > 97%), were purchased from Sigma-Aldrich (Oakville, ON, Canada). Cell culture agents, including Dulbecco's modified eagle medium (DMEM) low glucose, and phosphate buffer saline (PBS) were purchased from HyClone (Ontario, Canada). Fetal bovine serum (FBS) and trypsin-EDTA were purchased from Invitrogen Canada Inc. (Burlington, ON, Canada). A free comprehensive chemical drawing package, ACD/ ChemSketch Freeware (Toronto, Canada) was used to draw chemical structure of peptide molecules. This software optimizes all bond lengths and angles based on energy minimization.

3.2.2 Methods

3.2.2.1 Peptide Solution Preparation

Solutions of the APP8 peptide and DEG-conjugated AAP8 peptides were prepared by dissolving the peptide powder in pure water (18.2 MΩ; Millipore, Milli-Q system) at specified concentrations following by 10 min bath sonication for various experiments: including nanostructure visualization through Atomic Force Microscopy (AFM), hydrophobicity test by fluorescence spectroscopy, secondary structure evaluation and anticancer activity tests *in vitro* when peptides are in combine with anticancer drug.

3.2.2.2 Atomic Force Microscopy (AFM)

The self-assembled peptide nanostructures were imaged by atomic force microscopy (AFM) (PicoScan, Molecular Imaging, Phoenix, AZ) on a mica substrate. The samples were prepared with the following procedure: a 10 μL sample of the peptide solution (15 min after preparation) was put on the freshly cleaved mica substrate that was fixed on an AFM sample plate. The solution was incubated on the mica surface for 10 min, to allow the peptide nanostructures to adhere to the surface, and then rinsed with water twice. The extra water (moisture) on the surface was collected with tissue paper. The sample plate was then covered with a petri-dish to avoid possible contamination and left to dry overnight. AFM images were taken at room temperature using the AFM tapping mode. All images were acquired using 225 μm silicon single-crystal cantilever (type NCL-16, Molecular Imaging, AZ) with a typical tip radius of 10 nm and frequency of 175 kHz. A scanner with a maximum scan size of 6×6 μm^2 was used [152]. Data sets were subjected to third-order flattening. The AFM images underwent further dimension analysis with Gwyddion software (Free SPM data analysis software).

3.2.2.3 Steady-state Fluorescence Measurements

The hydrophobicity of the peptide assemblies was investigated through an ANS fluorescent probe. ANS (1-anilino-8-Naphthalene Sulfonate) with a molecular weight of 299.3 g/mol was the fluorescence label used to characterize the hydrophobicity of the prepared AAP8 assemblies. ANS is a fluorescent dye that binds with high affinity to the hydrophobic surfaces of protein assemblies. The emission maximum of ANS undergoes a blue shift, and fluorescence intensity increases significantly upon ANS binding to low polarity regions of the protein surface. These properties make ANS well suited for determining the hydrophobicity of peptide nanostructures. ANS can be excited at 360 nm in pure water and emits light at 520 nm; whereas, in hydrophobic solution, the emission wavelength moves toward a lower value. A solution of 10 μM ANS was prepared in a 10 mM phosphate buffer at a pH of 6. The fresh peptide solution was mixed with the same volume of ANS solution on a vortex mixer for 10 sec. The spectrofluorometer used in this study was type LS-100 (Photon Technology International, London, ON, Canada). The light source used was a pulsed xenon flash lamp. For solution samples, spectra were obtained using a quartz cell (1 cm × 1 cm). The ANS-containing samples were excited at 360 nm, and emission spectra were collected from 420 nm to 670 nm. The excitation and emission slit widths were set at 0.5 mm and 1.25 mm, respectively [147].

3.2.2.4 Fourier Transform Infrared (FT-IR) Spectroscopy

The secondary structure of the peptides was determined with Fourier transform infrared (FT-IR) spectroscopy (TENSOR 37, Bruker Optics Ltd, ON, Canada), with a Bio-ATR II cell. A 30 µL of sample solution was injected into an ATR-crystal (silicon) chamber. The scan ran wavenumber of 1550-1700 cm^{-1} for the 256 runs for each measurement. The obtained spectra were analyzed using OPUS software (version 6.5, Bruker Optics Ltd., ON, Canada).

3.2.2.5 Circular Dischroism (CD) Spectroscopy

The secondary structures of the peptides were evaluated using another standard method, which involves a Circular Dischroism (CD) spectrometer (J-815, JACSO Inc., Easton, MD). A 150 µL of the sample solution at a concentration of 0.5 mg/ml was transferred to a quartz cuvette with a path length of 1mm for each measurement. CD spectra were collected in a continuous scanning method from 190 to 260 nm at a scanning speed of 50 nm/min. Data were analyzed with JACSO software (J-810).

3.2.2.6 Dynamic Light Scattering (DLS)

The particle size distribution and zeta potential of peptide-drug complexes at different peptide-to-drug ratios were measured by a Zetasizer Nano ZS (Malvern Instruments, Worcestershire, UK). Appropriate settings, viscosity, refractive index, and dispersant solvent were set for each measurement at 25 °C. A small 50 µL volume of the sample was transferred from the vial to a disposable solvent resistant micro cuvette (ZEN0040, Malvern, Worcestershire, UK). The scattered light intensities of the samples were collected at an angle of 173°. This was known as backscatter detection, *i.e.*, the relationship between the size of a particle and its scattered light intensity obtained with the multimodal Contin algorithm, which was provided in the Dispersion Technology Software 5.1 package (Malvern Instruments, Worcestershire, UK).

The zeta potential of the complexes was investigated on a Zetasizer Nano ZS (Malvern Instruments Worcestershire, U.K.) with suitable viscosity and refractive index setting at 25°C temperature. Samples were injected into a disposable cell (folded capillary DTS-1060 from Malvern, Worcestershire, U.K.) with a volume of ~ 1ml for zeta potential measurements. The zeta potential distribution was directly calculated from electrophoretic mobility distribution based on Smoluchowski formula. For each solution, the measurements were repeated three times. The values reported herein correspond to average of the peak values of the zeta potential distribution from the triplicates.

3.2.2.7 Peptide and Ellipticine Complex Preparation

The complexes were made of ellipticine (0.1 mg/ml, 406 μM) with freshly prepared 0.5 mg/ml peptides: AAP8 (435 μM), AAP8-DEG (386 μM), and DEG-AAP8-DEG (347 μM). Ellipticine (1 mg/ml) crystals were dissolved in tetrahydrofuran (THF); aliquots of ellipticine-THF were transferred to a 1.5 ml centrifuge tube and dried under blowing air. A fresh peptide solution was then added to the tube, followed by continuous probe sonication for at 6 W-power for 10 minutes. An ellipticine control in pure water (in absence of peptide) at the same ellipticine concentration was prepared for comparison.

3.2.2.8 Cellular Toxicity of the Peptide-Drug Complexes

A cancer cell line, non-small lung cancer cell A549, and mouse macrophage cells RAW 264.7 were used for the cellular toxicity on the AAP8 peptide series and peptide-ellipticine complexes. Cells were cultured in Dulbecco's Modified Eagle Medium (DMEM), containing 10% fetal bovine serum (FBS) and 1% penicillin-streptomycin in an environment controlled incubator (37 °C with 5% CO2). After reaching ~ 95% confluence, the cells were detached and suspended in the DMEM, followed by centrifuging at 500 rpm for 5 min. The cell pellets were re-suspended in a fresh DMEM at a concentration of 2.5×10^4 cell per ml. A volume of 200 μl of the cell suspensions was added into each well of a clear, flat-bottom, 96-well plate (Costar) and incubated for 24 hr. The culture medium was replaced with 150 μl fresh culture medium, followed by an addition of 50 μl treatment (the complexes, their dilutions, and control samples) into each well. Each treatment was replicated in four wells. The plates were incubated for 24 hr prior to performing the cell viability assay.

MTT assay (TOX1 from Sigma–Aldrich, Oakville, ON, Canada) was used to determine the cell viability after each treatment. Solid MTT (5 mg) was first dissolved in PBS solution (3 mL), followed by a 10-time dilution in the culture medium. All the treatments were replaced by 100 μl MTT solution. The plates were incubated for 4 h prior to the addition of solubilization solution (100mL, anhydrous isopropanol with 0.1 N HCl and 10% Triton X-100). After overnight incubation, the absorbance at 570nm was collected on a microplate reader (BMG FLUOstar OPTIMA) and subtracted by the background signals at 690 nm. The absorption intensities were averaged from 4 replicates for each treatment and normalized to that obtained from the untreated cells (negative control) to generate the cell viability [24].

3.3 Results and Discussion

Self-assembly of short peptides into β-sheet fibril nanostructures paves the way for synthesis of novel biomaterials for a wide range of applications (e.g., drug delivery and tissue engineering). To develop peptide-based nanostructures, it is necessary to assure that the configuration of nanostructures is controllable and uniform (e.g., in either fibrillar or spherical shape). One of the main drawbacks of the β-sheet fibrillar structures is their tendency to aggregate in tangled form, which is unbearable in both *in vitro* and *in vivo* applications. We previously introduced the *de novo* design principle of amino acid pairing (AAP) and created a novel class of self-assembling peptides [26]. This design strategy focuses on amino acid pair interactions, including hydrogen bonding, ionic pairing and hydrophobic interactions. The current work concentrates on an AAP peptide with all three pairing interactions mentioned. This self-assembling peptide, AAP8, consists of eight amino acids: four Phenylalanine (F), hydrophobic side chains; Lysine (K) and Glutamic acid (E), an ionic pair; Glutamine (Q) and Asparagine (N), a hydrogen bonding pair. This peptide is phenylalanine-rich, which may generate β-sheet-rich fibrils but possibly reduce solubility of the peptide in aqueous solution. Since the β-sheet formation is mainly due to intermolecular hydrogen bonding and hydrophobic interactions, it is hypothesized that introducing organic molecules, such as polymers via conjugation, could regulate β-sheet formation and lead to more oriented, uniform nanostructure. This hypothesis is supported by earlier work of Burkoth et al. [81] and Collier et al. [85], who showed that PEG-modified Aβ and Q11 peptides avoided lateral aggregation. In addition to improvement of peptide self-assembly provided by PEG-conjugation, numerous biological advantages have been drawn for drug delivery, such as solubility, long circulation in the bloodstream and protection of the nanoparticles from enzymatic degradation[82,84,85].

In this work, a short segment of polyethylene glycol (PEG), diethylene glycol (DEG), with a molecular weight of 145 Da, was selected to functionalize AAP8 and make a peptide-DEG hybrid molecule. Since AAP8 is a short peptide, conjugating a short ethylene glycol (EG) would be appropriate, so that it does not interfere with peptide self-assembly, to any larger extent. Two hybrids were studied here: one is a conjugation of DEG to the C-terminal of AAP8, and the other a conjugation to both C- and N-terminals of AAP8. The schematic of molecular formulas is presented in (Figure 3.1) (ACD/ChemSketch Freeware, Toronto, Canada). Hydrophilic amino acid residues (lysine and glutamic acid) are positioned on one side of the molecule, and hydrophobic amino acid residues (phenylalanine rings) are located on other side, creating an amiphiphlic side-to-side

configuration. Diethylene glycol with hydrophilic characteristics is shown to conjugate to AAP8, first on the C-terminal, then on both C- and N-terminals.

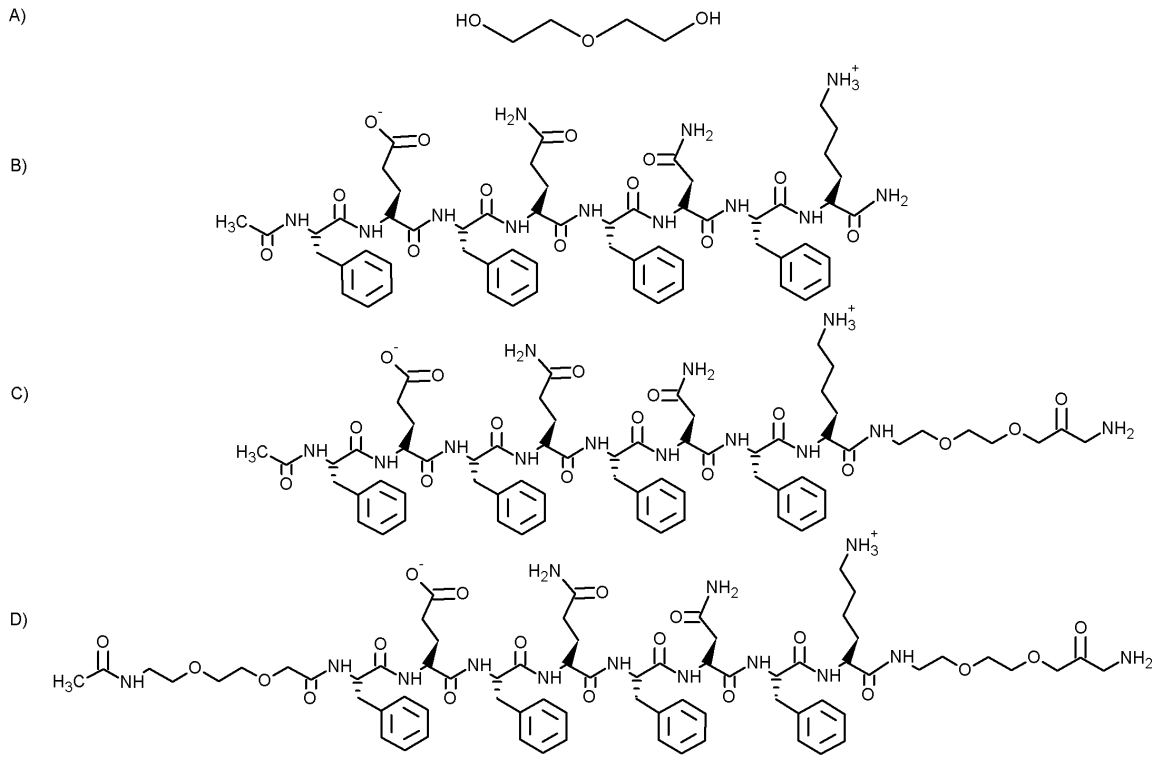

Figure 3.1. Molecular structure of **(A)** Diethylene Glycol (DEG), **(B)** amino acid pairing peptide AAP8 with monomer length: 3.53 nm, **(C)** AAP8-DEG with monomer length: 4.52 nm, **(D)** DEG-AAP8-DEG with monomer length: 5.51 nm. The width of all molecular structures are ~ 0.2-0.8 nm. All dimensions are estimated using ACD/ChemSketch Freeware (Toronto, Canada).

3.3.1 Effect of DEG-functionalization on Self-assembly of Nanofibers

3.3.1.1 Nanostructure Morphology

Atomic force microscopy (AFM) images of self-assembling peptide nanostructures on a mica surface showed significant differences in assembly morphologies between AAP8 and functionalized AAP8 (Figure 3.2). AFM images of AAP8 revealed that this peptide forms extremely tangled fibers with large aggregates (Figure 3.2(A)). In contrast, the modified AAP8 showed a greatly improved the

morphology, revealing more uniform fibrillar structures, with little evidence of aggregation (Figure 3.2(B), (C)).

Images were taken to observe the peptide assembly at two time points. AAP8 formed larger aggregates over time and in most cases did not attach to the mica surface (Figure 3.2(D)). This latter observation is due to AAP8's hydrophobicity, which reduces the likelihood of stabilization on mica. However, AAP8-DEG formed more structured fibers, with bundles consisting of a few fibers of an increased length (Figure 3.2(E)). The most interesting morphology observed was from DEG-AAP8-DEG, which produced highly uniform, long fibers, aligned in parallel and almost no evidence of aggregation or tangled fibers (Figure 3.2(F)).

In the analysis of dimensions of the peptide assemblies, the widths were deconvoluted using the method reported by Hong et al., to eliminate the convolution effect arising from the finite size of the AFM tip [149,152]. The observed dimensions have to be corrected; for spherical shapes with a radius R_m, the observed width of the sample follows a relationship: $W_{obs}=4(R_tR_m)^{0.5}$, where R_t is the radius of the AFM tip, which is 10 nm in the present case. If the sample is a sheet, the real width of the sheet can be calculated using this equation: $W = W_{obs} – 2(2R_tH – H^2)^{0.5}$, where H is observed height. Since we later show the significant amount of β-sheet in the peptide secondary structure, the assumption of using the sheet formula for dimension analysis is acceptable.

From the analysis of at least fifty independent fibers in each image, the corrected width and height were calculated and tabulated in Table 3.1 The heights of assembled nanofibers are 0.7-0.8 nm for all three peptides in the freshly prepared sample, a measurement is in agreement with corresponding molecular determinations using ACD/ChemSketch drawing software, which determined the width to be ~ 0.5-0.8 nm, from the topmost and bottommost atoms in the van der Waals-based structures. The height of AAP8 fibers increased, almost twice the initial height, over the ten-day span, which is likely due to aggregation progression and building of the peptide molecules to avoid attaching to a mica surface. The increase in height happened for AAP8-DEG to some extent, but the height of DEG-AAP8-DEG assemblies did not show significant increase. Since, DEG-AAP8-DEG is more hydrophilic and stable in aqueous solution, molecules have a tendency to attach to a mica surface.

AFM images of freshly made AAP8 demonstrated 16.86 ± 1.07 nm wide tangled short fibers, with aggregates of 76.08 ± 2.98 nm in diameter. The aggregates seemed to grow over ten days, to 109.4 ± 5.6 nm in width. The ACD/ChemSketch software determined the length of an individual AAP8 molecule to be 3.35 nm. Therefore, the fiber width observed by AFM corresponds to more than one peptide molecule length.

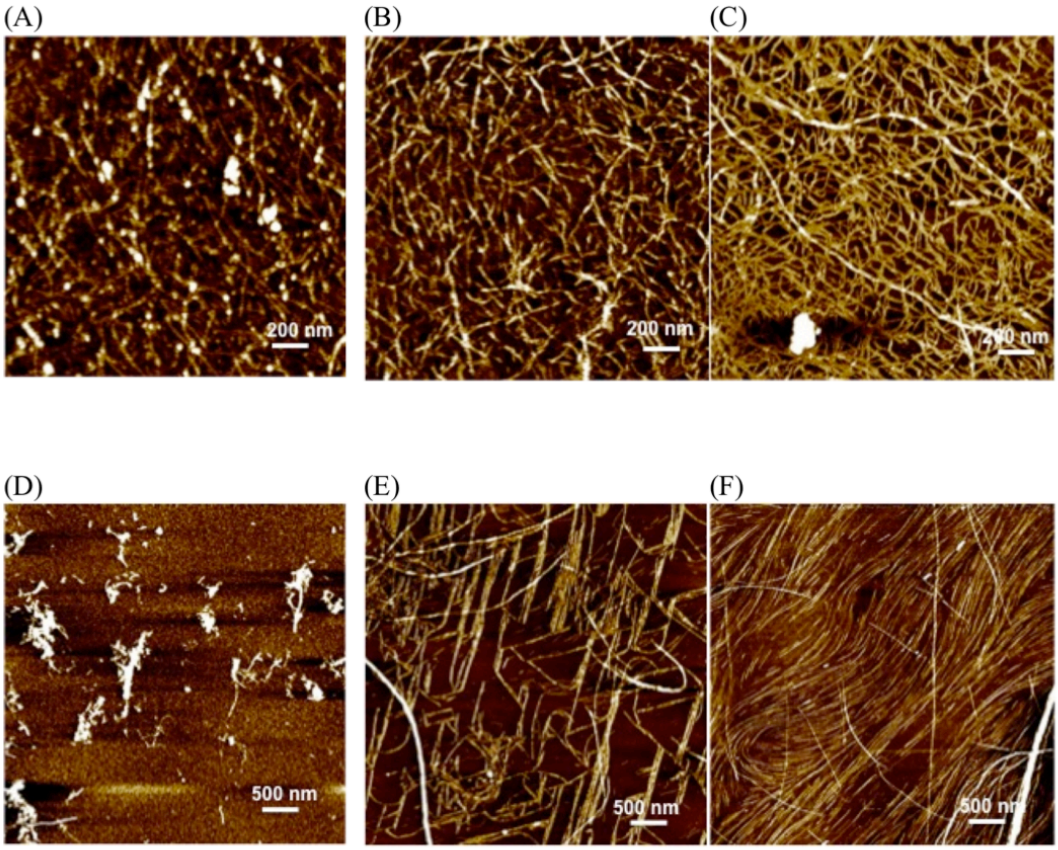

Figure 3.2. Nanostructure of freshly prepared **(A)** AAP8, **(B)** AAP8-DEG, **(C)** DEG-AAP8-DEG, and ten- day-old **(D)** AAP8, **(E)** AAP8-DEG, **(F)** DEG-AAP8-DEG taken by tapping mode of Atomic Force Microscopy (AFM) on mica surface. All concentrations are 0.5 mg/ml.

The dimension analysis of AAP8-DEG illustrated thinner fibers, 10.2 ± 0.61 nm in width, even though its molecule is longer than of AAP8, 4.52 nm, as predicted by ACD/ChemSketch software. Each fiber consists approximately two to three DEG-conjugated AAP8 molecules stacked together width-wise. It was shown that over ten days, the fibers only grew to about 13.53 ± 0.87 nm in width, and some of the fibers associated together and created bundles, 58.95 ± 3.99 nm in width. The DEG-AAP8-DEG presented the most uniform fibrillar structures, whether the samples were fresh or had aged for ten days: the initial fibers had 8.21 ± 0.79 nm width with no trace of aggregation. After ten days, the average fiber width was 10.97 ± 0.87 nm and the fibers were in an oriented and parallel pattern. The dimension of a DEG-AAP8-DEG molecule calculated by ACD/ChemSketch was about

5.7 nm in length, longer than those of AAP8 and DEG-AAP8, but the resulting thinner fibers indicate the lower possibility of aggregation. In comparison with AAP8, the DEG-conjugated AAP8s were shown to spread on the mica surface more expansively and assembled in a more uniform fashion. Conjugating DEG to the peptide changes the nanostructures significantly, which can be interpreted by steric shielding of the fibrils by diethylene glycol and an increase in stability in aqueous solution [85].

Table 3.1. Dimensions of AAP8, AAP8-DEG, and DEG-AAP8-DEG assemblies at two time points. Heights and widths are obtained by Gwyddion software (Free SPM Data analysis software), and the widths are corrected with the above deconvolution method [152]. *F, Fibrillar assemblies; A, aggregates, B, bundles.

	Fresh			10 Day		
	Shape*	Width (nm)	Height (nm)	Shape*	Width (nm)	Height (nm)
AAP8	F	16.86±1.07	0.69±0.06	F	17.06±2.02	1.21±0.21
	A	76.08±2.98	0.92±0.03	A	109.4±5.65	3.15±0.45
AAP8-DEG	F	10.2±0.61	0.74±0.06	F	13.53±0.87	1.03±0.09
				B	58.95±3.99	2.16±0.35
DEG-AAP8-DEG	F	8.21±0.79	0.81±0.081	F	10.97±0.87	0.86±0.09

3.3.1.2 Secondary Structure

To further investigate the DEG-conjugation effect on peptide assemblies, secondary structures of peptide-DEG hybrids were determined by Fourier Transform Infrared (FT-IR) spectroscopy and Circular Dischroism (CD). All results showed greater β-sheet content in their secondary structures, where the β-sheet content increased when DEG was conjugated to the peptide sequence. FT-IR results indicated a strong peak at 1614-1622 cm^{-1}, and CD spectra represented a strong negative peak at ~ 210-215 nm. The three main peaks in the amide I region are for the β-sheet (1614-1622 cm^{-1}), α-helix (1650-1658 cm^{-1}) and β-turn structure (1680 cm^{-1}). From the FT-IR spectra obtained from AAP8, AAP8-DEG and DEG-AAP8-DEG, the dominant peak is at 1620 cm^{-1}, which corresponds to the β-sheet secondary structure. There is no clear peak observed for the α-helix or β-turn. The intensity of these peaks increased from AAP8 to AAP8-DEG to DEG-AAP8-DEG (Figure 3.3), which showed that the β-sheet content increased when DEG was conjugated to AAP8. This evidence pointed out that functionalization of the peptide with a DEG has a significant impact on its secondary structure and modulates its β-sheet content due to self-association by hydrogen bonding between β-strands[159].

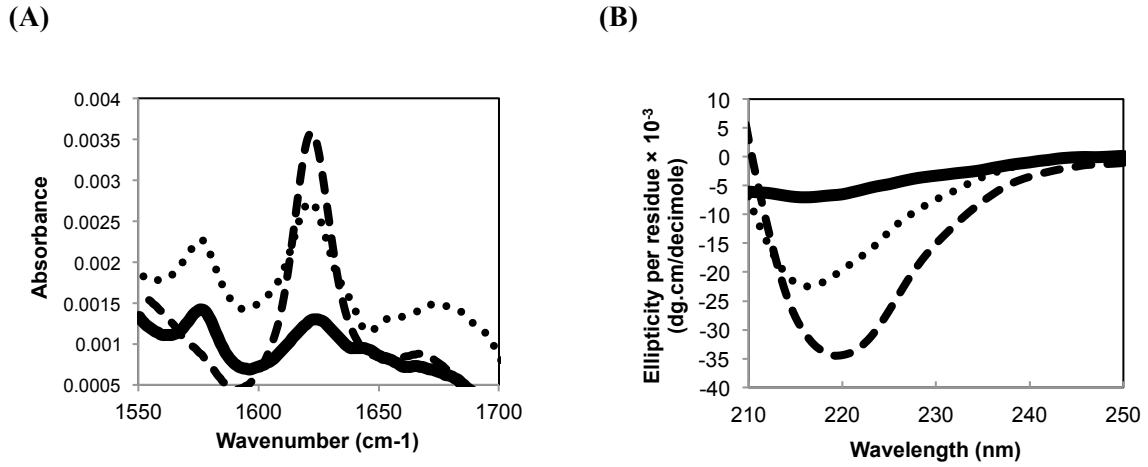

Figure 3.3. Secondary structure determination by **(A)** FT-IR spectra, **(B)** Circular Dichroism spectra, (—) AAP8, (**….**) AAP8-DEG, (**---**) DEG-AAP8-DEG, 0.5 mg.ml^{-1} in Milli-Q water.

3.3.1.3 Hydrophilicity and Critical Aggregation Concentration (CAC)

Since PEG is considered a hydrophilic polymer, we hypothesized that conjugation of a short segment of PEG, such as DEG, to our relatively hydrophobic peptide, AAP8 with four phenol rings, would reduce hydrophobicity of the peptide. In order to determine hydrophobicity, we utilized a fluorescent probe, which can bind to hydrophobic compounds and, as a consequence, emits light. We used the 1-anilino-8-Naphthalene Sulfonate (ANS) fluorescence probe, which emits light at 470 nm in a hydrophobic environment, whereas its emission wavelength in pure water is at 520 nm. Figure 3.4(A) shows the fluorescence spectra of the ANS probe in three different peptide solutions compared to in pure water. All spectra were normalized with light scattering of air at 360 nm, to correct the lamp fluctuations. The normalized fluorescence intensity of the ANS shows the following trend: AAP8≈AAP8-DEG>>DEG-AAP8-DEG>>H_2O. Meanwhile, the peak position of ANS in pure water (inset) is observed at ~ 520 nm, whereas it shifts to ~ 470 nm for AAP8 and its DEG-conjugates. In addition, the fluorescence intensity of the ANS probe decreases upon DEG functionalization of AAP8. Among AAP8, AAP8-DEG, and DEG-AAP8-DEG, the last one shows the lowest fluorescence emission intensity, and is thus the least hydrophobic. As expected, conjugation of DEG on both sides enhances the hydrophilicity of AAP8 compared to one-sided conjugation, which explains the significant reduction in aggregation likely caused by hydrophobic residues.

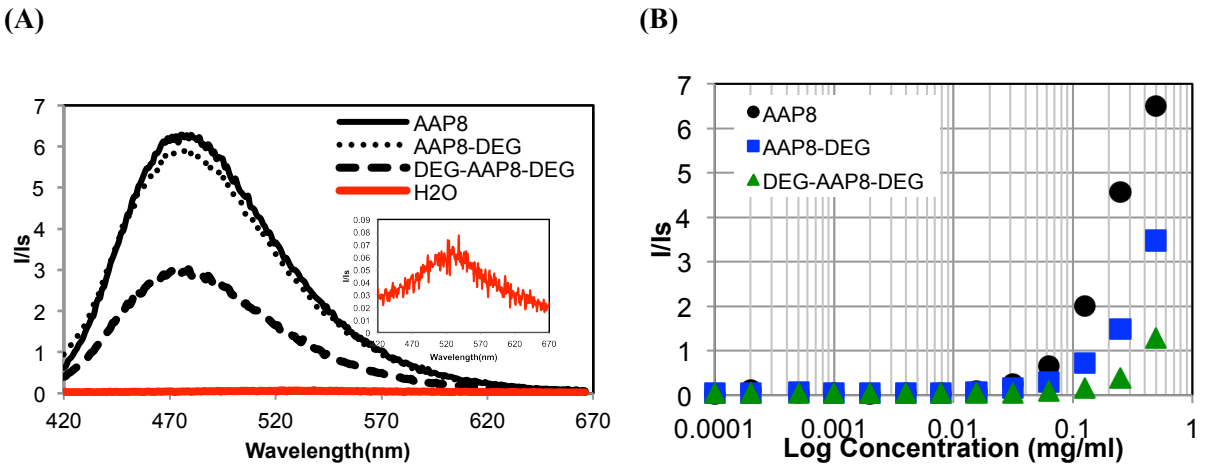

Figure 3.4. (**A)**Hydrophobicity of (—) AAP8, (**….**)AAP8-DEG, (----) DEG-AAP8-DEG, (—) pure water. The inset is fluorescence control of ANS probe in water with absence of the peptide. The peptide concentration is 0.5 mg/ml and the ANS concentration is 10 μM. (**B**) CAC determination by ANS fluorescence probe.

The same method was performed to determine critical aggregation concentration (CAC). Critical aggregation concentration (CAC) is a parameter to evaluate self-assembly strength. CAC is defined as the concentration of peptides that above that concentration the peptide aggregates are spontaneously formed. The lower CAC, the higher tendency to self-associate the system will have. In this study, the CAC of these three peptides were determined by (ANS) fluorescence assay. The fluorescence intensity of ANS probe does not change by increasing peptide concentration at low concentrations of peptide in pure water, however after a certain concentration, which we call it CAC, the fluorescence intensity of ANS increases significantly. AAP8 showed the lowest CAC amongst the DEG-conjugated AAP8, and DEG-AAP8-DEG showed the highest. The observed values are: ~0.015, ~ 0.06, and ~0.15 mg/ml for AAP8, DEG-AAP8, and DEG-AAP8-DEG, respectively (Figure 3.4). These values show that the CAC increases with DEG conjugation. With DEG conjugation, peptide becomes more hydrophilic, which means that more peptide chains would be necessary to form self-assembled nanostructures increasing the minimum peptide concentration required (i.e. higher CAC). DEG functionalization facilitates peptide to self-assemble in more organized ways and avoids aggregation at low concentrations. As we observed from AFM images, DEG-AAP8-DEG does not show lateral aggregation even at high concentration (0.5 mg/ml), however, both AAP8 and AAP8-DEG showed aggregation and tangled fibers. Therefore, DEG conjugation on both sides of AAP8 provides the more controllable and stable structure.

3.3.2 DEG-functionalization Effect on Encapsulation of Hydrophobic Drug and Cellular Toxicity

3.3.2.1 Ellipticine Encapsulation

In the next step, we investigated the potential use of AAP8 and its DEG-conjugates as carriers for hydrophobic anticancer drugs. Ellipticine (EPT), an anticancer drug, has been used as a hydrophobic model drug in our past drug delivery research [24,26,132,146]. Ellipticine (EPT), a cytotoxic plant alkaloid, is known as a polycyclic molecule that intercalates between DNA base pairs, inhibits Topoisomerase II, and induces G2/M phase cell cycle arrest [160]. The fluorescence properties of ellipticine make it easy to characterize for encapsulation and release of the drug. Despite of these advantages, clinical tests on ellipticine were suspended due to the drug's lack of target-ability, and accumulation in undesired sites, which can be explained by insolubility of ellipticine in aqueous media [161]. The challenges regarding delivery of hydrophobic compounds highlight a strong need for more effective delivery systems. We previously showed the great potential of AAP8 to deliver ellipticine into cancer cells [26]. However, AAP8 without modification might be challenging for further *in vitro* and *in vivo* tests due to its aggregation tendency and cytotoxicity. The therapeutic efficiency of drug carriers may be limited by particle recognition by macrophages of the mononuclear phagocyte system (MPS) and possibility of rapid elimination from the bloodstream after intravenous injection. Therefore, the current modification of AAP8 by DEG shows means to overcome aggregation and may improve its drug delivery potentialities [157,162,163].

Table 3.2. Complexes characterization.

	Zeta Potential (mV)	**pH**	**EPT State**
AAP8-EPT	36.6±0.41	5.0±0.1	Protonated
AAP8-DEG-EPT	30.46±0.64	5.1±0.1	Protonated
DEG-AAP8-DEG-EPT	30.86±0.38	5.36±0.03	Protonated

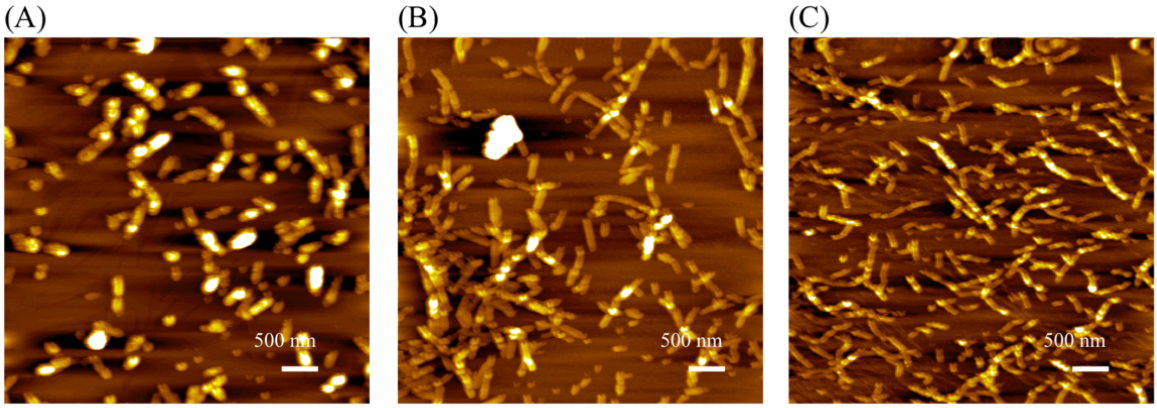

Figure 3.5. Nanostructure of freshly prepared ellipticine complexes with (**A**) AAP8, (**B**) AAP8-DEG, (**C**) DEG-AAP8-DEG taken by tapping mode of Atomic Force Microscopy (AFM) on mica surface. All concentrations are 0.5 mg/ml for peptides and 0.1 mg/ml for ellipticine.

Preliminary characterization has been performed on the peptide and drug complexes to investigate the differences between complexes formed from modified and non-modified AAP8. Table 3.2 summarizes the data for three complexes. Emission spectra of ellipticine collected with the spectrofluorometer showed the protonated state of ellipticine (peak at ~ 520 nm) for all AAP8-EPT, AAP8-DEG-EPT and DEG-AAP8-DEG-EPT complexes at 0.5mg/ml peptide and 0.1mg/ml ellipticine concentration. The difference between the current study and reference [26], regarding formation of ellipticine in solution, is due to the age of complexes in the experiments. Previously, AAP8 was added to EPT and mechanically stirred at 900 rpm for 24hr. However, in the current study, AAP8 was added to EPT and the complexes were made through the probe sonication method at a power of 6-8 W for 5-10 min and freshly analyzed with fluorescence spectroscopy and applied for cytotoxicity study. In this case, the complex product is a transparent yellow color, similar to that of the EAK-EPT complexes reported in Reference [24]. As it was shown in Figure 4 [24], the presence of protonation and crystalline states of ellipticine is time-dependent. For the freshly prepared complexes, protonated ellipticine is dominant, whereas after ~ 10hr, the crystalline form of ellipticine dominates in solution. Since in the current study the focus is not studying ellipticine state over time in solution and only freshly prepared samples were used in the experiments, the protonated state of ellipticine in AAP8-EPT complexes is reported. Note that the protonation of ellipticine usually occurs at higher peptide concentrations and relatively low pH (i.e. $\leq$ 5), lower than ellipticine pK_a (6.0) [147]. The pH of freshly prepared AAP8 was measured as 4.3, which provides an acidic environment for the protonation of ellipticine. Since ellipticine is stabilized in solution in protonated form, it is

expected to have positively charged species. This was confirmed with zeta potential measurements for complexes and no significant difference was observed from DEG-conjugated and non-conjugated AAP8s in complex with ellipticine. Since the zeta potential for all three complexes is more positive than +30 mV, they are normally considered stable particles in solution.

Table 3.3. Dimensions of ellipticine complexes with AAP8, AAP8-DEG, and DEG-AAP8-DEG assemblies. Heights and widths are obtained by Gwyddion software (Free SPM Data analysis software), and the widths are corrected with the above deconvolution method [152]. Hydrodynamic diameter (D_H) is calculated based on *L* and *w* [164].

	Width (nm)	**Length (nm)**	**Height (nm)**	**(D_H)**
AAP8-EPT	126.11±4.94	339.36±8.57	5.398±0.325	212.91
AAP8-DEG-EPT	98.79±3.369	283.891±1.374	1.21±0.106	-
DEG-AAP8-DEG-EPT	74.07±2.044	472.17±27	0.819±0.103	-

The interaction between hydrophobic drug, ellipticine and AAP8 peptide is based on hydrophobic interactions between phenylalanine side chain and ellipticine. The four F residues can provide strong hydrophobic interactions assisted by π-π stacking to stabilize nanostructure and consequently interact with ellipticine. This hydrophobic interaction between peptide and ellipticine remains constant by modifying AAP8 with DEG; however, DEG helps stabilizing the complex better in aqueous solution. Non-modified AAP8 tends to aggregate overtime when it is in complex with ellipticine in aqueous environment, whereas DEG-modified AAP8s provide more hydrophilic environment and assist stabilized fibers in complex with ellipticine in aqueous solution. AFM images illustrated the above hypothesis, where DEG-modified AAP8 suppress aggregation of AAP8 in complex with ellipticine and stabilize ellipticine more efficiently in aqueous solution. AAP8 in complex with ellipticine formed cylindrical shape particles with approximate hydrodynamic diameter of ~212 nm, which is comparable with DLS results (Table 3.3). However, both DEG-modified AAP8s in complex with ellipticine formed fiber structures (Figure 3.5). The nanostructure of peptide-EPT complexes observed in AFM images showed wider fibers compared to those formed in the peptide nanostructure, as shown in Figure 3.2. The mechanism of the complexation between peptide and ellipticine is not fully understood. As discussed in Reference [26], a model has been proposed for AAP8 nanofibers via amino acid pairing, where peptide molecules are aligned in anti-parallel fashion to form nanofibers with a width equals to the length of a peptide chain or a multiple of the length. This may be seen in Figure 3.2 and Table 3.1. However, in peptide-EPT complexes, this alignment is disrupted;

as a result, wider nanofibers may form, perhaps because of potential multiple interactions between peptide and EPT molecules (e.g., ionic, hydrogen bonding and hydrophobic interactions). It is observed from AFM images that the height of nanofibers does not increase significantly. One may postulate that fiber growth in peptide-EPT complexes is not isotropic, but the reason is unclear and it requires more investigation. The average hydrodynamic diameter of particles was calculated based on the Equation 3.1 for cylindrical shape particle with length of L and diameter (width) of w observed by AFM images. This equation is applied for AAP8 and ellipticine complex particles, since they formed cylindrical shapes, whereas this equation cannot be applied for fibril structures [164].

Equation 3.1- Correlation between Hydrodynamic diameter and length and width of cylinder observed by AFM

$$D_H = L\left(\sqrt{1-x^2}\Big/\ln\frac{1+\sqrt{1-x^2}}{x}\right), \qquad x = \frac{w}{L}\left[1+0.37\frac{(L-w)}{L}\right]$$

3.3.2.2 Cytotoxicity

Cytotoxicity of unmodified AAP8 and DEG-modified AAP8s was evaluated by MTT assay on non-small cells lung carcinoma (NSCLC), i.e., A549 cell line, for 24 and 48 hr incubation times. Cells treated with AAP8 showed around 30-40% cytotoxicity. However, cells treated with both DEG modified AAP8 in one end and two ends showed lower cytotoxicity (0-5%). DEG-functionalization of AAP8 has a clear beneficial effect on the cytotoxicity of the peptide, rendering it completely nontoxic for all concentrations evaluated (up to 100 uM) (Figure 3.6(A)).

Anticancer activity of ellipticine encapsulated with unmodified AAP8 and modified AAP8s were examined on A549 cell line for 24 hr and 48 hr incubation times by MTT assay. Results presented that the cytotoxicity of ellipticine in complex with modified AAP8s are lower than that of the corresponding unmodified AAP8, which can be understood by our two main observations: first, cytotoxicity of AAP8 compared to modified AAP8s is higher, which consequently may induce higher cytotoxicity together with ellipticine; second, the modified AAP8s, i.e., AAP8-DEG and DEG-AAP8-DEG, can stabilize ellipticine and suspend it longer in media, resulting in the slower release of ellipticine from the complex and delay in drug contact with adhesive cells, as compared to AAP8-ellipticine complexes. This is observed for 24 hr incubation time (Figure 3.6(B)). Despite the fact that complexes of modified AAP8s and ellipticine showed lower cytotoxicity to cancer cells than

corresponding unmodified AAP8 complexes at 24 hr treatment time, the cytotoxicity of the complexes is higher than the ellipticine control at highest concentration (100 µM). This indicates that both modified and unmodified AAP8 carriers are more effective to deliver ellipticine and cause cytotoxicity than the drug control. This is primarily because ellipticine can be stabilized in AAP8 and DEG-conjugated AAP8s in aqueous media.

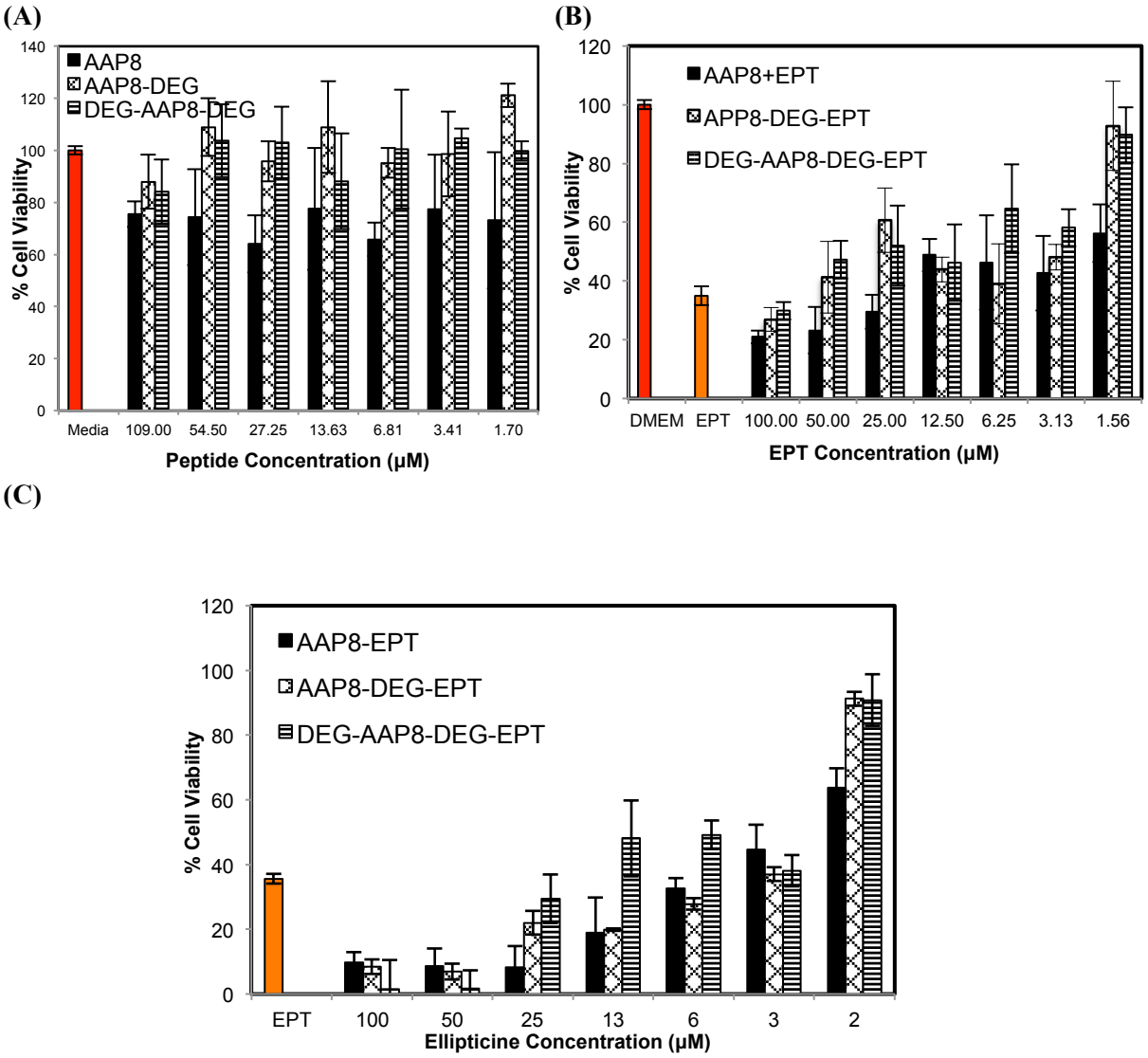

Figure 3.6. The cytotoxicity test of **(A)** controls (negative control, AAP8, AAP8-DEG, and DEG-AAP8-DEG (1.07-109 µM) for 24 hr incubation time; ellipticine in complex with above peptides and in pure water, **(B)** for 24 hr incubation time and **(C)** for 48 hr incubation time. The maximum ellipticine concentration was 100 µM diluted serially up to 1.56 µM. The peptide concentration ranges from (~ 1-100 µM). Note that the molar ratio between ellipticine and peptide is kept constant at 1:1. DMEM corresponds to non-treated cells. Error bars represent for standard error of means in 95% confidence interval.

However, the cells were treated with the complexes for 48 hr showed a reverse trend for the cytotoxicity results for modified and unmodified AAP8 in complex with ellipticine, up to 50-100 μM for both peptide and ellipticine. The cytotoxicity of the complexes showed the following trend: DEG-AAP8-DEG-EPT>AAP8-DEG-EPT>AAP8-EPT. This can be explained by aggregation of particles in AAP8 and ellipticine solution overtime and settling down in the cell containing wells without penetrating to cell membranes, whereas in shorter incubation time, within 24 hours, the possibility of aggregation is lower, which allows penetration into cell membranes and cause more toxicity. On the other hand, the cytotoxicity of the modified AAP8s and ellipticine complexes improved overtime as stabilized ellipticine in the solution will eventually reach the cells, causing higher cytotoxicity (Figure 3.6(C)). This phenomenon happened only for higher concentrations of complexes of DEG-modified AAP8 and ellipticine (50-100 uM of peptide and ellipticine), i.e., up to 4 times dilution, and it is expected, as the difference in aggregation between the modified and unmodified peptides is significant only at relatively high concentrations.

The effect of DEG-conjugation was observed on cellular uptake of ellipticine through fluorescence microscopy. As it was mentioned previously, EPT has an intrinsic fluorescence property that can be detected under green light (520 nm emission). The fluorescence intensity illuminated from the A549 cells treated with AAP8-EPT is the lowest among other DEG-conjugated AAP8 and EPT complexes, indicating the efficiency of the DEG delivering EPT into the cancer cells (Figure 3.7).

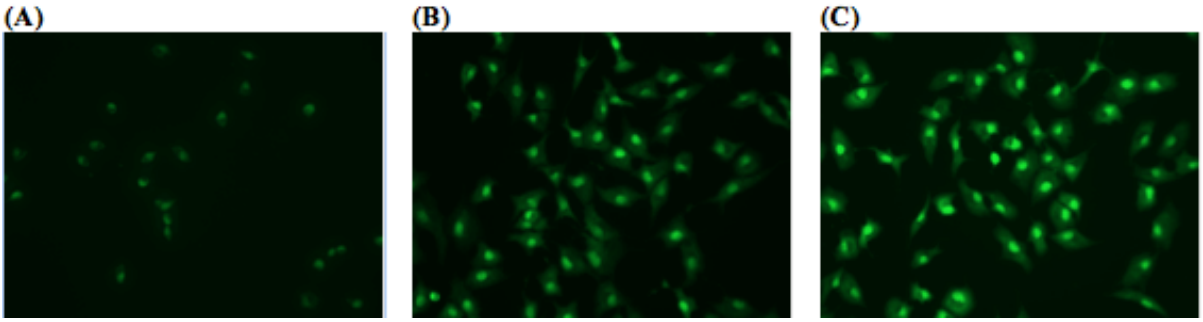

Figure 3.7. Cellular uptake of EPT carried by **(A)** AAP8, **(B)** AAP8-DEG, and **(C)** DEG-AAP8-DEG after 2hr incubation with the complexes.

3.3.3 Effect of DEG-conjugation on Macrophages

So far, DEG-functionalization showed positive results on aggregation control, nanostructure formation, hydrophobic drug encapsulation, and anticancer activity. Here, effect of DEG-conjugation was studied on interaction with macrophages as one of the acute immune system components.

Macrophages are responsible to eliminate foreign materials from body through phagocytosis mechanism. If the foreign nanomaterials are recognized by macrophages innate inflammation responses will be observed that can be observed *in vitro* such as macrophage toxicity, morphology change and other indications such as level of induced nitric oxide synthase (iNOS). iNOS expression is induced by immune stimulations such as lipopolysaccharide (LPS) in mammalian macrophages [165,166].

(A)

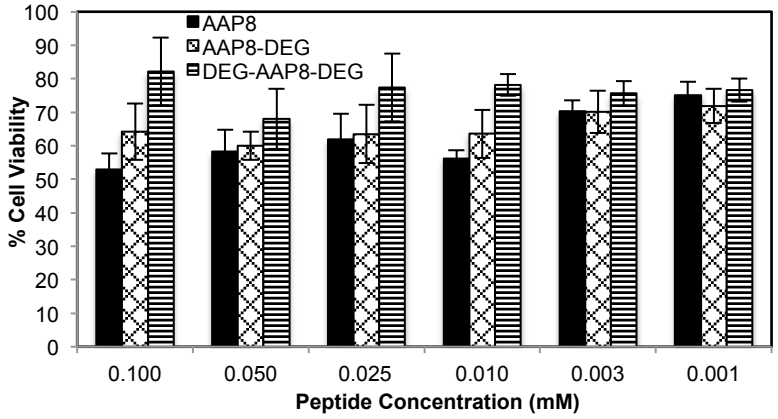

(B)

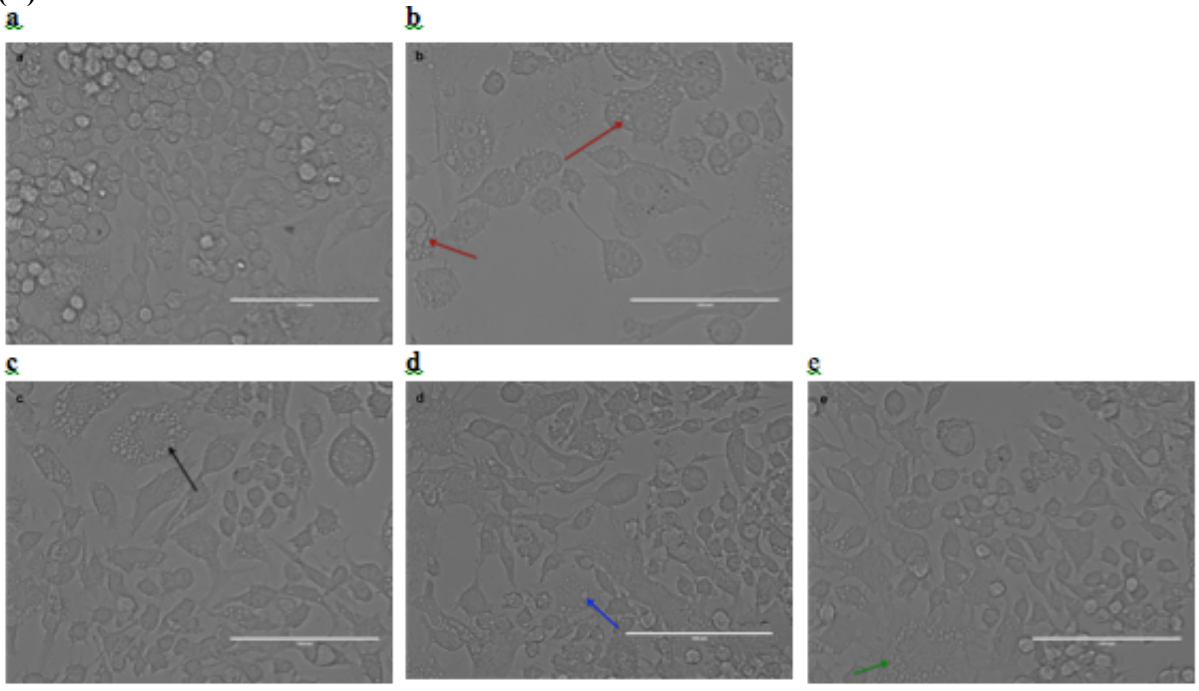

Figure 3.8. **(A)** Cellular viability of the macrophages treated by AAP8, AAP8-DEG, and DEG-AAP8-DEG (0.001-0.1 mM) for 48 hr. **(B)** Morphology of the macrophage cells after exposure to the peptides. Arrows point at the activated feature of macrophages. Treatments: a: untreated, b: LPS, c: AAP8, d: AAP8-DEG, e: DEG-AAP8-DEG (peptide concentrations are 0.1 mM)

The cell viability of the macrophages was evaluated after treated with the AAP8 and DEG-conjugated AAP8s peptides. First, all three peptides showed very negligible cytotoxicity towards macrophages after 48 hr treatment. Second, macrophage cellular toxicity decreased about ~ 10 and 30% when treated with DEG-AAP8 and DEG-AAP8-DEG, respectively (Figure 3.8 A). This result indicates the stealth properties of DEG for the peptide to protect it from phagocytosis. In addition, morphology of the cells has been changed after treated with AAP8, whereas the morphology of the cells treated with DEG-conjugated AAP8 stayed almost intact for the same less phagocytosis reason. LPS was applied on cells as a positive control sample, which is known as one of the main stimulators of macrophages. The cells exposed to LPS showed the most extreme morphological change (Figure 3.8 B).

3.4 Conclusions

Nanostructural characterization of the peptide AAP8 and diethylene glycol conjugated AAP8 indicates that functionalizing the short self-assembling peptide with diethylene glycol (DEG) is an effective means to enhance β-sheet content in secondary structure and modulate the nanostructure to an aligned and uniform fibrillar configuration, minimizing random aggregation. The unmodified AAP8 showed significant aggregation over time, whereas DEG-conjugated AAP8s, particularly DEG-AAP8-DEG overcame the aggregation problem. We also observed higher hydrophilicity, in particular, when DEG was conjugated to both ends of AAP8. The improvement of the peptide self-assembly upon DEG conjugation supports the hypothesis that conjugating a short chain of PEG to peptides helps obtain more uniform and organized nanostructure, increase β-sheet content and enhance solubility in aqueous solution, which all lead to low lateral aggregation. These peptides showed reduced cytotoxicity towards non-small cells lung carcinoma and macrophages as compared to unmodified AAP8, which is considered an advantage for drug carriers. Both modified and unmodified AAP8s showed impressive capability to stabilize the hydrophobic anticancer drug ellipticine in aqueous solution. All three complexes, AAP8, AAP8-DEG and DEG-AAP8-DEG with ellipticine, exhibited higher cytotoxicity against A549 cells than ellipticine control, indicating great capability of peptide-based carriers for stabilizing and delivering of ellipticine. The viability of the cells treated with both DEG-modified AAP8s in complex with ellipticine is higher than corresponding AAP8 and ellipticine complexes after 24 hr incubation time. This may be due to the delay contact of ellipticine, when formed complex with DEG-modified AAP8s, with adherent cells. After 48 hr incubation time, DEG-modified AAP8s have become more effective than unmodified AAP8 in complex with ellipticine, possibly due to aggregation associated with AAP8 and ellipticine in aqueous

solution over a relatively long time. The results reported here provide a means to overcome critical issues in aggregation and inherent cytotoxicity associated with the use of biomaterials, and pave the way to further design of functionalized biomaterials for improved drug delivery applications.

Chapter 4‡

Self/Co-Assembling Peptide, EAR8-II, as a Potential Carrier for a Hydrophobic Anticancer Drug Pirarubicin (THP)-Characterization and *in vitro* Delivery

Abstract

A short ionic-complementary peptide, EAR8-II, was employed to encapsulate the hydrophobic anticancer drug pirarubicin (THP). EAR8-II was designed to inherit advantages from two previously introduced peptides, AAP8 and EAK16-II, in their self/co-assembly. This peptide is short, simple, and inexpensive to synthesize, while possessing a low critical assembly concentration (CAC). The choice of alanine (A) residues in the peptide sequence provides moderate hydrophobic interactions, causing a minimal degree of aggregation, compared with other more hydrophobic residues. EAR8-II is an ionic-complementary peptide, similar to EAK16-II, can self/co-assemble with hydrophobic compounds such as THP, and forms a stable fibular nanostructure in aqueous solution. Physiochemical properties and cellular activities of the EAR8-II and THP complexes are evaluated and show dependency on the peptide-to-drug ratio. The complex at the peptide-to-drug mass ratio of 5:1 provides a stable solution, uniform nanostructure, and highly effective anticancer activity against various cancer cell lines. This work forms the basis for detailed studies on EAR8-II and THP formulations *in vitro* and *in vivo*, for future development of peptide-based delivery systems for hydrophobic anticancer drugs.

Key Words: ionic-complementary; self/co-assembly; encapsulation; stability; anticancer activity

‡ This chapter is based on a paper "Sadatmousavi, P.; Chen, P. Self/Co-Assembling Peptide, EAR8-II, as a Potential Carrier for a Hydrophobic Anticancer Drug Pirarubicin (THP)—Characterization and *in vitro* Delivery. *Int. J. Mol. Sci.* **2013**, 14, 23315-23329."

4.1 Introduction

In the last chapter, I discussed a strategy for designing amino-acid-pairing peptides, and their potential for drug and gene delivery [26,167]. A short amino-acid-pairing peptide (AAP8), with a sequence of Ac-FEFQFNFK-NH_2, was introduced and showed promise for delivering the anticancer drug Ellipticine. Despite its practicability in anticancer drug encapsulation, AAP8 shows uncontrollable aggregation, which is not favorable for many biological applications. Therefore, a DEG-functionalization procedure was explored as a strategy to improve the multi-functionality of the nanocarrier by avoiding aggregation and to enhance bioavailability of the drug delivery system [168]. The current work focuses on a new amino-acid-pairing peptide called EAR8-II for drug delivery. This peptide, like other ionic-complementary peptides, can spontaneously organize itself into a nano/micro structure that stabilizes hydrophobic therapeutic molecules and further facilitates passive targeting [3,24]. Additional advantages of using such a peptide as a carrier for drug delivery are the ease with which it can be synthesized and functionalized to incorporate long circulation, active targeting, and low immunogenic properties [23]. In particular, EAR8-II has the benefit of two well-known amino-acid-pairing peptides, EAK16-II [24] and AAP8 [26]. The design strategy exploits the ionic-complementarity of EAK16-II and the short sequence of AAP8. The shorter sequence of the peptide is the easier and less expensive synthesis procedure, and alternative charged residues in the sequence provide spontaneous self/co-assembly of the peptide with hydrophobic compounds such as Ellipticine and Pirarubicin.

EAR8-II (Ac-AEAEARAR-NH_2) is a unique amphiphilic structure (Figure 4.1) of eight amino acids, including Glutamic acid (E), Alanine (A), and Arginine (R). Negatively charged Glutamic acid and positively charged Arginine residues are positioned in the first and second block of the sequence, providing ionic-complementarity. Alanine residues with hydrophobic side chains are located alternatively through the sequence, offering hydrophobic properties to the peptide as a whole. Self/co-assembly characteristics of this peptide arise from its ionic pairs (E and R), and hydrophobic pairs (A) that both promote self-assembly in peptides as well as co-assembly with hydrophobic molecules such as Pirarubicin (THP).

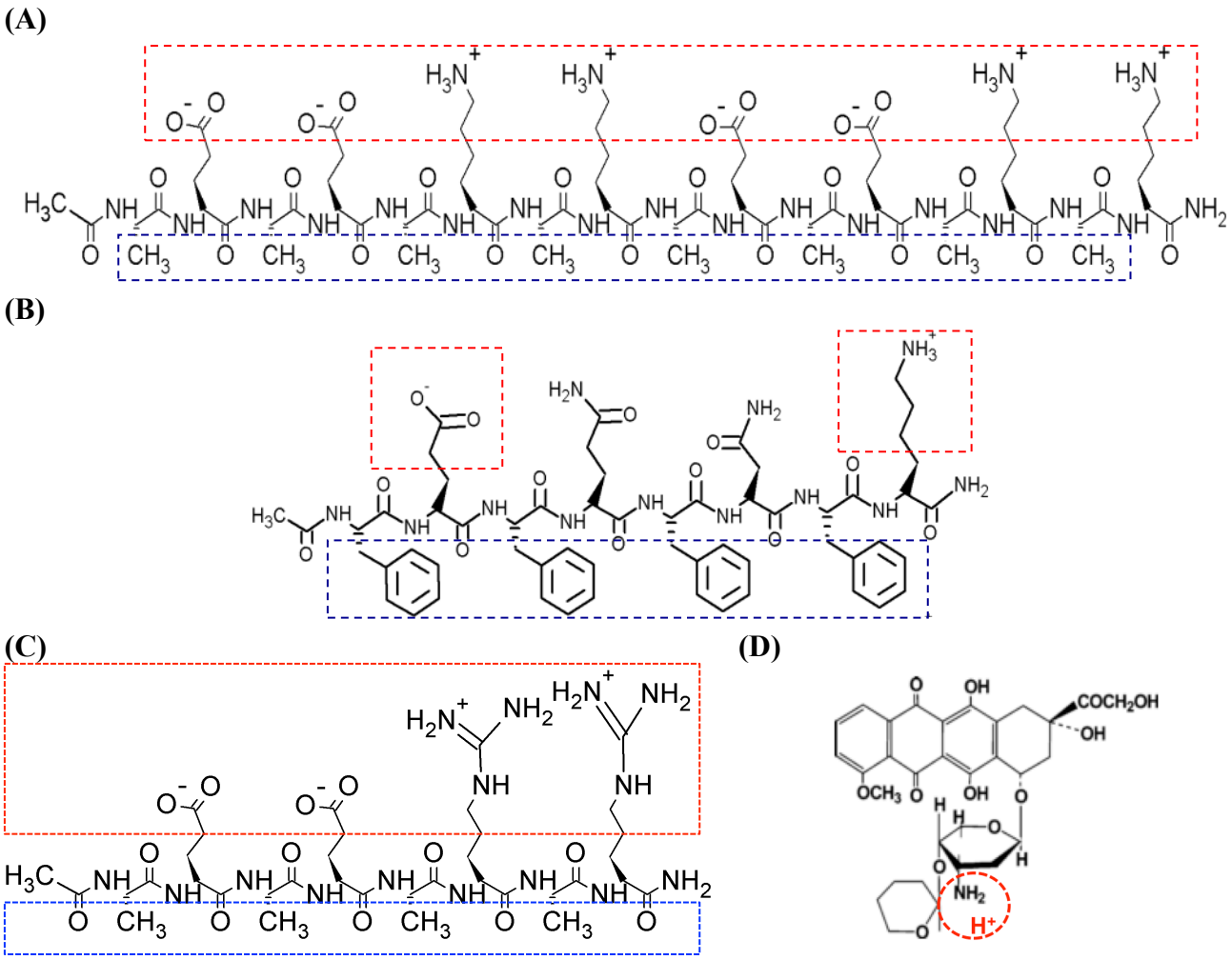

Figure 4.1. Molecular structure of **(A)** EAK16-II (Ac-AEAEAKAKAEAEAKAK-NH_2) [24]; **(B)** AAP8 (Ac-FEFQFNFK-NH_2) [26]; **(C)** EAR8-II (Ac-AEAEARAR-NH2). The red and blue box regions indicate the charged and hydrophobic residues, respectively. E: Glutamic acid (Glu); A: Alanine (Ala); K: Lysine (Lys); R: Arginine (Arg), F: Phenylalanine (Phe); Q: Glutamine (Glu); N: Asparagine (Asn); and (D): Pirarubicin (THP) [169].

Pirarubicin (4-*O*-tetrahydropyranyladriamycin, or THP), a derivative of doxorubicin, is an anthracycline antibiotic, and acts against colorectal cancer [170], liver metastases [171], breast cancer [172], acute leukemia, and malignant lymphomas [11]. It has been reported that THP has fewer cardiotoxic effects than doxorubicin [173]. THP is applied as an anticancer drug model in the current study for the following purposes: intrinsic fluorescence property, hydrophobicity (Figure 4.1), promising anticancer activity, and deleterious side effects in clinical trials [174]. The fluorescence property of THP enables us to monitor the interaction of this drug with peptides and detect it in different physiological environments [169,175,176]. The low solubility of THP in aqueous

environments and its possible side effects in humans highlight the important role of a delivery system for THP. Our self/co-assembling peptide-base carriers have shown characteristics to overcome problems associated with THP delivery.

The main objective of the current study is to find the effective peptide-to-drug ratio for high encapsulation efficiency, drug stabilization, and effective anticancer activity. The techniques applied are fluorescence spectroscopy, dynamic light scattering, and cellular toxicity. Emission fluorescence intensity is correlated proportionally to the concentration of encapsulated THP. Dynamic light scattering is used to determine the stability of THP in peptide solutions by measuring the average particle sizes and surface charge of peptide-drug complexes at different ratios. Anticancer activity and cellular uptake of the complexes against two cancer cells (e.g., A549 and HeLa) are also evaluated to determine the effect of peptide-to-drug ratio on therapeutic efficiency of the complex. This work provides comprehensive knowledge of the formation of peptide and drug complexes and their cellular toxicity at different ratios, paving the way for future cellular, immunological and animal studies in the development of a self/co-assembly peptide-based delivery system for hydrophobic anticancer drugs. Self/co-assembly peptide-based carriers have many advantages over other delivery systems including biocompatibility, low immunogenicity, and capability of sequence alteration based on the required interactions with therapeutic agents.

4.2 Experimental

4.2.1 Materials

The EAR8-II (Ac-AEAEARAR-NH_2) peptide with a molecular weight of 913.94 g/mol and a purity of >75% was synthesized in our laboratory by the solid-phase peptide synthesis (SPPS) method [177]. The *N*-terminus and *C*-terminus of the peptides were protected by acetyl ($COOCH_3$) and amine (NH_2) groups, respectively. The molar mass of this peptide was verified by Matrix-assisted laser desorption ionization time of flight mass spectroscopy (Q-TOF Ultima Global, Waters, Milford, MA, USA). The anticancer drug Pirarubicin (THP) (AB2000083), with the commercial name of THP and molecular weight of 627.63 g/mole, was purchased from ABBLIS (Houston, TX, USA).

All cell lines, purchased from Cedarlane (Burlington, ON, Canada), were used in the current study and cultured in their respective culture medium as follows: Human Cervical Adenocarcinoma: HeLa (CCL-2) in Eagle's Minimum Essential Medium (EMEM) (ATCC30-2003), Human lung

cancer: A549 (CCL-185) in F-12 medium (ATCC30-2004). All medium solutions were prepared with 10% fetal bovine serum (FBS-F1051).

4.2.2 Methods

4.2.2.1 Sample Preparation

EAR8-II peptide solutions in the concentration range of 0.05–2 mg/ml (0.0547–2.188 mM) were prepared by dissolving peptide lyophilized powder in Milli-Q (18.2 MΩ) water (EMD Millipore, Billerica, MA, USA) followed by bath sonicating for 10 min. Freshly prepared peptide solutions were added to THP to reach fixed [THP] concentrations at 0.1 mg/ml (0.159 mM), followed by mechanical stirring at 900 rpm for 24 h.

4.2.2.2 Material Characterizations Methods

Material characterizations techniques such as dynamic light scattering method for estimating size and zeta potential (3.2.2.6), Fourier transformed IR (FT-IR) spectroscopy for secondary structure analysis (3.2.2.4), and atomic force microscopy (AFM) for nanostructure evaluation (3.2.2.2) in this chapter followed the same procedures as presented in Chapter 3.

4.2.2.3 Steady-state Fluorescence Emission

The THP fluorescence emission spectra were acquired on a photon technology international spectrofluorometer (Type QM4-SE, London, ON, Canada) with a continuous xenon lamp as the light source. The emission spectra were collected in the wavelength range of 500–800 nm, while samples were excited at 480 nm. The maximum emission peak of THP is at a wavelength of 590–600 nm. The excitation spectrum was collected in the wavelength range of 200–500 nm. The maximum excitation peak of THP is at wavelength of 470–490 nm. The excitation and emission slit widths of the monochromators, which control the amount of light coming in and out of the sample chamber, were set at ½ and 2 turns to yield a spectral resolution of 1 and 4 nm, respectively. The fluorescence intensity at 590 and 480 nm for emission and excitation were obtained by taking the average of twenty points around each value, respectively. Each fluorescence spectrum was divided by lamp intensity to account for eventual lamp fluctuations [132]. The normalized fluorescence intensity for both emission and excitation spectra at 590 and 480 nm was plotted for various peptide-to-drug ratios.

4.2.2.4 Cellular Toxicity and Uptake

Two human cancer cell lines (A549 and HeLa) at 10^4 cells per well concentrations, were seeded in 96-well plates, followed by treatment with different peptide-drug complex ratios for 24 h. Cellular toxicity experiments were performed with sensitive colorimetric assay called Cell counting kit-8 (CCK-8) (Dojindo Molecular Technologies, Inc. Burlington, ON, Canada). CCK-8 contains highly water-soluble tetrazolium salt (WST-8), which is reduced by dehydrogenase activities in cells to give the yellow color of the formazan dye, which is soluble in culture media. The amount of formazan dye is measured by absorption (O.D.) at 450 nm, which is directly proportional to the number of living cells.

Cellular uptake of THP was also carried out by spectroscopy, exploiting the intrinsic fluorescence properties of THP (excitation wavelength: 480 nm, emission wavelength: 590 nm). Cells were plated in 12-well plates, with concentrations of 2×10^5 cells per well. They were then treated with peptide-drug complexes for 2–4 h. For spectroscopy with the PTI system, after 6 h incubation at 37 °C, the cells were lysed with 1% SDS in Tris-EDTA, followed by probe sonicating to complete cell lysis. The lysed cell suspensions were excited at 480 nm, and emission spectra were collected from 500 to 800 nm to quantify the THP content of the treated cells. Each spectrum was corrected by spectra of lysed untreated cells. The amount of drug uptake is directly proportional to the emission peak intensities. Higher fluorescence emission intensity indicates higher cellular uptake of THP.

4.3 Results and Discussion

The details of the complexation between EAR8-II and Pirarubicin (THP), peptide concentration effect on the complex formation, cellular uptake, and anticancer activity of the formulation are reported here.

4.3.1 Effect of Peptide to Drug Ratio on Complex Formation

EAR8-II, similar to other ionic-complementary peptides such as EAK16-II, was observed to self-assemble into a dense fibular nanostructure with an average width and height of 10 and 15 nm, respectively. However, there was evidence of large aggregates among the fibers, which occurred due to the high concentration of peptide intermolecular interactions of amino acids. The hydrodynamic diameters of these aggregates were measured at ~500 nm resemblance to the particle size distribution observed by DLS, but fibers were in the range of one or two peptide monomers wide. Interestingly, EAR8-II combined with the hydrophobic drug THP forms a fibular bundle nanostructure with a

hydrodynamic diameter of 712.4 ± 17.43 nm, indicating molecular interactions between the peptide and the drug called "co-assembly". The uniformly shaped fibular structure of the peptide-drug complex provides stability and prevents uncontrollable aggregation in an aqueous solution (Figure 4.2).

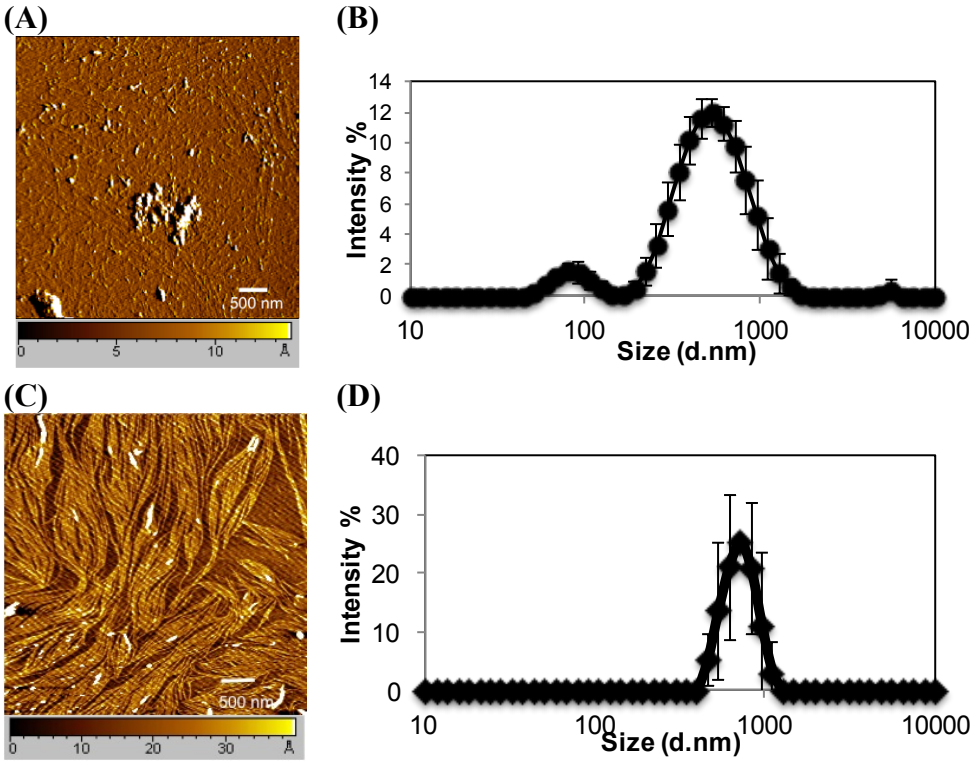

Figure 4.2. Nanostructure of (**A**) EAR8-II and (**C**) EAR8-II-THP complex by tapping mode atomic force microscopy; Intensity-based particle size distribution of (**B**) EAR8-II and (**D**) EAR8-II-THP complex in aqueous solution by dynamic light scattering. EAR8-II concentration is 0.5 mg/ml, and THP concentration is 0.1 mg/ml.

The absorbance peaks from the FT-IR spectrum at 1614–1622 and 1630–1637 cm^{-1} correspond to β-sheets, and peaks at 1650–1658 and 1548 cm^{-1} correspond to α-helical secondary structures. As shown in Figure 4.3, EAK16-II formed β-sheets dominantly, and AAP8 formed a mixture of β-sheets and α-helices. However, EAR8-II showed stronger formation of α-helical structures than the other two self-assembling peptides, probably due to the length of peptide, because intramolecular interactions causing a helical structure in short sequences are stronger than the ones in longer sequences. The FT-IR spectrum collected from the complex containing EAR8-II and THP illustrated a significant increase in absorption intensity at wavenumbers corresponding to α-helical secondary (1654 and 1548 cm^{-1}) structures, compared to the spectrum collected from the peptide solution. The higher absorption intensity in the FT-IR spectrum implies higher amounts of corresponding secondary

structures. The helical fibular bundle structures formed in EAR8-II-THP complexes demonstrate the strong interactions between the peptide and drug to form an organized nanostructure.

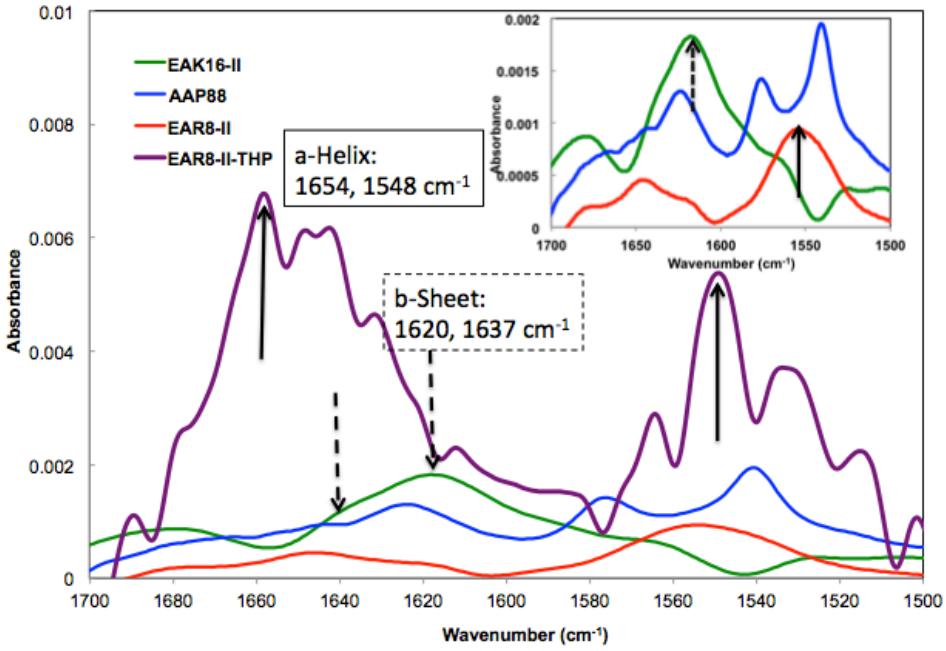

Figure 4.3. Absorbance spectrum of (—) EAK16-II; (—) AAP8; (—) EAR8-II; and (—) EAR8-II-THP complex collected by FT-IR presenting secondary structures.

To determine a suitable concentration of required EAR8-II for THP encapsulation, different concentrations of EAR8-II, in a range of 0.05–1.0 mg/ml, were prepared and combined with THP at 0.1 mg/ml concentration in aqueous solution. Solubility of THP in water is very low, whereas it can be dissolved and stabilized in an EAR8-II solution at a minimum concentration of 0.2 mg/ml. As illustrated in Figure 4.4 (A), at lower EAR8-II concentrations (0.05–0.1 mg/ml), THP molecules were not fully dissolved, and crystalline THP particles floated in the solution. However, at higher EAR8-II concentrations (0.2–0.6 mg/ml), THP molecules were fully dissolved, and consequently, a clear-transparent solution of the peptide-drug complexes formed. At much higher peptide concentrations (above 0.6 mg/ml), THP molecules were still fully soluble, but the excess amount of EAR8-II produced a cloudier solution, with clearly a higher particle size distribution. Note that amphiphilic features of EAR8-II, including the ionic and hydrophobic residues, stimulated binding with hydrophobic molecules of THP through protonation of NH_2 to NH_3^+ in THP molecules and hydrophobic interactions between alanine residues and aromatic rings in the THP structure. Figure 4.1

shows the hydrophobic and hydrophilic regions of EAR8-II peptide, as well as protonation of the amine group in THP. Both ionic and hydrophobic interactions are the possible main interactions of EAR8-II and THP, *i.e.*, the protonation of THP in an acidic EAR8-II solution and hydrophobic interaction between THP and hydrophobic side chains of EAR8-II are the dominant forces in complexation of EAR8-II-THP.

To evaluate the characteristics of the complex formation, the change in size, pH, surface charge, and the THP fluorescence of the peptide-drug complex was monitored at different peptide concentrations. Increasing the concentration of EAR8-II made the THP become more soluble and stable in the solution. The average particle size in these complexes measured by dynamic light scattering (DLS) presented a size increase of up to [EAR8-II] = 0.3 mg/ml, followed by stabilization of the particles in the smaller range of hydrodynamic diameter ~500–700 nm, where at higher [EAR8-II] = 0.8–1 mg/ml, the solution become unstable with larger particles (Figure 4.4). At low concentrations of EAR8-II, non-soluble THP molecules were visible by the naked eye, and the solutions were cloudy. At concentrations of EAR8-II above 0.2 mg/ml, a uniformly suspended complex formed, where THP was fully dissolved. At a very high concentration of EAR8-II (1.0 mg/ml), peptide fibers appeared to aggregate, and the diameter measured by DLS showed a significant size increase.

The surface charge and the pH of the complex were also affected by concentration of EAR8-II. EAR8-II has an isoelectric point of ~6.55, in which at lower pH, the net charge of the peptide in aqueous solution is positive. Results showed that when the peptide concentration was increased, the pH of the solution decreased from pH 5.5 to 3.5 at a concentration of 0.05-1 mg/ml, owing to the higher $[H^+]$ at higher peptide concentrations. Since THP has a pK_a of ~7.3 (pyridine-like nitrogen) it can be protonated in a weakly acidic environment. Consequently, acidic EAR8-II produced protonation of THP at higher peptide-to-drug ratios and led to more positive zeta potential values (Figure 4.5). Basically, an acidic environment provided higher $[H^+]$, and accordingly a higher positive surface charge reflected in zeta potential values. In Figure 4.5, the zeta potential values increased with increasing peptide concentration in the complex. Zeta potential values reached a plateau at EAR8-II concentrations above 0.5 mg/ml, indicating saturation of the positive charge on the surface at high peptide concentrations. Note, negatively charged glutamic acid residues in the peptide sequence may also help to stabilize the protonated THP. The high zeta potential values at very low peptide concentrations did not follow the above trend, due to the presence of non-stabilized protonated THP on the surface.

(A)

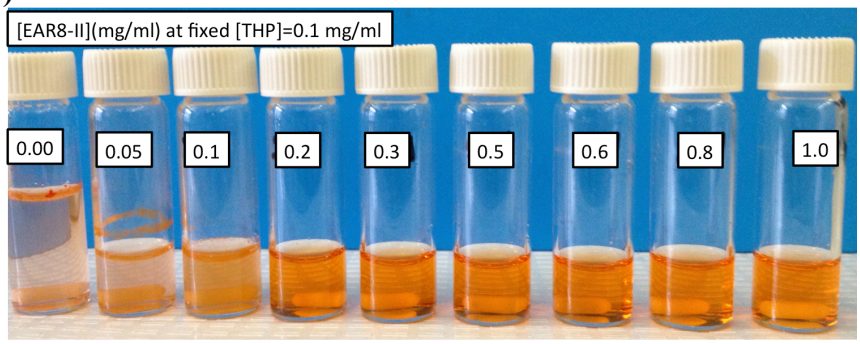

(B)

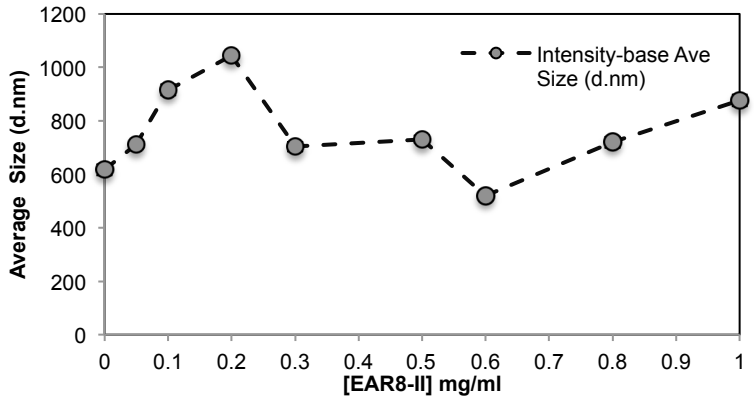

Figure 4.4. (**A**) Appearance of complexes formed by EAR8-II and THP and different EAR8-II:THP mass ratios. (From left to right: THP in water, 1:2, 1:1, 2:1, 3:1, 5:1, 6:1, 8:1, 10:1 mass ratios); (**B**) Intensity-base average hydrodynamic diameter of EAR8-II-THP complexes at fixed [THP] = 0.1 mg/ml. Error bars are standard deviation (i.e. < +/- 3%)

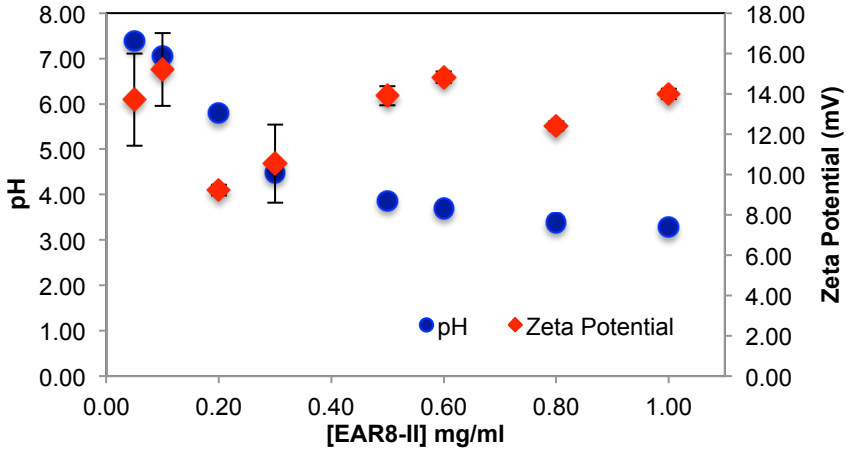

Figure 4.5. Zeta potential and pH of complex at fixed [THP] = 0.1 mg/ml and varied [EAR8-II].

The amount of protonated THP in EAR8-II is also determined by measuring the fluorescence intensity of the excitation and emission by THP at different EAR8-II concentrations. Protonated THP absorbs light at 480 nm, and emits light at 590–600 nm. Normalized fluorescence intensity for both the excitation and emission spectra is proportional to the concentration of protonated THP stabilized in the peptide solution. Although the initial concentration of THP was constant in each complex, the amount of protonated THP varied due to the dependency of the THP encapsulation efficiency on peptide concentration. As shown in Figure 4.6, when peptide concentration increased, the THP fluorescence intensities increased, and plateaued at peptide concentrations above 0.5 mg/ml. At lower peptide concentrations, substantial amounts of non-stabilized THP were present in the solutions, and the fluorescence intensities were significantly low, whereas at higher peptide concentrations where all the THP molecules were stabilized in the peptide aqueous environment, higher fluorescence intensities were collected. Our results showed that the minimum concentration of peptides required to fully encapsulate THP was ~0.5 mg/ml.

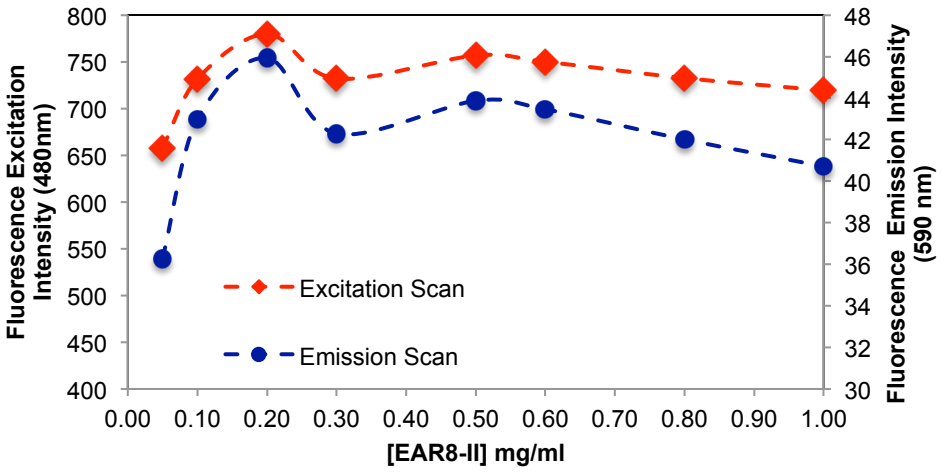

Figure 4.6. Normalized fluorescence emission and excitation intensities from EAR8-II-THP complexes at fixed [THP] = 0.1 mg/ml and varied [EAR8-II].

4.3.2 Cytotoxicity and Cellular Uptake of the Peptide-Drug Complexes

So far, I have illustrated that EAR8-II can stabilize THP in protonated form in aqueous solutions. It is expected that, due to stability and the peptide-to-drug mass ratio, different anticancer activity against cancer cells will be obtained [24,178].

Here, a series of peptide-to-drug mass-ratio complexes at a constant THP concentration of 0.1 mg/ml and EAR8-II at a range of concentrations of 0.05-1 mg/ml were employed to investigate cellular uptake and toxicity against two cancer cell lines (HeLa and A549). Cellular viability profiles for both HeLa and A549 cells at different ratios followed a similar trend, where the cell viability of A549 was relatively higher than that of HeLa, indicating more sensitivity of HeLa cells toward EAR8-II-THP complexes. In the absence of peptide in the complex, THP has been shown to induce non-significant cellular toxicity against both cell lines. Whereas, when EAR8-II stabilized THP in aqueous solution, cellular toxicity of both cells increased significantly. Due to the instability of the THP molecules in aqueous solution they do not penetrate the cell membrane effectively.

As shown in Figure 4.7, the complexes with a peptide concentration below 0.2 mg/ml and above 0.6 mg/ml had lower anticancer activity than the complexes with a peptide concentration between 0.2 and 0.6 mg/ml. Cellular viability of the complexes with an EAR8-II concentration beyond 0.2-0.6 mg/ml was significantly high, in the range of cellular viability observed in the THP control sample. This finding indicated effectiveness of EAR8-II in stabilizing THP in certain concentration ranges. As discussed above, the particle size in complexes in the 0.2-0.6 mg/ml ranges were smaller than those in other ratio complexes, which can be correlated to anticancer activity of the complexes. At lower EAR8-II concentrations, not all the THP molecules co-assembled with the peptide molecules, shown in the particle size distribution and in less efficiency toward cancer cells. However, at higher peptide concentrations, the excess presence of peptide suppressed the proficiency of THP by inhibiting the drug release effectively. The lower cytotoxicity at higher peptide concentration can also be explained by particle size effect, in which with the increased size endocytosis to the cancer cells is inhibited and consequently lower number of cells were killed.

It is speculated that protonated THP molecules were inclined to interact with negatively charged cell membrane and promoted cellular uptake [179]. The hydrophobic properties of THP further stimulated molecules cross the cell membrane and localized in the cytoplasm. As shown in Figure 4.8, cellular uptake of complexes with a peptide concentration between 0.3 and 0.6 mg/ml presented higher cellular uptake for both cell lines than the complexes beyond that ratio. The exception was the peptide-to-drug ratio 1 to 1 and the THP control, showing dramatically high uptake due to accumulation of free THP molecules on the cell membrane without them being fully localized in the cytoplasm. On the other hand, the complexes with higher EAR8-II concentrations (0.8–1.0 mg/ml) showed significantly lower cellular uptake due to highly bound EAR8-II to THP and inhibiting release of hydrophobic THP to the cell membranes.

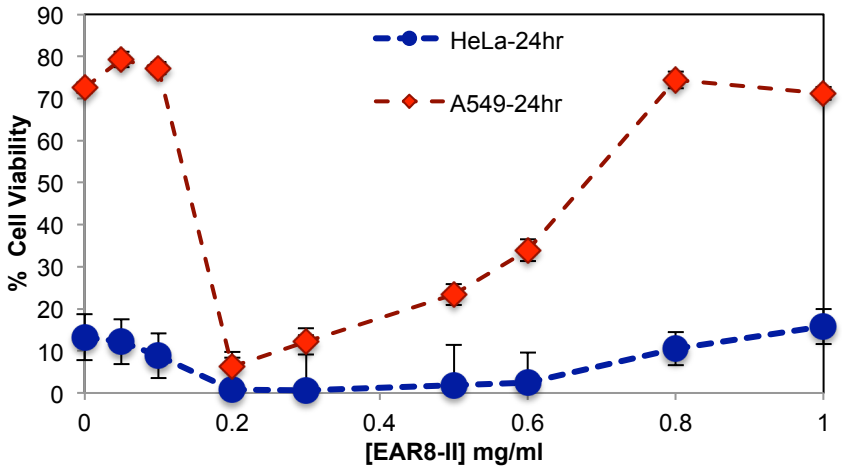

Figure 4.7. Cellular viability of HeLa and A549 cells treated with the complexes for 24 h at fixed [THP] = 0.1 mg/ml and [EAR8-II] = 0.05–1.0 mg/ml.

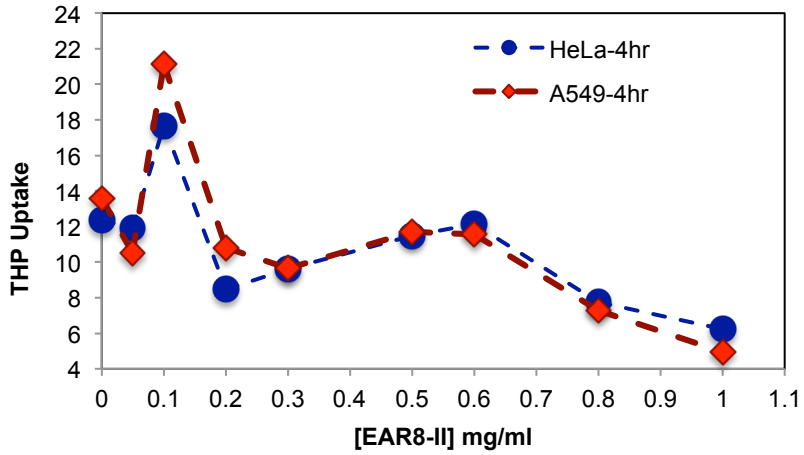

Figure 4.8. Normalized fluorescence emission intensity of THP uptake by HeLa and A549 cell lines treated with the complexes for 4 h at fixed [THP] = 0.1 mg/ml and [EAR8-II] = 0.05–1.0 mg/ml.

A similar pattern was observed in the fluorescence microscopy images from the cells treated with EAR8-II-THP complexes at different ratios. For both cell lines, complexes with peptide concentrations of 0.3 and 0.5 mg/ml resulted in the highest cellular uptake of THP in cytoplasm. In contrast, complexes at lower and higher concentrations of the peptide showed lower localization of THP in cytoplasm. Note that the bright red fluorescence observed in 1:2 and 1:1 ratio complexes were from non-dissolved THP not localized in cytoplasm. At the ratios of 3:1 and 5:1, the localization of

THP in cytoplasm was very uniform, whereas other ratio complexes had THP randomly localized or just accumulated on the membrane (Figure 4.9). These results led us to select appropriate formulations to treat different cancer cells. So far, from the cumulative characterization and cellular uptake and toxicity results, the complex with the peptide-to-drug ratio of 5:1 has been shown to be a more stable and efficient solution for drug delivery, because of its high encapsulation efficiency, uniform nanostructure, relatively high cellular toxicity and uptake.

Au *et al.* emphasized the importance of drug stability upon dilution during treatment time in clinical trials [180]. Since, the peptide-drug complex at a 5:1 ratio illustrated appropriate properties such as size, charge and toxicity against cancer cells, cytotoxicity testing was performed for this particular complex, and its serial dilution solutions were tested against two human cancer cell lines, including the non-small lung cancer cell A549, cervical adenocarcinoma HeLa. Figure 4.10 represents the viability of the cells treated with the 5:1 ratio complex and its serial dilution in water, where the final concentration of THP is between 0.3 and 38 μM. The IC_{50} values of the complex for the cancer cells were calculated, and followed the following trend; THP concentration at ~19.3 μM for A549 >~1.8 μM for HeLa cells [181].

Toxicity results for both serially diluted and variable peptide-to-drug ratio complexes revealed relatively higher cell viability of A549 compared to HeLa cells, denoting that A549 cells are highly resistant towards the EAR8-II-THP complex. Similar results were observed previously for EAK16-II and EPT complexes against MCF-7 cells and A549, in which A549 cells showed higher resistance than other tested cells [24]. The reason for different levels of toxicity of the same complex towards various cancer cells is not fully clear, but it might arise from different reactions of cancer cells to the EAR8-II-THP complex.

Note that the cell viability of the THP control solution (no peptide) for both types of cell lines was significantly higher than for the respective THP concentrations in the presence of EAR8-II. For THP at 38 μM in water, the cellular viability was 64.9 ± 6.4, 29.58 ± 3.69 (%) for A549, HeLa cells, respectively. These findings clarify the important role of EAR8-II in stabilizing THP in an aqueous environment, and consequently delivering it into cells and causing cellular toxicity.

(A)

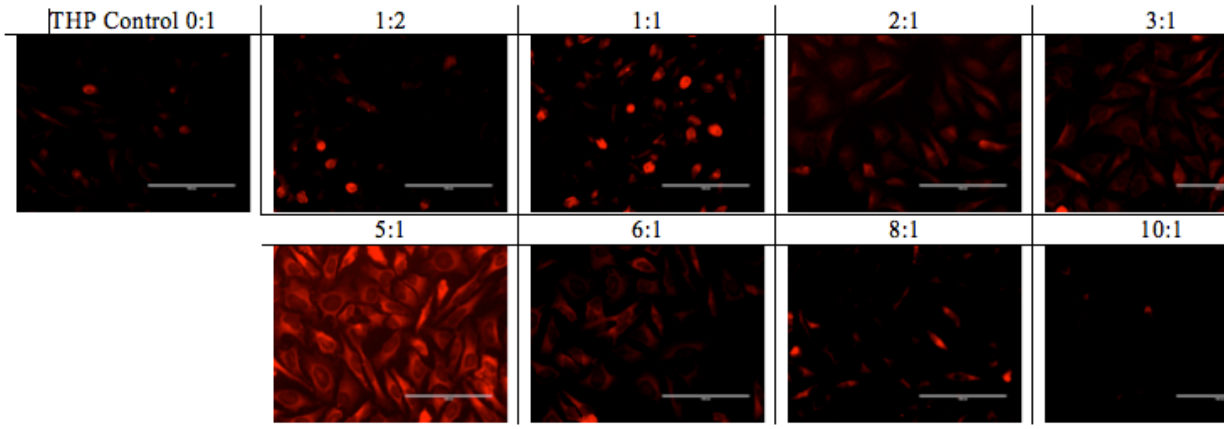

(B)

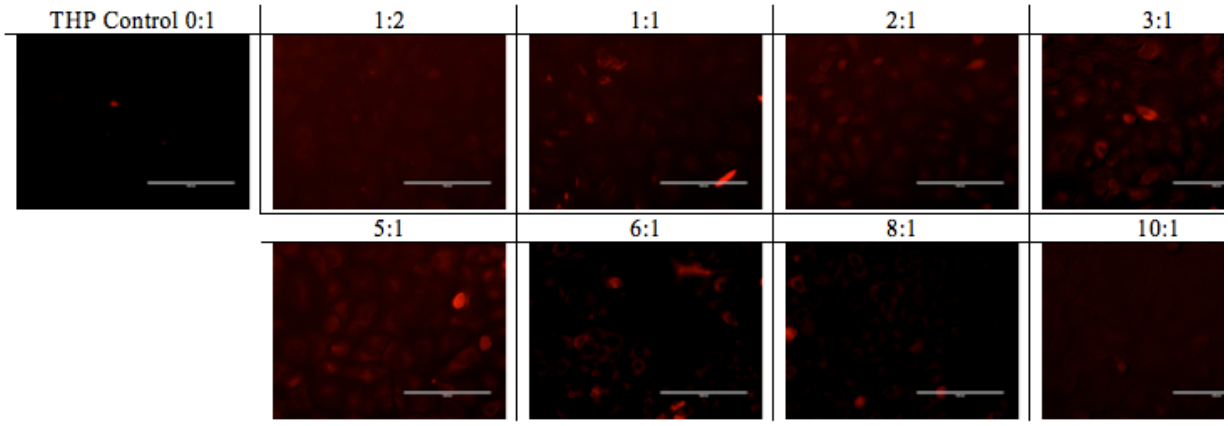

Figure 4.9. (**A**) HeLa cells; (**B**) A549 cells, treated with EAR8-II-THP at fixed [THP] = 0.1 mg/ml and varied [EAR8-II]. The ratios between EAR8-II to THP are indicated above each image. EAR8-II concentrations: (0:1) = 0.0 mg/ml; (1:2) = 0.05 mg/ml; (1:1) = 0.1 mg/ml; (2:1) = 0.2 mg/ml; (3:1) = 0.3 mg/ml; (5:1) = 0.5 mg/ml; (6:1) = 0.6 mg/ml; (8:1) = 0.8 mg/ml; (10:1) = 1.0 mg/ml. Scale bar is 100 μm. Note, all the images are taken with the same exposure time.

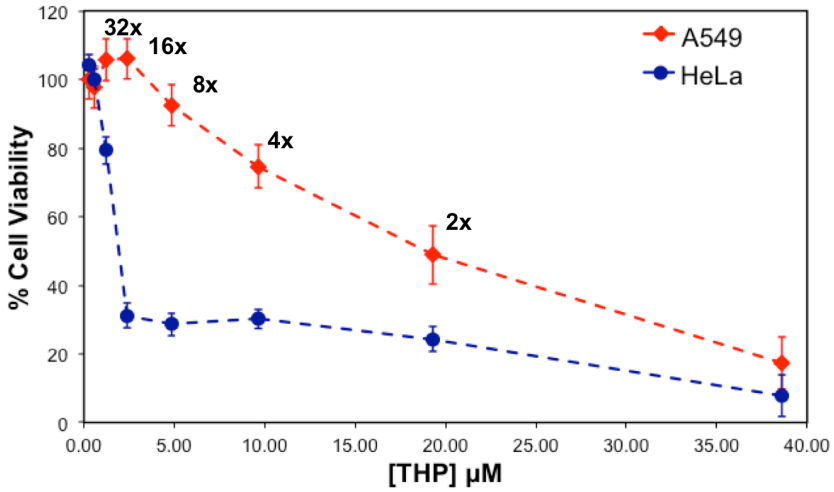

Figure 4.10. Viability of A549, HeLa cells treated with serially diluted complexes at 5:1 EAR8-II to THP complex for 24 h.

In the case of a stable complex upon dilution, the increase in cellular viability happens smoothly and gradually due to the lower drug concentration. Based on the observed cell viability results at 24 h incubation time, the viability of A549 increased gradually, when the complex was diluted. In contrast, the viability trend for HeLa cells did not increase as smoothly as for A549 cells. The increase of HeLa cell viability after sixteen times dilution was sharp, indicating instability of the complex at high dilution factors in water, in the presence of a medium. One reason for complex instability is the instability of protonated THP in a highly diluted complex. As discussed, protonated THP is stabilized in peptide environments at low pH. Higher amounts of water lead to increased pH and consequently lower THP stability in solution. This effect might also arise from the stability of the complex in the different culture media used for different cell lines. The content of each culture medium varied, and THP might have distinct properties in each medium. Further experiments are required to confirm this phenomenon. Overall, EAR8-II-THP complexes at a peptide-to-drug ratio of 5:1 demonstrated promising results against cancer cells and stabilized in the cell culture environment.

4.4 Conclusions

The current article introduced a new self/co-assembling ionic-complementary peptide, EAR8-II, stabilizing the hydrophobic drug pirarubicin (THP) in protonated form in aqueous environments, as shown by surface charge and fluorescence measurements. Results show the complex formation to be peptide-to-drug ratio dependent. Increasing EAR8-II concentration at a constant THP concentration

reduced the pH value of the complex and consequently caused protonation of THP stabilized in solution. At lower peptide-to-drug ratios, an insubstantial amount of THP molecules were solubilized in aqueous solution, according lower fluorescence emission intensity than in complexes with higher peptide-to-drug ratios, in which more THP is stabilized. The peptide-to-drug ratio affected the particle size distribution within a complex; where at very low and very high concentrations of EAR8-II, the average particle size was large, indicating the presence of long fibers and large aggregates in the solution. However, in complexes with peptide concentrations between 0.2 and 0.6 mg/ml, the average particle size observed was ~600 nm. Cytotoxicity and cellular uptake by cancer cell lines demonstrated peptide-to-drug ratio dependent behavior, in which, at very low and very high ratios, the anticancer activity was lower than that of peptide-to-drug mass ratios between 2:1 and 5:1. Deficiency and excess of the peptide in stabilizing THP caused not fully encapsulated and highly trapped THP molecules, respectively. The complex at a 5:1 peptide-to-drug mass ratio was recognized as an optimum peptide-to-drug ratio complex where the highest encapsulation efficiency was observed for the lowest peptide concentration present in the complex. This complex also offered the highest anticancer activity and cellular uptake against cancer cells compared to other ratio complexes. The anticancer activity of this complex and its serial diluted solutions were further studied against two cancer cells. The IC_{50} of THP was calculated as ~19.3 μM for A549 >~1.8 μM for HeLa cells, indicating sensitivity of HeLa cells compared with A549 toward EAR8-II-THP complexes. This study provides a platform for using self/co-assembly peptides as carriers for hydrophobic drugs in future for *in vitro* and *in vivo* applications by introducing a stable complex with relatively high therapeutic efficacy against cancer cells.

Chapter 5[§]

Thermodynamic Characterization of the Interaction between a Peptide-Drug Complex and Serum Proteins

Abstract

The interaction between a peptide-based drug delivery system and two serum proteins, bovine serum albumin (BSA) and immunoglobulin G (IgG), is investigated using fluorescence quenching and calorimetric techniques. An ionic-complementary self/co-assembling peptide, EAR8-II, is employed to encapsulate the hydrophobic anticancer drug pirarubicin (THP) and stabilize it in protein environments. Self/co-assembling properties of the peptide-drug complex (EAR8-II-THP) are shown to be different while interacting with serum proteins compared with the properties of the isolated complex. The results from thermodynamic studies suggest that the drug delivery system has a strong binding affinity (K_{sv} 1689 M^{-1}), exothermic and enthalpy-driven interaction, with BSA and a relatively weak affinity with IgG (K_{sv} 295.2 M^{-1}). In the presence of salt ions, the enthalpy and binding affinity remain unchanged, implying other interactions such as hydrophobic and Van der Waals interactions are present that are not affected by reduced polarity. This work forms the basis for further studies of EAR8-II-THP complexes in the presence of important proteins and for further evaluation of the complexes' immune response and anticancer activity.

Keywords:

Self/co-assembling peptide, drug delivery, serum albumin, immunoglobulin G (IgG), complex-protein interaction, free energy

[§] This chapter is based on a manuscript. ***Sadatmousavi, P.;*** *Kavalenko, E.; Chen. P.* "Thermodynamic Characterization of the Interaction between a Peptide-Drug Complex and Serum Proteins". Submitted ACS- Langmuir**, Jan 2014-** under review

5.1 Introduction

In the past few decades, nanotechnology has emerged as a versatile approach for different applications, including nanomedicine[25], cancer therapy and diagnosis, siRNA[182,183] and drug delivery[184]. At the same time, increasing concern about the toxicological effects of nanoparticles has led to an increase in toxicological studies of nanoparticles, involving interactions between nanoparticles and physiological biomolecules (e.g., plasma proteins). Interactions between nanoparticles and proteins result in the formation of a "bio-nano interface". This interface is also called the protein "corona" and is significantly different from the original engineered nanoparticle's surface. Therefore, what cells and tissues "see and process" are protein-nanoparticle complexes that are formed in the physiological environment [87,89]. The protein coronas of nanoparticles play an important role in determining their circulation half-life, controlled by the process of phagocytosis. Hence, understanding the interaction of nano-materials with plasma proteins is critical to improve the control of therapeutic efficiency, pharmacokinetics and pharmacodynamics [185].

In the current study, we focus on the characterization of serum proteins binding to the previously introduced peptide-drug complex, EAR8-II-THP[**]. EAR8-II is a simple ionic-complementary self/co-assembling peptide that can stabilize Pirarubicin (THP) in aqueous solution [186]. High loading efficiency, stability, and anticancer activity of this complex against different cancer cells encouraged us to further study this complex for its behavior in the physiological environment. Any drug or delivery system applied either orally or intravenously is transported by the blood, which primarily encounters a large quantity of plasma proteins and various cellular components. The chemical composition, size, charge, and shape of nanoparticles influence the protein binding affinity and in consequence affect their interactions with cells and tissues [187]. On the one hand, strong binding between nanoparticles and serum albumin proteins is considered to be an advantage associated with a drug delivery system that provides long-circulating nanoparticles in the bloodstream, protected from immune cells, and consequently enhances drug safety [10]. On the other hand, nanoparticles that bind with IgG as one of the opsonin proteins [188] or fibrinogen as one of the plasma glycoproteins with high affinity to many nanoparticle (e.g. gold, metal oxide, single-wall carbon nanotubes) [189] are considered to have a disadvantage that promotes the macrophage uptake, blood coagulation, protein aggregation and complement activation of the nanoparticles. In addition to effect of nanoparticles shape and structure on protein corona composition, the temperature at which the NPs and proteins are

[**] The term nanoparticle NP and complex are used in this article interchangeably for the peptide-drug complex EAR8-II-THP.

stabilized in physiological environment is an important factor affecting the formation of protein corona. For instance, application of NPs in hyperthermia treatment of tumors can benefit from protein corona composition change at slight changes in temperature [190,191].

In the current study, serum albumin and immunoglobulin G are the two main plasma components studied here to evaluate the binding affinity of the nanoparticle. Serum albumin, with a molecular weight of 65 kDa, is the most abundant protein in plasma, with a concentration of 35-45 mg/ml and a 19-day half-life in humans. Albumin maintains the plasma pH, osmolality, and blood pressure and serves as a carrier for many drugs and small molecules [185,192]. Immunoglobulin and complement activation proteins such as IgG, C3, C4 and C5, on the other hand, are known as opsonin proteins and cause the opsonization process. The low binding affinity of nanoparticles to IgG leads to a lower possibility of phagocytosis followed by lower clearance and enhanced therapeutic efficiency of a drug delivery system [157,193,194].

To evaluate the stability and binding properties of the peptide-drug complex (or NP) in plasma protein solutions, the following methodologies are applied. First, NPs were prepared at their optimal concentration ratios (peptide-to-drug 5:1 mass ratio), followed by incubation with serum proteins at different concentrations. Particle size distributions were measured to determine the effective protein concentrations in stabilizing NPs. Second, a fluorescence quenching technique at different temperatures was employed to assess the thermodynamic binding parameters by exploiting the intrinsic fluorescence of albumin and IgG. Third, isothermal titration calorimetry (ITC) was used to further estimate the binding properties of the protein-nanoparticle. The detailed theory and observations obtained from the above methods are discussed in the following sections.

5.2 Experimental

5.2.1 Materials

The EAR8-II (Ac-AEAEARAR-NH_2) peptide and the anticancer drug Pirarubicin with commercial name of THP were used from the sources presented in Chapter 4 (4.2.1). All serum proteins (including albumin from bovine serum (A7906) and human serum (A8763) and IgG from bovine serum (I5506)) were purchased from Sigma-Aldrich (Oakville, ON, Canada) with > 95% purity. The schematic of the molecular structures of EAR98-II, THP, and BSA are shown in Figure 5.1.

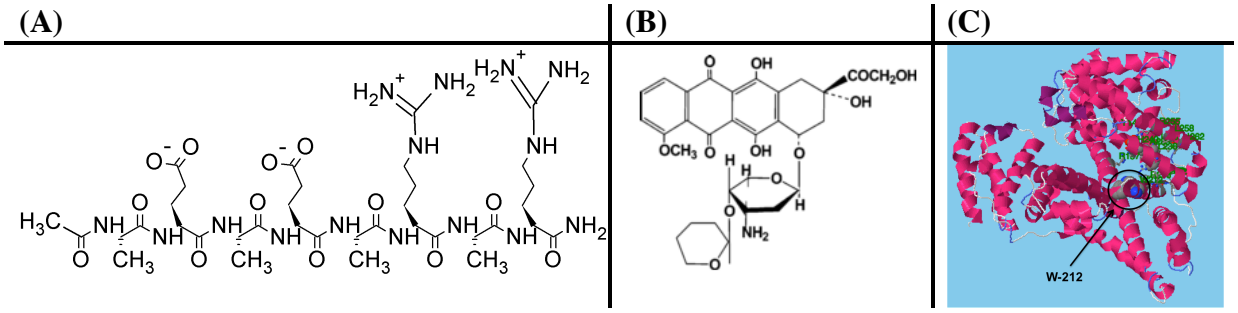

Figure 5.1. Schematic of molecular structure of **(A)** EAR8-II, drawn by ACD/ChemSketch Freeware (Toronto, Canada), **(B)** pirarubicin (THP) [169], **(C)** BSA and Trp-212 is known as a binding site using protein structure prediction by the RaptorX web server.

5.2.2 Methods

5.2.2.1 Sample Preparation

EAR8-II peptide solutions in the concentration range of 0.5 mg/ml (0.547 mM) were prepared by dissolving peptide lyophilized powder in Milli-Q (18.2 MΩ) water followed by bath sonication for 10 min. Freshly prepared peptide solutions were added to Pirarubicin (THP) to reach fixed [THP] at 0.1 mg/ml (0.159 mM) followed by mechanical stirring at 900 rpm for 24 hr. Bovine and human serum albumins were reconstituted in pure water at a concentration range of 4 to 224 µM. IgG from bovine serum was prepared at concentration of 0.1 mg/ml (0.66 µM) in saline solution (150 mM). To study protein and nanoparticle interactions, prepared EAR8-II-THP complexes were mixed with freshly made proteins in a 1:1 [v/v] ratio and was incubated for 2 hr at different temperatures according to the experimental requirements.

5.2.2.2 Fluorescence Quenching of Proteins

Serum albumin and IgG from serum have intrinsic fluorescence with emission wavelength of 350 nm when excited at 285 nm. This fluorescence property comes from tryptophan in binding site II of the albumin structure. This characteristic leads to a simple and reliable fluorescence quenching method to find the binding properties of proteins and the peptide-based drug delivery system. Quenching experiments were conducted on a steady state spectrofluorometer (QM4-SE, Photon Technology International (PTI), London, ON, Canada). Eighty µL of sample were transferred to quartz black 3.0 mm followed by irradiation at 285 nm. The emission spectra were collected from 300 to 800 nm. The excitation and emission slit widths of the monochromators were set to be 1 and 5 nm bandpath, respectively, to control the amount of light coming in and out of the sample chamber. For each

sample, the lamp intensity of the fluorometer was monitored and used to normalize the scattering intensity to correct lamp fluctuations over time. Each collected spectrum from the protein-NP was corrected by subtracting the corresponding spectrum acquired from the peptide-drug complex in the absence of protein. The normalized fluorescence intensity (F_0/F) is plotted against the concentration of the quencher for further Stern-Volmer analysis. A drop in the fluorescence emission intensity due to the existence of other molecules is called fluorescence quenching. Dynamic and static quenching are the two main categories of fluorescence quenching [195]. Both quenching phenomena can be described by the Stern-Volmer equation (Equation 5.1). In this equation, F_0 and F are fluorescence intensities in the absence and the presence of the quencher, respectively. K_{sv} is a Stern-Volmer quenching constant or association constant in the case of static quenching that can also be shown as $K_q^{App}\tau_0$. K_q^{App} is the apparent bimolecular quenching constant; τ_0 is the lifetime of the fluorophore in the absence of a quencher and [Q] is the quencher concentration.

Here, the fluorophores are the serum proteins, and the quencher is the EAR8-II-THP complex. To fit the quenching data, the THP concentration was considered as [Q]. The fluorescence lifetime for BSA is ~ 5 ns [196].

Equation 5.1. Stern-Volmer quenching equation

$$\frac{F_0}{F} = 1 + K_{SV}[Q] = 1 + K_q\tau_0[Q]$$

5.2.2.3 Isothermal Titration Calorimeter (ITC)

Binding properties of proteins from serum and the peptide-drug complex have been thermodynamically characterized by an isothermal titration calorimeter technique. The EAR8-II-THP complex at a 5:1 mass ratio concentration was titrated into protein solutions (BSA at 640 μM and IgG at 6.6 μM) at 25°C. Titrations were performed in NanoITC standard volume with a Hastelloy reaction vessel (TA Instruments, Delaware, USA). The reference vessel was filled with the buffer solution. For serum albumin tests, because the solutions were made in pure water, reference cells were filled with water, whereas for IgG tests, because IgG was prepared in saline (150 mM) the reference cells were filled with saline solution. Each titration consisted of 25 injections at 200-second intervals with a stirring speed of 250 rpm. A 300-second baseline was collected before the first injection and after the last injection. Prior to starting the titration, the calorimeter was equilibrated to a baseline with a drift of less than 100 nW over a thirty-minute period. The data were fitted using an independent

method (1:1 binding isotherm) to estimate the thermodynamic parameters, including the binding constant, stoichiometry, ΔH, ΔS, and Gibbs free energy (ΔG).

5.2.2.4 Transmission Electron Microscopy (TEM)

The nanostructure of bovine serum albumin, self-assembled peptide-drug complexes, and the protein-NP was observed by transmission electron microscopy (type CM20, Philips Electronics Ltd, Guidford, U.K.) at an accelerating voltage of 200 kV. Images were digitized using a Gatan 679 slow-scan CCD camera and analyzed using Digital micrograph (version 2.1, Gatan Inc. Pleasanton, CA). Freshly prepared sample solutions were incubated on a 400-mesh carbon coated Formvar copper grid (Marivac Ltd., St. Laurent, QC) for 10 min. Extra moisture was taken from the edge of the grid with tissue paper. After air-drying for 20 min, the grid was negatively stained with 2% (w/v) uranyl acetate for 5 sec. Excess stains were drawn off with tissue paper and the grid was air-dried before TEM imaging. The TEM images underwent further dimension analysis with Gwyddion software (Free SPM data analysis software). Detailed experimental methods for, FT-IR spectroscopy, circular dichroism, and dynamic light microscopy were adapted from Chapter 3 (3.2.2.4 and 6) [25,168].

5.3 Results and Discussion

5.3.1 Effect of Protein Binding on Peptide-Drug Complex Structure

EAR8-II-THP nanoparticles (NPs) form a fibril bundle nanostructure in aqueous solution with helical secondary structures with an effective diameter of ~ 712 nm. EAR8-II is an amphiphilic ionic-complementary peptide that stabilizes hydrophobic THP molecules. These NPs are positively charged (pH 3.87) due to the protonation of THP (pK_a = 7.3) in the peptide environment and have a zeta potential of +11.5 mV. On the other hand, bovine serum albumin (BSA) is a negatively charged protein at pH 7 with a zeta potential of ~ -28 mV and has an effective diameter of ~ 10 nm. This protein forms predominantly α-helix secondary structures observed by FT-IR (1654 and 1548 cm^{-1}). BSA is known for its hydrophobic functional groups that can be initial targets for its association to other molecules such as surfactants or hydrophobic molecules. Interestingly, we found exceptional stability of EAR8-II-THP nanoparticles in BSA solution in biological studies. Therefore, we determined that it is worth studying the detailed binding properties of NPs and BSA using different methods to demonstrate the nature of binding and understand the effect of binding in biological applications.

The morphology of the EAR8-II-THP nanoparticles was changed due to binding to the BSA molecules (64 μM). The images obtained by TEM presented an alteration in the fibular structure of EAR8-II-THP nanoparticles into a more globular structure similar to the BSA nanostructure (Figure 5.2A-C). In order to understand the behavior of NPs in BSA solution, a range of BSA concentration solutions were mixed with a constant concentration of NPs and characterized for self-assembling properties. The particle size distribution of solutions containing BSA and NP has shown a bimodal distribution of particles including a peak at ~ 2-20 nm and a peak at 200-1000 nm. To identify what each peak represents, the BSA-NP mixture was centrifuged for 1 hr at 17000 rcf, and then the size of supernatant was measured. The intensity of the peak around 200-1000 nm for supernatant was lower than the sample before centrifugation, indicating the unbound nanoparticles were precipitated. The population of the particles in a range of 2-20 nm, which is slightly larger than particle size for isolated BSA particles, remained unchanged representing stable BSA-bound NPs in the solution (Figure 5.2D).

Dynamic light scattering results showed the particle size dependency on the BSA concentration in BSA-NP complexes. By increasing BSA concentration the population of BSA-bound NPs increased, whereas the population of unbound-NPs decreases (Figure 5.2E). At lower BSA concentrations there was not enough protein to bind with all present NPs, at BSA concentration higher than 64 μM (above molar ratio [BSA]/[NP] = 0.4), the population of unbound EAR8-II-THP nanoparticles remained constant ~ 10% showing binding saturation between NPs and BSA. Therefore, increasing BSA concentration above 64 μM would only induce free proteins in the solution not participating in binding process. Therefore, for further characterization, BSA at concentration of 64 μM was selected to ensure free protein did not exist in the solution and the amount of unbound NPs is minimum.

The intensity-based particle size distribution showed a significant decrease in the size of the complexes when it was combined with BSA. This change was more noticeable with longer incubation times. After two days of incubation, the majority of the particles were in the size range of 2-20 nm. This suggested that over time most of the unbound EAR8-II-THP particles disassemble and reorganize into smaller spherical structures. Stabilizing nanoparticles in serum albumin is considered a great advantage for future drug delivery purposes.

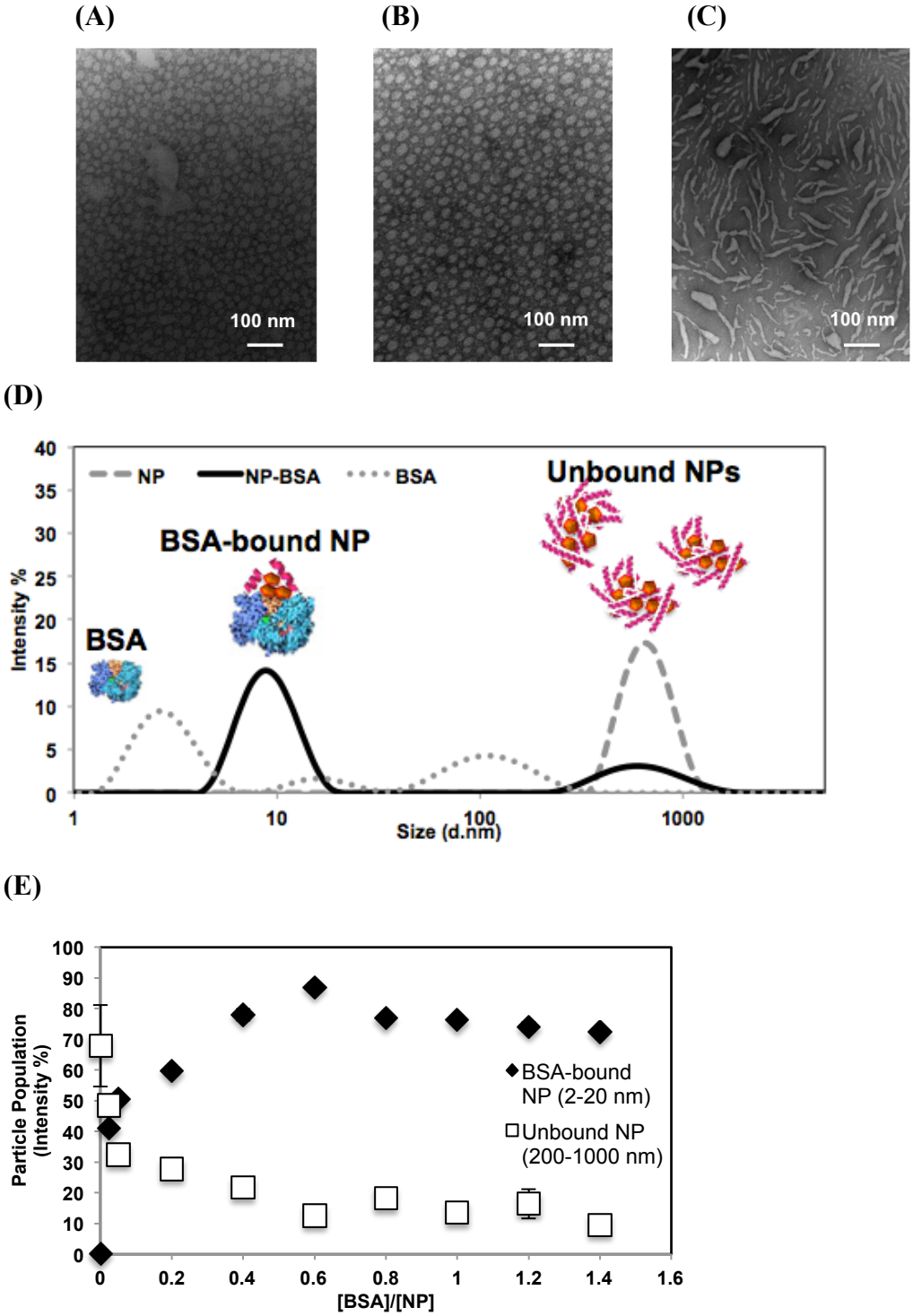

Figure 5.2. Particle size analysis of EAR8-II-THP and serum albumin. TEM images; **(A)** BSA (64 µM), **(B)** EAR8-II-THP (NP)-BSA complex, **(C)** EAR8-II-THP (NP). **(D)** Intensity-based particle size distribution of the above samples measured by DLS. [BSA] = 64 µM, [EAR8-II]= 0.547 mM, [THP]=0.159 mM **(E)** Effect of BSA concentration on particle size distribution of BSA-NP compounds. The error bars are standard deviations (i.e., +/- 3%)

The secondary structures of BSA and BSA combined with the NPs were determined by collecting absorbance spectra by CD and FT-IR methods. Both CD and FT-IR spectra showed a dominant α-helix structure for BSA solution, and combination of α-helix and β-sheet for the EAR8-II-THP complexes. The spectrum from EAR8-II-THP compound resulted in formation of a mixture of α-helix (1654 cm^{-1}) and β-sheets (1620 cm^{-1}) as secondary structures. The spectrum from the BSA solution showed a mainly α-helix secondary structure (two main peaks at 1654 and 1548 cm^{-1}) with significantly higher intensity than the one observed with isolated nanoparticles [196–198]. When the NPs are combined with BSA, the results no significant change is spectrum compared to BSA in the absence of NPs, indicating no significant conformational change in BSA secondary structure while bound with EAR8-II-THP complexes. (Figure 5.3).

(A)

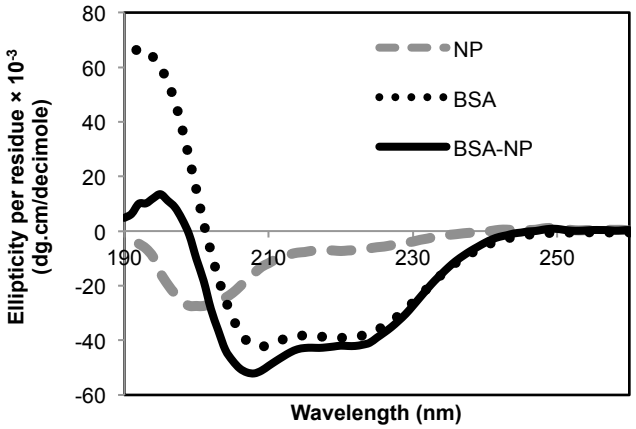

(B)

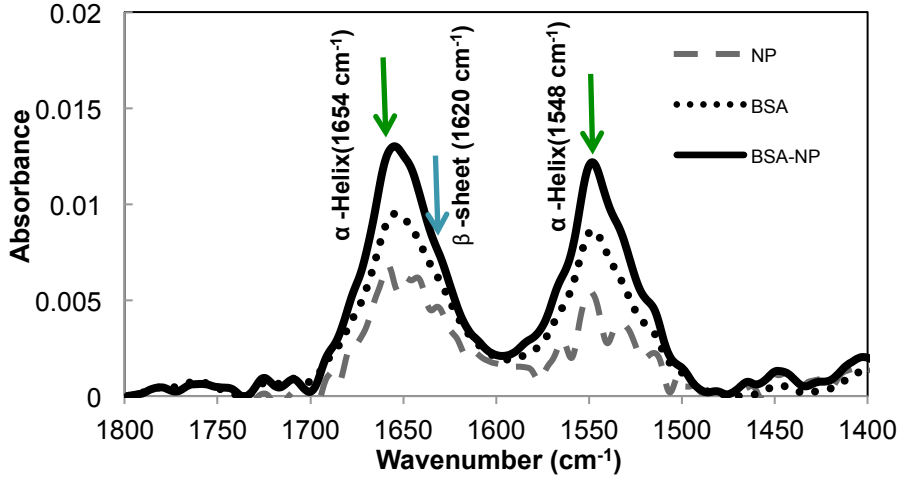

Figure 5.3. **(A)** CD spectra collected from EAR8-II-THP (NP), BSA and NP-BSA complexes. All four spectra are baseline corrected., **(B)** FT-IR spectra of above complexes collected by Bio-ATR FT-IR at [BSA] = 8 μM, [EAR8-II]= 0.547 mM, [THP]=0.159 mM

5.3.2 Thermodynamic Characterization of Peptide-Drug Complex Binding with Serum Proteins

As discussed above, the EAR8-II-THP complex showed noticeable stability in a serum albumin environment without the tendency to aggregate over time. To evaluate the binding properties of the peptide-drug complex and serum albumin (BSA), a fluorescence quenching technique and an isothermal titration calorimeter (ITC) were applied in the current study.

5.3.2.1 Fluorescence Quenching of Serum Proteins

BSA contains a single polypeptide chain of 607 amino acids with two tryptophan residues (Trp-134, and Trp-212) located in the first and second domains of the protein hydrophobic regions [199]. Exploiting the tryptophan residue's fluorescence emission, BSA quenching experiments have been employed to evaluate the binding affinity of nanoparticles to BSA. A drop in the fluorescence emission intensity due to the existence of other molecules is called fluorescence quenching. The fluorescence emission of BSA at 350 nm was reduced as the complex's concentration [THP] was increased due to tryptophan quenching (Figure 5.4A). The plot of F_0/F vs. concentration of [THP] (Figure 5.4C) represents the Stern-Volmer quenching relation, in which the slope corresponds to the binding constant K_{SV}. Dynamic and static quenching are the two main categories of fluorescence quenching that can be presented by linear Stern-Volmer plot [195]. Dynamic quenching is also known as collisional quenching in which the quencher diffuses to the fluorophore during its excitation lifetime. After contact, the fluorophore returns to the ground state without any emission. In dynamic quenching, there is no permanent change in the molecules, whereas in the case of static quenching, a complex between the fluorophore and the quencher is formed and the complex does not emit strong fluorescence. It is important to realize that linear Stern-Volmer plot does not prove that collisional quenching has certainly occurred, however, static quenching is also results in linear Stern-Volmer plots. Static and Dynamic quenching can be distinguished by their differing dependence on fluorescence lifetime measurements, and the following factors that were considered in the current study : (i) temperature dependence; higher temperatures result in faster diffusion and therefore more possibility for collisional quenching. In other words, increasing the temperature will increase the slope of the Stern-Volmer plot during dynamic quenching. This is due to the dissociation of weakly bound complexes. However, in static quenching, increasing the temperature leads to a lower Stern-Volmer slope. Increasing temperature results in decreased stability of bound complexes, which leads

to lowering the quenching constant driven from the Stern-Volmer plot. In the current study, BSA was prepared at a 64 μM concentration and incubated with a series of EAR8-II-THP concentrations at 4°C, 25°C, and 37°C for two hours. The fluorescence spectra of BSA were collected for all solutions and normalized by air light scattering (to correct for lamp fluctuation) followed by subtracting the corresponding EAR8-II-THP spectra. F_0/F was plotted versus the THP concentration to find the Stern-Volmer fitting parameters at different temperatures. The association constant is decreased by increasing temperature, indicating a weakening of the bound complexes at higher temperatures, suggesting static quenching (see Figure 5.4C).

(ii) Absorption spectra of the fluorophore; in collisional quenching, only excited states of the fluorophore change and the absorption spectra are expected to remain unchanged. However, in static quenching, the formation of the ground-state complex results in a slight shift in the absorption spectra. This effect for the NP-BSA is shown in Figure 5.4 B, in which the absorption spectra of BSA showed a strong peak at 280 nm, where this absorption reduced significantly in BSA combined with EAR8-II-THP complex suggesting the static quenching of BSA by the complex.

(iii) Bimolecular quenching constant: diffusion-controlled quenching typically shows the k_q^{App} value near 1×10^{10} $M^{-1}.s^{-1}$. For dynamic quenching, this value is smaller than this threshold due to steric shielding of the fluorophore. Static quenching typically shows higher values, which indicates stronger binding interactions between the fluorophore and the quencher [195,200]. In the current study, the calculated apparent bimolecular quenching constants (K_q^{App}) for all three temperatures have higher values than 1×10^{10} M^{-1} s^{-1}, which suggests that the quenching was initiated not by collisional quenching but by static quenching, and a compound formed between the BSA and the EAR8-II-THP complex.

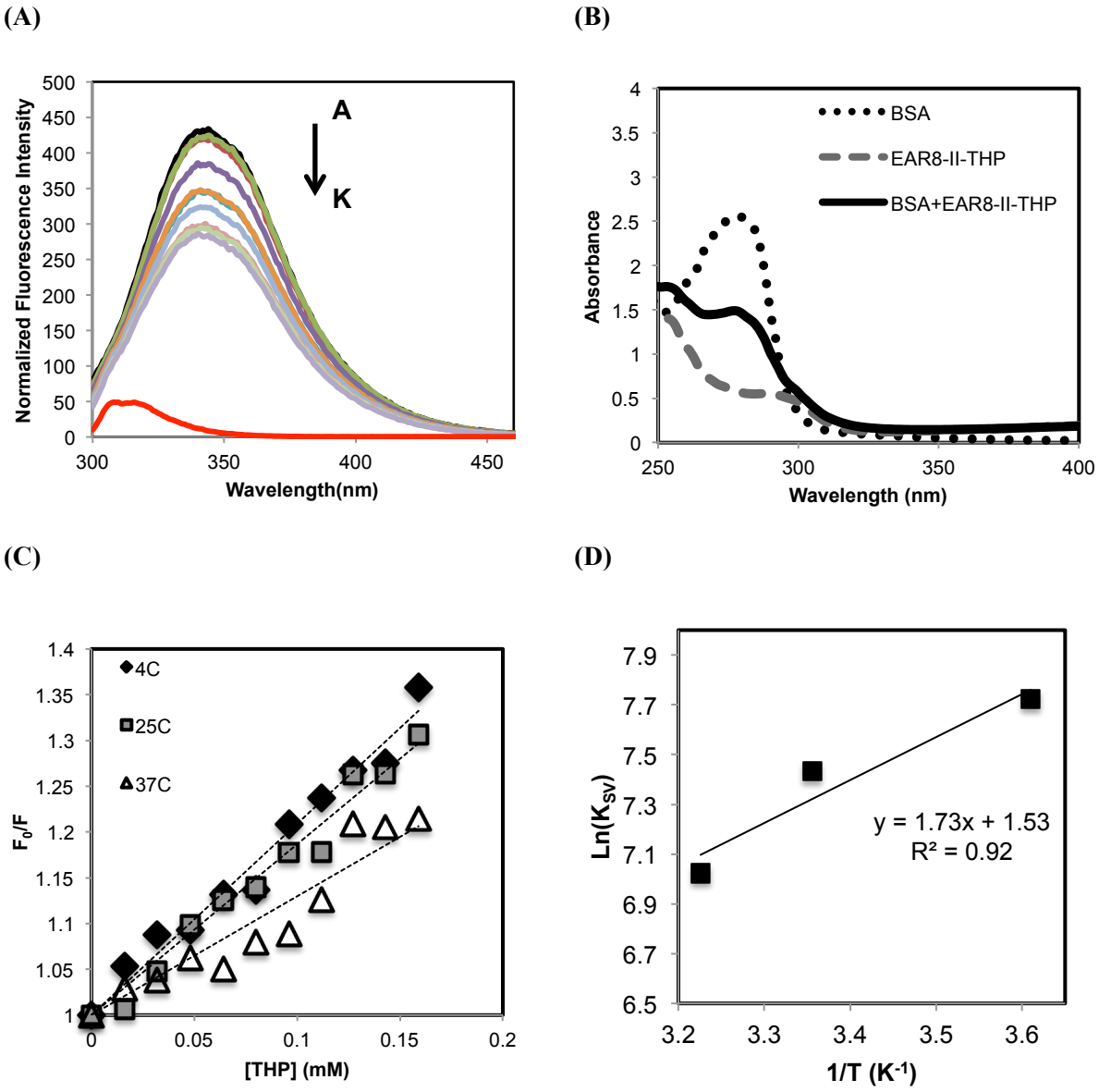

Figure 5.4. Quenching of BSA by the EAR8-II-THP complex. **(A)** Effect of the EAR8-THP complex on the intrinsic fluorescence of BSA at 298K (25°C). (Black) [BSA]: 64 µM, and (Red) EAR-THP complex is at [EAR]: 0.55 mM and [THP]: 0.159 mM. (A-K): [THP] in mixture is: 0, 0.016, 0.032, 0.048, 0.064, 0.080, 0.096, 0. 2, 0.127, 0.143, 0.159 mM, respectively. **(B)** Absorption spectrum of BSA (dotted), EAR8-II-THP complex (dashed) and the mixture of BSA and EAR8-II-THP (solid) **(C)** Stern-Volmer plot at different temperatures**. (D)** Van't Hoff plot for the interaction of EAR8-II-THP and BSA at different temperatures. ΔH = -14.35 kJ/mol, and ΔS = 12.7 J/mol.K.

The interaction between the fluorophore and the quencher can occur due to various forces, including hydrophobic, electrostatic, hydrogen bonding, and Van der Waals interactions. To calculate the thermodynamic parameters of BSA binding to the EAR8-II-THP complex, the Van't Hoff

equation has been applied to the static quenching binding constant (K_{LB}) at different temperatures [202]. When enthalpy (ΔH) does not change significantly in the range of temperatures, ΔS can be driven from this equation (Equation 5.2).

Equation 5.2. Van't Hoff thermodynamic equation

$$\ln(K_{SV}) = -\frac{\Delta H}{RT} + \frac{\Delta S}{R}$$

In the BSA-NP system, the enthalpy and entropy can be driven from the slope and y-intercept of the ln(K_{SV}) versus 1/T plot. The Gibbs free energy is also estimated from $\Delta G = \Delta H - T\Delta S$ at each corresponding temperature (Table 5.1). Negative values of ΔG (~ -18 kJ/mol) and ΔH (-14.35 kJ/mol) convey that the interaction between BSA and the peptide-drug complex is a spontaneous and exothermic reaction. The small value of ΔS (12.71 J/mol.K) indicates that the reaction is more enthalpy driven and entropy is unfavorable showing hydrogen bonding and van der Waals forces are dominant forces. Notably, this protein quenching is only observed when encapsulated THP by EAR8-II was interacting with BSA, whereas naked THP (without EAR8-II) does not show any significant quenching of tryptophan in serum albumin. This proves the unique capability of the self-assembling peptide in stabilizing a hydrophobic agent in the physiological environment. By increasing the temperature, the binding affinity decreased slightly, suggesting weakening the forces between BSA and peptide-drug complexes. Furthermore, the effect of salt is investigated in this work to confirm the nature of the binding. The interaction between BSA molecules and THP only occurs when THP is already stabilized in an EAR8-II solution; otherwise, THP molecules alone are not solubilized in a BSA solution and do not induce fluorescence quenching. EAR8-II as an amphiphilic peptide first stabilizes THP in an aqueous environment, promoting the BSA interaction.

The fluorescence quenching results suggested a binding between BSA and the peptide-drug complex, however, for more confirmation on nature of quenching whether is static or dynamic fluorescence lifetime measurement is highly recommended.

Table 5.1. Summarized data on BSA quenching by EAR8-II-THP

Stern-Volmer				
T (°C)	$K_{sv}(M^{-1})$	$K_q(M^{-1}\ s^{-1})$	R^2	ΔG(kJ/mol)
4	2259.9	3.83E+11	0.974	-17.87
25	1688.6	2.86E+11	0.975	-18.14
37	1123.2	1.90E+11	0.903	-18.29

5.3.2.2 Isothermal Titration Calorimeter (ITC)

Isothermal titration calorimetry (ITC) is a powerful procedure for investigating the thermodynamics and stoichiometry of molecular binding processes. This technique can be used in nanoparticle and protein assemblies to directly determine (a) binding stoichiometry, (b) nature of binding (entropy or enthalpy driven), (c) binding affinity between titrant and titrate [90,203,204]. In the current study, ITC was applied to evaluate the binding and thermodynamic parameters of the NP to BSA at 25°C to complement the quenching data. Titration was performed by slowly adding a peptide-drug complex (NP) solution into the protein solution and monitoring the heat difference that needs to be added to the sample and reference cells to maintain the two cell temperatures constant. The results are plotted as a heat rate against time plot. If the reaction is exothermic, the heat that must be added to the sample cell is less and a negative signal is observed (Figure 5.5). When both titrant and titrate concentrations are known by an isothermal fitting analysis of enthalpy vs. [NP]/[Protein] ratio curves, we estimate thermodynamic parameters such as binding constants K_a (M^{-1}), enthalpy changes ΔH (kJ. mol^{-1}), ΔS (kJ $mol^{-1}K^{-1}$), and binding stoichiometry *n*. The Gibbs free energy (ΔG) is also determined from common thermodynamic relations: $\Delta G = \Delta H - T\Delta S$ or $\Delta G = RT \ln (K_a)$. Table 5.2 summarizes the binding parameters for the NP-BSA complex and compares the corresponding values with the fluorescence quenching data at 25°C. Note that the concentration of titrant (NP) is ten times higher than the original concentration of NP used in the quenching experiment. This concentration adjustment is due to the need to obtain a substantial heat rate at the very first injections and low volumes.

Thermodynamic values from both techniques indicate that the protein-nanoparticle interaction is a spontaneous reaction, with data showing a negative free energy change ($\Delta G < 0$). The peptide-drug complex and protein interaction involves an unfavorable negative entropy change ($\Delta S < 0$) that is compensated by a favorable highly negative enthalpy change ($\Delta H < 0$). Negative enthalpy change is indicative of an exothermic process, which is comparable to the albumin bindings to NPs observed by ITC. The stoichiometry value acquired from ITC is at 1.87 for [NP]/[BSA], which is fairly comparable with the results of ratio effect on particle size analysis. At the ratio of [BSA]/[NP] ~ 0.6 and higher, which corresponds to [NP]/[BSA] ~ 1.67, most NPs are bound to BSA and beyond that ratio binding saturation occurs similar to what happens in ITC thermal profile. Despite the difference observed between thermodynamic values from both quenching and calorimetry methods, the binding behavior in the NP-BSA system showed a similar trend. ITC is the method that offers thermodynamic values directly by measuring the heat transfer while binding, whereas the fluorescence quenching

method is an indirect technique using the Van't Hoff equation; therefore, more error is associated with the obtained values.

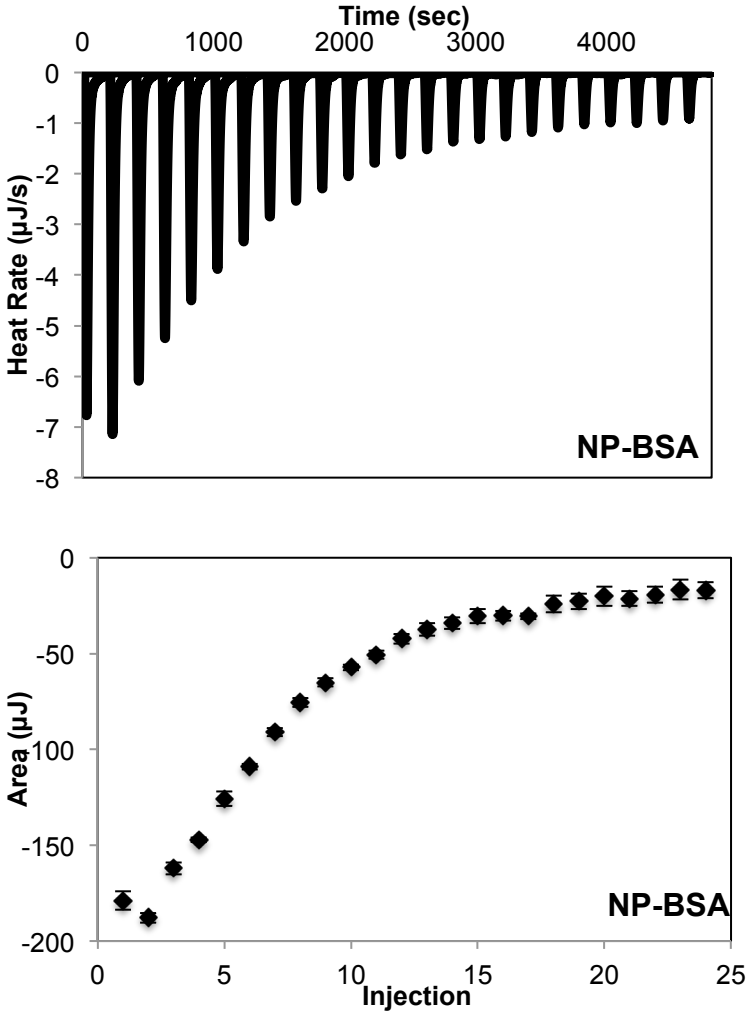

Figure 5.5. ITC result plots for (NP). EAR8-II-THP (5:1 mass ratio) complexes were titrated to BSA 64 µM at 25°C. [EAR8-II]=5 mg/ml, [THP]=1 mg/ml.

Table 5.2. Thermodynamic parameters obtained by ITC and fluorescence quenching for NP and BSA binding

	K_a (M^{-1})	ΔH (KJ/mol)	ΔS (J/mol. K)	ΔG (KJ/mol)	n
ITC	3.97E+04	-66.2	-134.1	-26.24	1.87
Quenching	1.68E+03	-14.35	12.71	-18.14	-

5.3.3 Effect of Salt on Binding Properties

To determine the nature of binding between tryptophan residues in BSA and EAR8-II-THP complexes, all of the samples were made in saline solution (150 mM) to further examine the particle size and thermodynamic binding parameters. Theoretically, salt molecules prefer to hydrate with water molecules in the solution, so they differ in binding behaviors between protein and nanoparticle molecules. Increasing the salt concentration reduces the polarity of the solution and decreases the amount of surrounding water on the surface of the protein and nanoparticles. Therefore, the presence of the salt molecules causes a change in the binding affinity of the protein interaction and provides energy for dehydration. If the main driving force in the protein-nanoparticle interaction is electrostatic force, increasing the salt concentration reduces the polarity of the system and lower binding affinity will be observed. However, when hydrophobic interaction is the main driving force in protein interaction, adding salt contributes to dehydration and leads to a higher binding affinity [202]. One of the major reasons for stronger hydrophobic interaction in the presence of salt is that decreasing the amount of water on the protein surface causes instability in the protein structure.

Adding salt to the EAR8-II-THP and BSA system did not significantly affect the binding affinities. The Stern-Volmer parameters and thermodynamic values from calorimetry were not altered considerably in the presence of salt. In addition, based on the results that the binding is mainly enthalpy-driven and entropy in unfavorable for it, hydrogen bonds and van der Waals interactions played major roles in the reaction between BSA and EAR8-II-THP complexes (Figure 5.6, and Table 5.3).

Table 5.3. Effect of salt in the binding properties of BSA and EAR8-II-THP.

	Stern-Volmer			ITC				
	K_{sv} (M^{-1})	K_q (M^{-1} s^{-1})	R^2	K_a (M^{-1})	ΔH (kJ/mol)	ΔS (J/mol.K)	ΔG (kJ/mol)	n
No Salt	1688.6	2.86E+11	0.975	3.97e4	-66.20	-134.1	-26.24	1.87
With Salt	1734.2	2.94E+11	0.931	3.73e4	-54.97	-96.92	-26.08	1.46

(A)

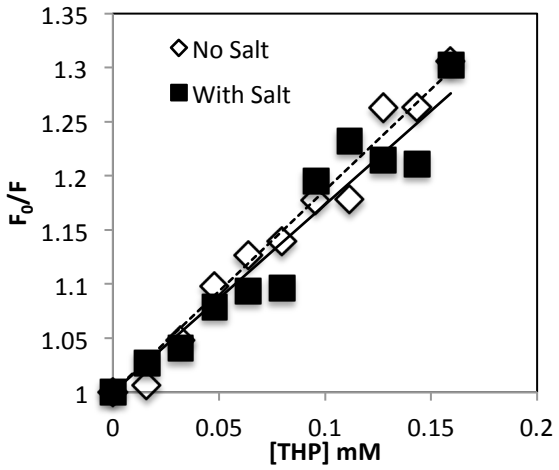

(B)

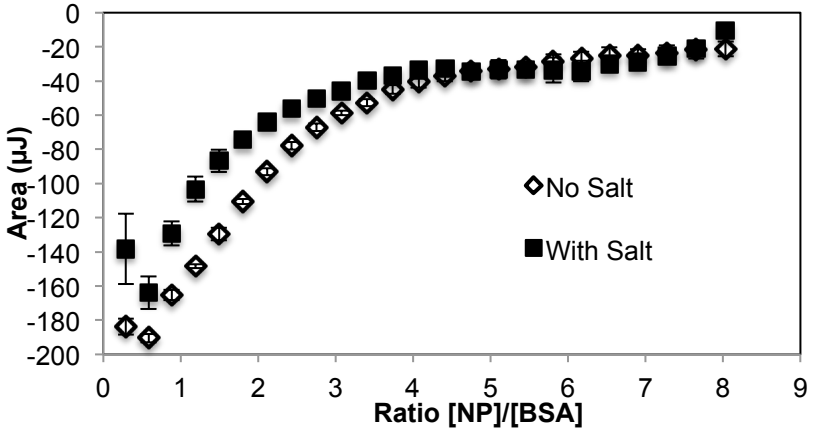

Figure 5.6. Effect of salt (155 mM) on the protein interaction, **(A)** Fluorescence quenching: Stern-Volmer plots for BSA quenched by EAR8-II-THP, **(B)** ITC: integrated heats in each injection versus molar ratio of [NP]/[BSA].

5.3.4 Immunoglobulin G Binding Properties

The same techniques (ITC, fluorescence quenching and particle size) that were applied to determine albumin-binding properties were employed to characterize the immunoglobulin G binding parameters to the EAR8-II-THP nanoparticles. Immunoglobulin G (IgG) is a protein containing four peptide chains: two identical heavy chains and two identical light chains formed in a typical Y-shape antibody monomer. Similar to serum albumin, IgG also has a typical intrinsic fluorescence due to a tryptophan residue when excited at 285 nm [205,206]. The results from the fluorescence quenching of immunoglobulin G (IgG) by EAR8-II-THP molecules showed the Stern-Volmer constant to be significantly lower than what it was calculated from the quenching of BSA. The quenching constant is lower than the dynamic quenching threshold, suggesting collisional quenching of IgG by NPs. The Stern-Volmer equation fit poorly with a low fitting parameter (R^2), indicating no significant binding between the molecules (Figure 5.7A). As discussed above, collisional quenching is due to the random contact of molecules and does not induce a strong binding between the quencher and the protein molecules. In contrast, BSA protein molecules have shown to be quenched by NPs in a static manner representing the formation of BSA-NP bound molecules. Similarly, the heat produced by calorimetry is considerably low, suggesting minimal binding of NP with IgG (Figure 5.7C). The binding profile from IgG and the particles did not follow a standard ITC trend to be modeled with a one-site binding model to derive binding parameters. In addition, the particle size of the NP did not change noticeably when combined with IgG, which represented no change in the peptide-drug complex in the IgG environment (Figure 5.7B). All of these results suggest that IgG binding to NPs is relatively low compared to one observed from NP-BSA binding. It is postulated that this low binding affinity is due to the position of tryptophan residues and their accessibilities to the other molecules such as THP.

Since formation of protein corona can either enhance or prevent biological responses of the nanoparticles, it is critical to study the molecular interactions and determine whether the nanoparticles have high or low affinity to certain proteins, and consequently predict the biological responses. It has been suggested that tightly bound proteins are the main components in nanoparticles fate *in vivo* and control the biodistribution of nanoparticles. At the same time, surface modifications of nanoparticles to avoid undesirable protein bindings provide the safer therapeutic nanoparticles for drug delivery [189,207].

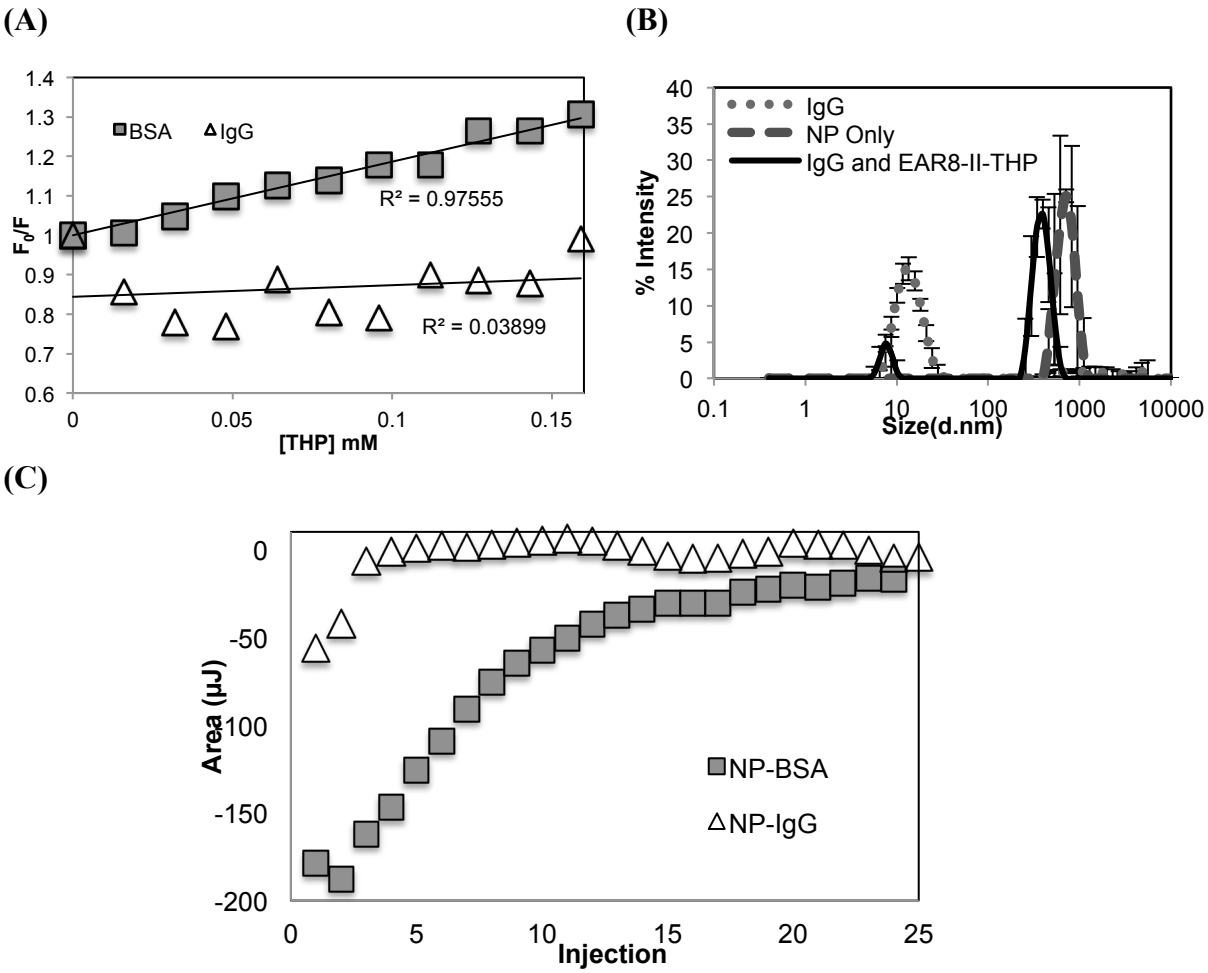

Figure 5.7. Binding properties of EAR8-II-THP and IgG. **(A)** Stern-Volmer plot from the fluorescence quenching method, **(B)** Particle size distribution (DLS), **(C)** ITC: integrated heats in each injection versus injection number.

5.4 Conclusions

We reported in this work that the peptide-based drug delivery system interacts strongly with serum albumin and relatively weakly with IgG proteins. The self/co-assembling peptide EAR8-II plays an important role in stabilizing the hydrophobic drug Pirarubicin (THP) in the physiological environment with serum albumin. The EAR8-II-THP complex self-assembles into a fibrillar nanostructure, whereas in the presence of serum albumin this structure is reorganized around albumin's spherical structure and binds to it non-covalently with no significant conformational change in the albumin protein structure. The results from both quenching and calorimetry

experiments illustrate spontaneous, exothermic, and enthalpy-driven binding (negative ΔG and ΔH) between the complex and BSA, with a reasonably high binding affinity (K_{sv} 1867 M^{-1}). Results from thermodynamic analysis showed that the main interaction between BSA and NPs is mainly hydrogen bonds and van der Waals forces (e.g. π-π stacking).

Chapter 6

Effect of Protein Binding to Peptide-Drug Complex on Immune Response

Abstract

Interactions between therapeutic agents and immune systems are critical in the development of drug delivery systems. Macrophages are immune cells that recognize and clear foreign materials from the body through phagocytosis. The ability to evade phagocytosis, and thus enable both extended circulation and site-specific targeting, is a key in designing effective drug delivery systems. For this purpose, serum albumin was used as a co-carrier for our peptide-based drug delivery system. The EAR8-II-pirarubicin (THP) complex, a peptide-anticancer drug assembly, had shown strong binding (exothermic and spontaneous) with serum albumin and relatively weak binding with immunoglobulin G (IgG). Here, we demonstrate the role of serum albumin in safe delivery of the peptide-drug complex, presenting reduced macrophage uptake and toxicity, inflammatory response, hemolytic activity (both *in vitro* and *in vivo*), and complement activation. Cellular toxicity and uptake results revealed that more than half of the cells survived in the complex solution with albumin, and that the phagocytosis rate of THP was three-fold lower compared to that in the complex solution without albumin. Cellular toxicity and uptake of the drug by macrophages was highest in the presence of IgG, possibly due to the IgG opsonin effect. The cytokine expression level by macrophages, as measured by qPCR, was also found to be much lower in the presence of albumin. Hemolytic activity was at minimum when albumin was used. However, the level of the final complement product, C5b-9, did not differ significantly between the albumin-associated complex and the complex alone; in both cases, complement product levels were biologically irrelevant (10-60% increase). These outcomes illustrate a promising role of serum albumin in enabling safer peptide-based delivery systems, which will help further development into clinical applications.

Keywords

Macrophages, cytokine, biocompatibility, hemolysis, cytotoxicity

6.1 Introduction

We previously introduced a newly designed self/co-assembling peptide, EAR8-II, and its unique capabilities to encapsulate the hydrophobic anticancer drug, Pirarubicin, and to remain stable in a physiological environment [186]. For the first time in peptide-based drug delivery research, thermodynamic interactions between peptide-drug complexes and serum proteins were investigated, and we presented a spontaneous and exothermic interaction between the peptide-drug complex and serum albumin. This effective binding of the EAR8-II-THP complex to serum albumin protein encouraged us to further investigate the effect of protein binding on *in vitro* immune response and biocompatibility. One of the main challenges of using such complexes is their rapid elimination by macrophages. Therefore, in this current study we focus on macrophages' reaction to the complex in the presence and the absence of bovine serum albumin (BSA) and immunoglobulin G (IgG). The fact that macrophages are widely located in many tissues of the body, invading and eliminating foreign particles, has provided an opportunity to design effective therapeutic compounds to evade macrophage recognition. Surface modifications, size, and shape of the particles have important roles in developing delivery systems capable of extended circulation and target specificity [208].

It has been demonstrated that plasma protein binding is a successful approach for improving the pharmacokinetic properties of short-lived molecules [185]. Drugs tend to bind to plasma proteins such as albumin [209], lipoproteins, immunoglobulin [194,210], transferrin [211], fibrinogen [89,98], and α1-acid glycoprotein [212], but due to the large amount and small size of albumin in the bloodstream, most particles bind to albumin [192]. It has been reported that many drugs, peptides [185], and fatty acid molecules [213] have the affinity to bind to serum albumin. This binding is usually through covalent or non-covalent interactions between albumin and other molecules [12]. For example the albumin-paclitaxel nanoparticle formulation, Abraxane, is a well-known compound for treating solid tumors. Paclitaxel comprised of lipophilic molecules, is encapsulated with human serum albumin in a solvent-free and high-pressure condition to form 130 nm nanoparticles. Abraxane has been approved by the FDA, and was administrated intravenously first in 2005 by Niel Dasai [67]. His trial revealed a significant improvement in therapeutic efficiency of Abraxane compared to standard paclitaxel, indicating the positive impact of albumin binding for both therapeutic and safety concerns. We speculate that serum albumin covers the nanoparticles and renders them invisible to macrophages, resulting in the observed improvement in nanoparticle longevity.

Immunoglobulin and complement proteins play an important role in modulating inflammation by clearing foreign materials from the body. Lin *et al.* showed that immunoglobulin G proteins bind to

antigens and facilitate Fc receptor mediated-phagocytosis that consequently activates the complement system [214]. This effect is crucial in preventing inflammation against pathogens, although the objective of the current study is protecting the nanoparticles from being recognized as pathogens by macrophages of the immune system. As observed in the previous studies, the affinity of peptide-drug complex binding to IgG was significantly lower than to serum albumin. It is hypothesized that high affinity to BSA and low binding to IgG offers low macrophage uptake and accordingly low inflammation responses.

Following physiochemical characterization analysis of binding presented in an earlier study, we evaluate *in vitro* the effect of protein binding to the peptide-drug complex. Macrophage cellular toxicity, uptake, cytokine expression, hemolysis, and complement activation were assessed by CCK-8, fluorescence, real-time RT-PCR, and ELISA assays, respectively. First, the cytotoxicity of the macrophages (RAW 264.7) treated with the complex in the presence and absence of BSA and IgG suggested higher cell viability with BSA bound to NPs[††]. Second, cellular uptake results of macrophages showed the lowest uptake in the presence of BSA, followed by the complexes with both BSA and IgG. Third, albumin-bound NPs showed significantly lower cytokine expression levels than naked NPs. Finally, hemolysis experiments were performed, and C5b-9 complement protein consumption was evaluated through ELISA, demonstrating protein binding effect on enhancement of the biocompatibility features of peptide-based delivery systems.

Overall, serum albumin binding to nanoparticles plays an important role in nanoparticle stabilization in a physiological environment and cellular responses. Therefore, a comprehensive study of protein interaction with nanoparticles provides useful guidelines for designing appropriate nanoparticles for drug delivery systems that are less susceptible to rapid removal by the human immune system.

6.2 Experimental

6.2.1 Materials

The EAR8-II (Ac-AEAEARAR-NH_2) peptide and the anticancer drug Pirarubicin with commercial name of THP were used from the sources presented in Chapter 4 (4.2.1). The supplies for BSA and IgG were similar to the ones presented in Chapter 5 (5.2.1). The mouse macrophage cell line

[††] Note that in this chapter EAR8-II-THP complex is presented as NP. NP only: NP - -, NP with BSA: NP + -, NP with IgG: NP - +, NP with BSA-IgG: NP + +

(RAW264.7) was purchased from Cedarlane (Burlington, ON, Canada). Cells were grown in Dulbecco's modified medium (DMEM) with high glucose including 10% fetal bovine serum and 1% penicillin-streptomycin (Sigma P4333).

TRI reagent (T9424), Chloroform (C2423), isopropyl alcohol (I9516) for RNA purification, and designed primers for real-time RT-PCR were purchased from Sigma-Aldrich (Oakville, ON). The qScript cDNA SuperMix (95048), and Perfecta SYBR Green Fast Mix, Low ROX (95074) for real time RT-PCR experiments were purchased from Quanta Biosciences (Gaithersburg, MD). Human C5b-9 ELISA kit (558315) for complement activation assay was purchased from BD Biosciences (Mississauga, ON). Lipopolysaccharides (LPS) from Escherichia coli 0111:B4, γ-irradiated (L4391) was purchased from Sigma-Aldrich (Oakville, ON) as a positive control for macrophage activation.

6.2.2 Methods

6.2.2.1 Cellular Toxicity and Uptake

Macrophage cells (RAW 264.7) were cultured in Dulbecco's Modified Eagle Medium (DMEM), containing 10% fetal bovine serum (FBS) and 1% penicillin-streptomycin in an environment controlled incubator (37°C with 5% CO_2). After 95% confluence, cells were detached and then seeded at concentration of 1.5×10^4 cells per well in 96-well plate, followed by treating with NPs for different incubation times for cellular toxicity assay (Cell counting kit CCK-8). For cellular uptake experiments cells were seeded at concentration of 2×10^5 cells per well in 12-well plates. THP cellular uptake tests were conducted by cell lysis after treatment with 1% SDS in Tris-EDTA and pipetting up-and-down to complete cell lysis. The fluorescence emission intensity was measured by spectrofluorometer at 590 nm indicating amount of THP uptake by the cells (Refer to 4.2.2.4). Note that cells were treated in serum free medium to isolate the effects of BSA and IgG.

6.2.2.2 RNA Extraction

RAW 264.7 cells were seeded in 12-well plate at concentration of 2.5×10^5 cells per well. After 6 hr incubation time with NPs the total RNA was extracted from the cells using the TRI reagent protocol (Sigma-Aldrich). RNA concentration was determined by measuring absorbance at 260 nm (OD_{260}) using NanoDrop system. The quality of purified RNA was assessed by absorbance ratio of 260/230 and 260/280. Note that nucleic acid and proteins have absorbance at 260 and 280 nm, respectively. A ratio of ~ 2.0 is generally accepted for pure RNA for 260/280. And the absorbance at 230 nm is

indication of other contaminants including phenol. The ratio of ~ 2.0-2.2 is acceptable for 260/230 for pure RNA.

6.2.2.3 Real-Time Reverse Transcription Polymerase Chain Reaction (RT-PCR)

Single stranded cDNA was synthesized from 100 ng of total RNA using MMLV (Moloney–Murine leukemia virus) reverse transcriptase. The cDNA for β-actin as a housekeeping gene and other cytokines were amplified by RT-PCR using Agilent Technologies (Paq5000). Briefly, 2 µl of each cDNA samples was amplified in a 20 µl PCR reaction containing 10 µl of PerfeCta SYBER Green Fast Mix, Low ROX and 0.75 µl of 10 µM primers (reverse and forward). The list of primers used for each cytokine is presented in Table 6.2. Samples were amplified under the following temperature profile: Initial denaturation for 1 min at 95°C, 45 cycles of 10 sec at 95°C and 30 sec in 60°C. Data are collected at the end of melt curve. Relative transcript levels were calculated using relative standard curve method [215,216].

6.2.2.4 Hemolytic Activity Test

To evaluate *in vivo* toxicity of the NP-BSA complexes, 0.4 ml of three THP dosages (5, 10, 20 mg/kg) was injected into 12-weeks-old male C57BL/6 mice (30-32 g) via intraperitoneal injection (i.p.). Subjects were monitored for their acute responses; 1 hr after injection, their blood, urine, and four tissue samples (heart, spleen, liver, and kidney) were collected for testing potential hemolysis and off-target effects. Collected blood was processed for hemolysis activity and red blood cell aggregation tests. All animal studies followed the protocols approved by the University of Waterloo Office of Research Ethics and the Animal Care Committee.

In addition to *in vivo* hemolysis testing, the hemolytic activity of the EAR8-II-THP complexes in the presence and absence of BSA was studied *ex vivo* using fresh blood from 2 year-old rabbits (White New Zealand female rabbit- 4.5 kg). In order to separate red-blood cells (RBCs), blood was washed 3 times with 3 ml PBS and centrifuged at 1500 rpm for 15 min followed by collecting the RBC and diluting in PBS at 5% (volume). The test samples were diluted in PBS and added to RBC with final RBC concentration of 1%. For each sample 5 different dilutions were tested in triplicate and each dilution was triplicated. Pure water and PBS were used as positive and negative controls, respectively. The mixtures were incubated at 37°C for two hours, then centrifuged at 1500 rpm for 5 minutes; the supernatant was transferred to 96-well plate for absorbance (Abs) reading at 570 nm. The sample absorbance was compared with positive control (PC) and negative control (NC) samples and hemolysis percentage was calculated using the following formula:

$$Hemolysis\% = \frac{Abs(samples) - Abs(NC)}{Abs(PC) - Abs(NC)} \times 100\%$$

The hemolysis activity of the blood samples collected from mice was also analyzed using the above method. At the same time, 2 µl of RBCs isolated after centrifugation was transferred to a glass slide monitoring possible RBC aggregation.

Three groups of samples were evaluated for hemolysis activity. The original complex was made at [THP] = 0.5 mg/ml or 0.8 mM, and [EAR8-II] = 2.5 mg/ml or 2.73 mM. Since in hemolytic activity test samples were diluted 5-fold in PBS, samples were made at concentrations 5 times higher than our working concentrations to keep the sample conditions consistent through out the current study. The first group contained serially diluted EAR8-II-THP complexes in water, with a final THP concentration range of 10 –160 µM. In the second group, EAR8-II-THP complexes were diluted in BSA (320 µM). The third group included samples with fixed complex concentration ([THP] = 80 µM) with varying BSA concentration (64 –512 µM). In addition, solutions containing only BSA at different concentrations were also tested as controls for hemolytic activity.

6.2.2.5 *In vitro* Complement Activation Test (C5b-9)

An enzyme-linked immunosorbent assay (ELISA) was used to quantify NP-induced formation of a complement cascade endpoint, the C5b-9 complex, in human serum. C5b-9 formation in the presence of NPs was measured using the Human C5b-9 ELISA Set (BD Biosciences, Mississauga, ON, Canada). 96-well micro-plates were prepared overnight with capture antibody, washed, and blocked using assay diluent, as provided in the kit.

NP treatments were prepared with the same conditions as for the hemolysis assay and added (60 µL) to a separate 96-well micro-plate, followed by the addition of 40 µL of freshly thawed pooled human serum (Innovative Research, Novi, MI, USA). NP-serum samples were then incubated at 37 °C for 60 minutes with periodic mixing. Following incubation, all sample wells were diluted 2500x in assay diluent, and 100 uL of each well was transferred to the washed ELISA plate for a 120 minute incubation at room temperature.

Separate washing and incubation steps followed for the working detector mixture (detection antibody and enzyme; 60 minutes) and substrate (3,3',5,5'-Tetramethylbenzidine, TMB; 30 minutes in dark environment). After adding the stop solution, absorbance values were measured using a BioTek Epoch spectrophotometer at 450 (signal) and 570 (background) nm.

% C5b-9 formation was calculated relative to a 100% baseline, containing only serum and buffer, and a positive control, containing serum and Zymosan microparticles (utilized for well-known complement activating properties). Estimated C5b-9 concentrations were established using log-log regression of the standard curve also obtained during the experiment and accounting for the large dilution factor.

6.3 Results and Discussion

Previously, EAR8-II was introduced as a potential nanocarrier for the hydrophobic anticancer drug Pirarubicin (THP). The EAR8-II-THP complex demonstrated efficient anticancer activity at different peptide-to-drug ratios. However, macrophages were able to rapidly recognize and capture the free and unbound complexes [186]. As macrophage uptake remains a key disadvantage of such drug delivery systems [217], designs or strategies to evade this uptake are necessary for advancement in this field. Polyethylene glycol modification of nanoparticles is an established strategy whereby stealth nanocarriers avoid phagocytosis [31]. In this present study, a protein-binding strategy is introduced to further mitigate macrophage uptake and cellular responses. Thus far, EAR8-II-THP complexes have illustrated exclusive binding to serum albumin proteins (spontaneous and exothermic interaction). It has been reported that in the presence of serum, the size and charge of nanocarriers play important roles in opsonin adsorption and subsequent phagocytosis [218]. We hypothesize that protein binding can decrease interactions with macrophages and other immune components. Here, the effect of protein binding to peptide-drug complexes on cellular responses is presented through macrophage cytotoxicity, uptake, cytokine expression level, hemolysis, and complement activation.

6.3.1 Macrophage Cellular Toxicity and Uptake

Phagocytosis by mononuclear phagocytes and macrophages is the first interaction of particles in the bloodstream with the immune system [219]. Macrophages are among the main cells involved in both innate and adaptive immune systems, and are used in this study to evaluate immune recognition of our peptide-based drug delivery system. Mouse macrophages, RAW 264.7 cells, were treated with different concentrations of EAR8-II-THP (NP) complexes in the presence and the absence of serum proteins, including BSA and IgG, for various incubation times.

The viability of the cells treated with NPs in the presence and the absence of proteins at 2 and 4 hr incubation times did not differ significantly, where only about 20% of the cells died when IgG was

present. However, cell viability dropped considerably after a 6 hr incubation period as the effect of protein binding became more noticeable. Among the various treatments, the cytotoxicity of NPs in the presence of IgG was the lowest, due to the opsonization effect of IgG. However, when both IgG and BSA were present in a culture environment, strong BSA binding to the NPs compensated for the opsonized particles and led to a higher viability of cells treated with NP and IgG. The highest cell viability was observed among cells treated with NPs and only BSA, indicating protection of NPs from macrophages while bound to BSA (Figure 6.1A). In addition, as is expected, increasing concentration of THP reduced the cell viability with all four treatments. Corresponding IC_{50} values for the treatments at a 6 hr incubation time in the presence of proteins, were in increasing order: NP -+ (NP+IgG) < NP -- (NP only) < NP ++ (NP+ BSA and IgG) < NP +- (NP+ BSA) (Table 6.1). Note that IC_{50} values were calculated through interpolation and extrapolation of data from cell toxicity values (100 – % cell viability) for evaluating the concentration of a drug required for 50% cytotoxicity *in vitro*. Similar trends were observed for cellular uptake observed by fluorescence microscopy. NPs in the presence of IgG showed the highest uptake, followed by unprotected NPs, NPs with BSA and IgG, and NPs with only BSA (Figure 6.1B).

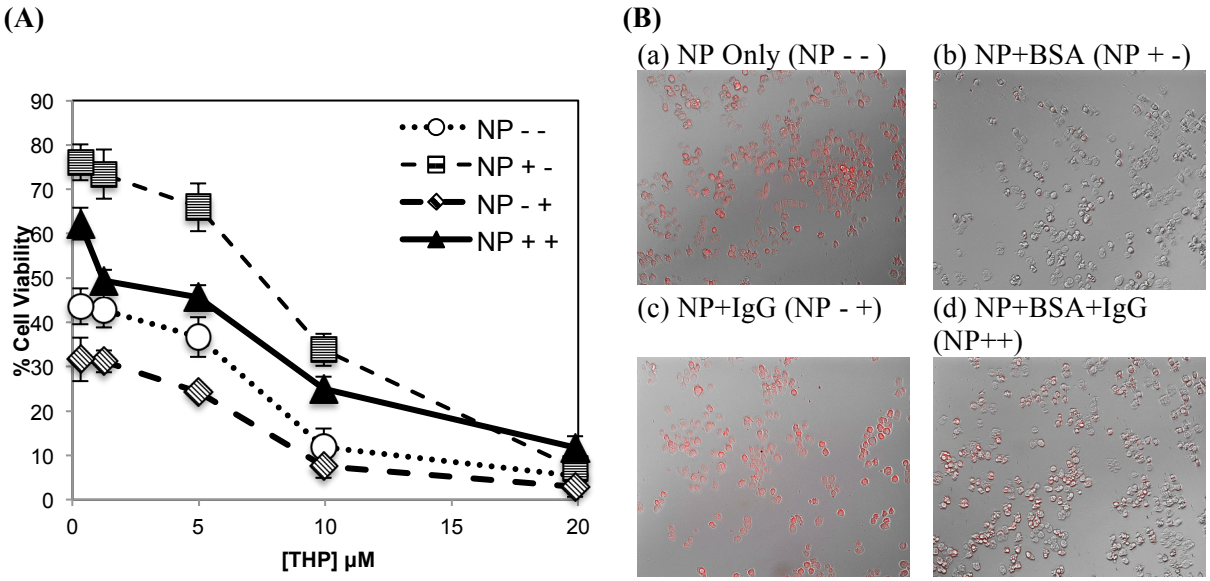

Figure 6.1. **(A)** Cellular viability of RAW 264.7 cells treated with EAR8-II-THP (NP), in the presence of BSA and IgG at 6 hr treatment time. **(B)** Cellular uptake of EAR8-II-THP by macrophages (a-d) fluorescence microscopy images. NP -- : EAR8-II-THP complex (no protein), NP +-: complex with BSA, NP - +: complex with IgG, NP ++ : complex with BSA and IgG.

A study was also conducted using different concentrations of the complex, in the presence and in the absence of BSA, to verify the above results. Macrophages treated with multiple combinations of NPs and proteins were lysed after a 2 hr incubation time. The lysed cells were collected for fluorescence studies, utilizing the intrinsic fluorescence properties of THP. Cellular uptake of THP by macrophages was measured using excitation and emission wavelengths of 480 nm and 590 nm, respectively [220]. Higher intensities of emitted light corresponded to higher cellular uptake of THP. Figure 6.1D displays the normalized fluorescence intensity of emitted light at 590 nm with respect to light fluctuation, representing the THP content of cells after a 6hr incubation period [221]. By increasing the complex concentration, the emission fluorescence intensity of THP was increased for NPs alone, more than for the NPs in the presence of BSA. As shown in Figure 6.2C, the slope of fluorescence intensity against THP concentration was more than double that measured with NPs and BSA, indicating protection of NPs by BSA and subsequent reduction of cellular uptake. Localization of red fluorescence represented THP uptake, yielding higher intensities when NPs were delivered in the absence of serum albumin (Figure 6.2A-B).

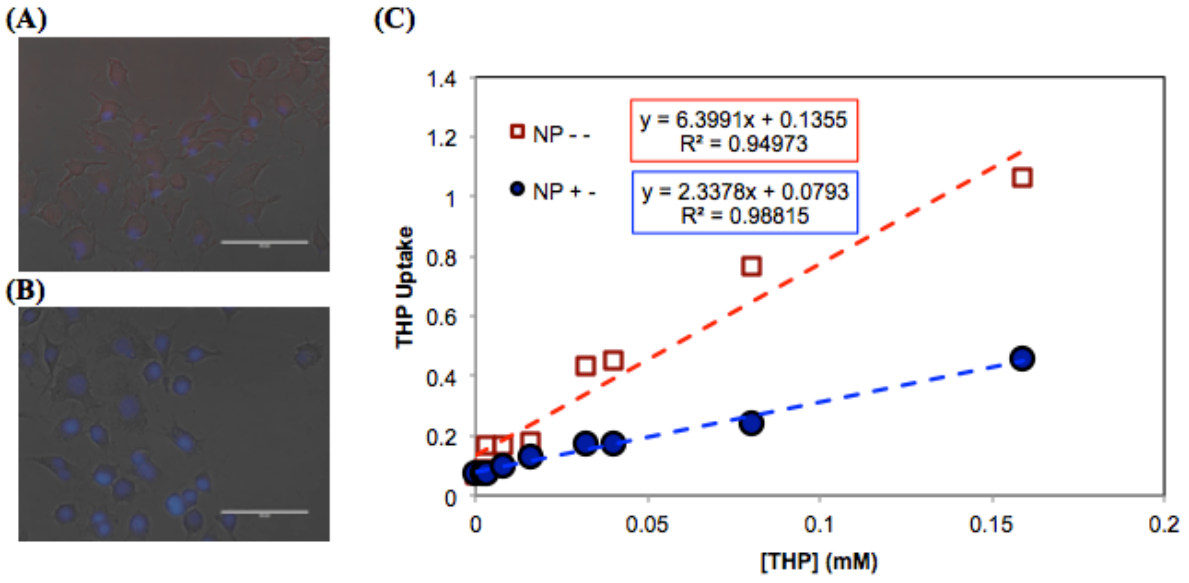

Figure 6.2. Cellular uptake of EAR8-II-THP **(A)** 5:1 ratio complex without BSA, **(B)** with BSA, **(C)** normalized emission fluorescence intensity of THP at different complex concentration monitored by fluorescence spectroscopy (Excitation: 480 nm, emission 590 nm)- 2 hr incubation time.

One of the main explanations of macrophage uptake and toxicity is particle size-dependent phagocytosis. Larger sizes and surface areas of particles increase in the attachment of opsonin

proteins, leading to higher macrophage uptake and elimination from the circulatory system [222]. Uptake results presented here follow the trend of particle sizes observed from NPs in their specified combinations with IgG and BSA proteins (Table 6.1). NPs with IgG and unprotected NPs showed distinctly larger particle sizes and thus appeared to be more visible to macrophages. However, when NPs were bound to BSA, particle sizes decreased significantly and the chance of macrophage uptake reduced by 50%. When both proteins were in the culture environment, BSA binding was a dominant force and particle size distribution was mainly in a small range of ~10 nm; as a result, cellular uptake behavior was similar between NPs with BSA and NPs with both proteins. We postulate that BSA can act as a carrier for the NP by reorganizing the NP structure within BSA molecules, thus helping the NPs to evade macrophage recognition.

Another key factor in uptake is particle surface charge-dependent phagocytosis. It has been previously reported that mammalian macrophages have negatively charged plasma membranes, based on electrophoresis and cell membrane staining (TEM) results in which cationic markers attached to cell membranes strongly in comparison to neutral and anionic markers [223,224]. As such, measuring the surface charge of NPs aids in a more thorough understanding of uptake behavior. The zeta potential of the complex in different protein environments was measured and presented in Table 6.1. Unprotected NPs exhibit positive surface charge due to protonated THP in the EAR8-II solution. When combined with BSA, the zeta potential dropped significantly, to negative values, while with IgG, zeta potential values decreased but still remained positive. Strong ionic attraction between positively charged particles and cell membranes resulted in high measured values of cellular uptake. However, for negatively charged particles stabilized with BSA, repulsion forces between particles and cell membranes resulted in significant reductions of cellular uptake and toxicity.

Table 6.1. Zeta potential, average diameter, and macrophages IC_{50} of the EAR8-II-THP complexes (NP) in the presence of BSA or IgG. NP - -: NP only, NP+ -: NP with BSA (64μM), NP -+: NP with IgG (0.66 μM), NP++: NP with BSA and IgG

	Zeta Potential (mV)	**Size (d.nm)**	**PdI**	**IC_{50} THP(μM)**
NP - -	11.205 ± 0.28	566.55 ± 44.15	0.44	~ 0.3
NP + -	-11.33 ± 0.57	15.07 ± 0.82	0.48	6.5
NP - +	1.71 ± 0.12	244.03 ± 66.19	0.47	<< 0.3
NP + +	-11.51 ± 0.89	19.46 ± 3.79	0.48	1.25

6.3.2 Macrophages Cytokine Expression

The innate immune response is one of the primary defense mechanisms against microbial infection and cellular damage. Macrophages are crucial components of the innate immune system that produce cytokines to mediate inflammatory responses. Foreign particles that cannot be destroyed by macrophages after producing some therapeutic effect in the body can cause prolonged chronic inflammatory responses initiated by macrophage activity [225,226]. The aim of the current study was to establish a model system to examine the effect of our peptide-drug complex (NP) and its combination with IgG and BSA proteins on cytokine expression in mouse macrophage cells. Expressions of different cytokine mRNA levels were examined here, including inducible nitric oxide synthase (iNOS), cyclooxygenase-II (COX-2), tumor necrosis factor (TNF-α), interleukin-1 Beta (IL-1β), interleukin-2 (IL-2), and interleukin-6 (IL-6). These pro-inflammatory cytokines are important regulators of both innate and adaptive immunity. When a stimulator such as LPS activates macrophages, a large amount of nitric oxide (NO) is produced by iNOS through the conversion of *L*-arginine to *L*-citrulline, which results in inflammatory disorders [225,226]. Production of iNOS provides macrophages with cytotoxic efficacy against viruses, bacteria, fungi, and tumor cells [166,227]. COX-2, an inducible enzyme with functional significance in many organs and diseases, is responsible for catalyzing the rate-limiting step in prostaglandin (PG) and leukotriene synthesis [228,229]. COX-2 is expressed by growth factors and pro-inflammatory stimuli, including LPS and activated oncogene in macrophages [230]. Induction of tumor necrosis factor- α (TNF-α) by macrophages leads to the development of chronic inflammatory diseases such as rheumatoid arthritis; therefore, down-regulating this gene is an established medical method to prevent and treat the disease [231]. LPS-stimulated macrophages also tend to overexpress interleukins, such as IL-1β, IL-2, and IL-6, that can promote differentiation of T and B cells [232].

The immune response of macrophages towards our peptide-based drug delivery system was studied at the mRNA level through quantitative RT-PCR. The expression levels of cytokines, including iNOS, COX-2, IL-1β, TNF-α, and IL-2, were measured for the cells treated with NP only and NP with BSA and IgG. The quality of the RT-PCR results, reflected in the % efficiency values and the R^2 value of standard curves, is presented in Table 6.2. Similar to cytotoxicity and uptake results, cytokine expression levels were significantly higher for cells treated with unprotected NPs than for cells in the presence of NPs with BSA and IgG (Figure 6.3). Cytokine expression levels of all the treatments, including unprotected NPs, were still considerably lower than those treated with LPS (100 ng/ml) as a positive control for macrophage activation, indicating the relative non-immunogenicity of

our peptide-drug complex, especially in the presence of serum proteins. The cytokine expression values of LPS-treated cells are reported in Table 6.2. An exception in cytokine expression was observed in COX-2, where the expression level was higher for cells treated with NP than those treated with LPS. Likewise, TNF-α expression in macrophages appeared to be down-regulated by our NP treatment. According to recent advances in anti-inflammatory treatment, secretion of TNF-α by macrophages plays a predominant role in reducing both local and systemic inflammation [231]. Since the peptide-based drug delivery system showed secretion of this gene in macrophages, it presents an opportunity for further investigating and developing similar systems for synergetic anticancer and anti-inflammatory effects.

Table 6.2. List of murine primers for Quantitative Real-time RT-PCR, and Standard curve parameters. * Relative Normalized quantities for cells treated with LPS (100 ng/ml)

Cytokines	**Primers**	**qRT-PCR values**		**LPS***	**Reference**
		R^2	**% Efficiency**		
B -Actin	**F:** AGAGGGAAATCGTGCGTGAC **R:** CAATAGTGATGACCTGGCCGT	0.999	97.8	180.03± 32.15	[233]
iNOS	**F:** CAGCTGGGCTGTACAAACCTT **R:** CATTGGAAGTGAAGCGTTTCG	0.949	85.1	114.72± 21.65	[233]
COX-2	**F:** AGAAGGAAATGGCTGCAGAA **R:** CTCAATACTGGAAGCCGAGC	0.542	258	25.57± 4.96	[234]
IL-1β	**F:** CCCAAGCAATACCCAAAGAA **R:** GCTTGTGCTCTGCTTGTGAG	0.993	98.2	7271± 1821	[235]
TNF-α	**F:**AGACCCTCACACTCAGATCATCTTC **R:** TTGCTACGACGTGGGCTACA	0.997	97	43.76± 10.04	[236]
IL-2	**F:** CCTGAGCAGGATGGAGAATTACA **R:** TCCAGAACATGCCGCAGAG	0.965	76.1	1937± 414	[233]

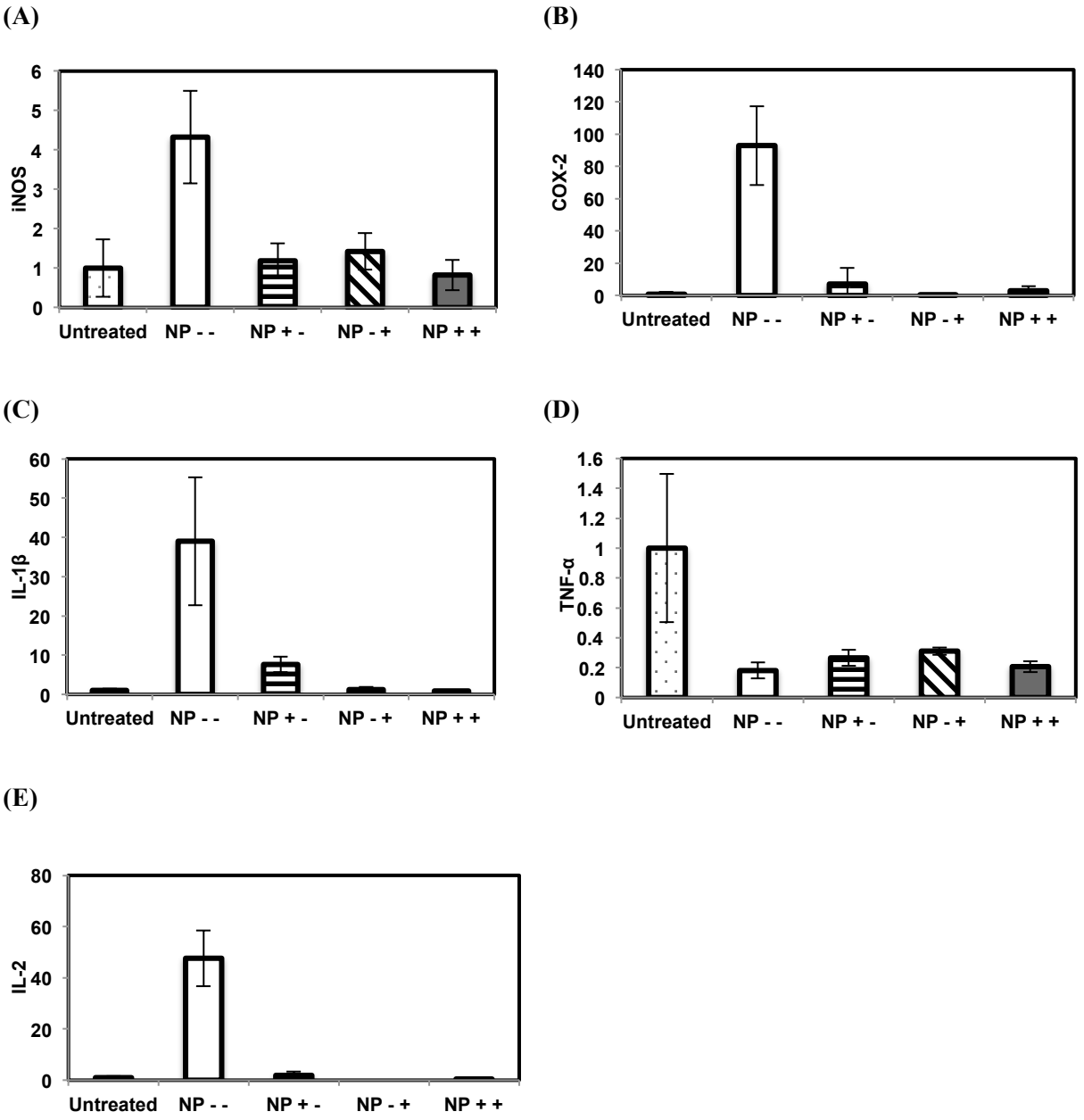

Figure 6.3. Relative normalized cytokine expression at the mRNA level of RAW 264.7 macrophage cells treated by EAR8-II-THP (NP) only, NP with BSA (NP + -), NP with IgG (NP - +), and NP with BSA and IgG (NP + +). **(A)** Inducible nitric oxide synthase (iNOS), **(B)** Cyclooxygenase-II (COX-2), **(C)** Interleukin-1Beta (IL-1β), **(D)** Tumor necrosis factor (TNF-α), **(E)** Interleukin-2 (IL-2)

6.3.3 Hemolytic Activity

Hemolytic activity is one of the most important criteria in the development of therapeutic agents destined for circulation in the bloodstream. The hemolysis assay evaluates the compatibility of nanomaterials with red blood cells, providing a measure of the acute response to foreign materials [154,237]. This phenomenon is quantified by reading and comparing the absorbance at 570 nm with negative and positive controls. In more severe cases, hemolytic activity can be visually assessed in whole blood after centrifugation, since the supernatant color tends to become red if RBCs are lysed and hemoglobin is released. Here, EAR8-II-THP complexes were tested in a hemolysis assay and found to be more compatible with red blood cells when pre-incubated with BSA. Fresh rabbit blood cells were treated with serially diluted EAR8-II-THP at a final THP concentration range from 10 – 160 μM, either in water or BSA. Table 6.3 summarizes the hemolysis results for different treatments. Note that materials inducing hemolysis values below 5% are generally considered safe and blood compatible [238].

EAR8-II-THP complexes at the highest THP concentration were highly hemolytic; however, when these complexes were serially diluted, hemolytic activity reduced significantly. This reduction was more noticeable when the complex was pre-incubated in BSA, indicating the positive effect of BSA binding on blood compatibility of the peptide-based anticancer drug delivery system. As shown in Figure 6.4, plasma collected from samples treated with only NPs is redder than plasma from samples treated with NPs pre-incubated with BSA (at the same THP concentrations). Also, decreasing THP concentrations corresponded to lower hemolysis values. These results were confirmed with absorbance readings (Figure 6.4D), verifying that at each concentration of NP, pre-incubated with BSA, resulted in hemolysis reductions of 37-56%. Moreover, results showed that the hemolytic activity of NP-BSA complexes at a fixed NP concentration and varied BSA concentrations is independent of BSA concentration. Increasing BSA concentration did not affect the hemolysis significantly, suggesting that BSA binding to NPs is effective even at low BSA concentrations.

To move forward with hemolytic activity, three selected dosages of THP pre-incubated with BSA were tested *in vivo*. Mice were injected with EAR8-II-THP complexes containing 4% BSA at 5, 10, and 20 mg/kg and monitored for one hour; selected mice were treated with saline as a control. Blood was then collected and tested for hemolytic activity. While a high dosage of THP (20 mg/kg) in the presence of EAR8-II and BSA was shown to be slightly hemolytic, with a hemolytic activity of 7.16 ± 2.22 % (Figure 6.5), lower dosages of THP (10 mg/kg and 5 mg/kg) caused lower hemolysis (<

5%), showing their blood compatibility. Red blood cells after centrifugation were observed by microscope to rule out aggregation.

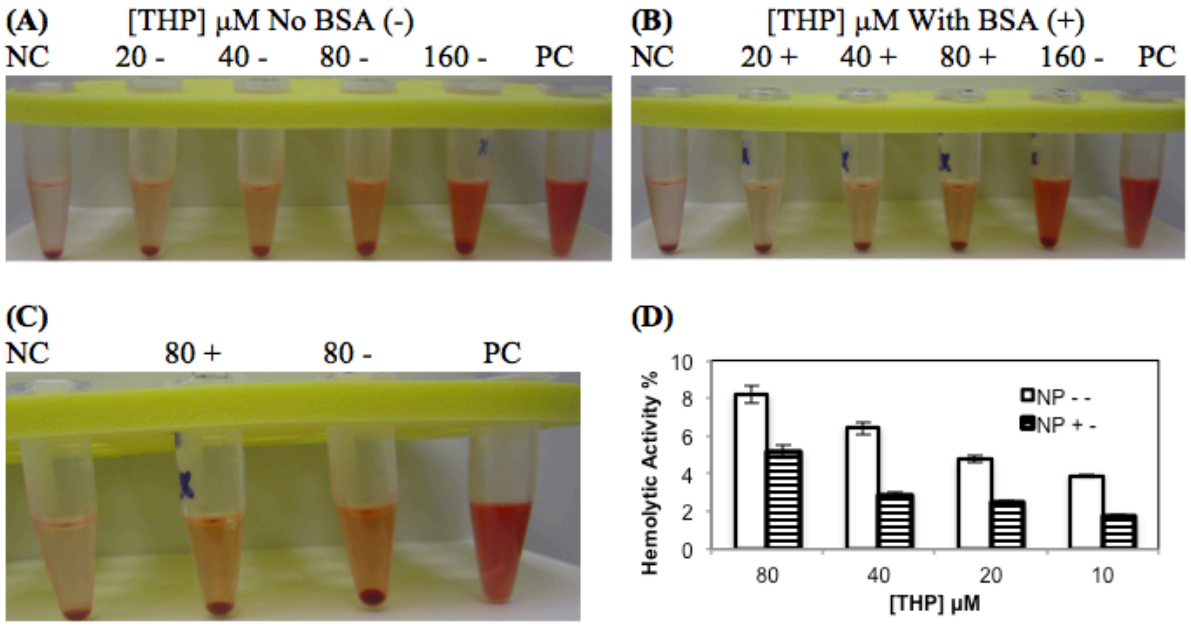

Figure 6.4. Images from plasma collected from the blood samples treated with EAR8-II-THP complexes; (**A)** Complexes without BSA (-), **(B)** complexes with BSA (+), **(C)** direct comparison between with and without BSA complexes at 80 µM of THP. NC: negative control (normal saline), PC: positive control (pure water) **(D)** Hemolytic activity of EAR8-II-THP complexes (NP). NP--: NP diluted in water, NP +-: NP diluted in BSA. Error bars represents standard error of the means for 95% confidence interval.

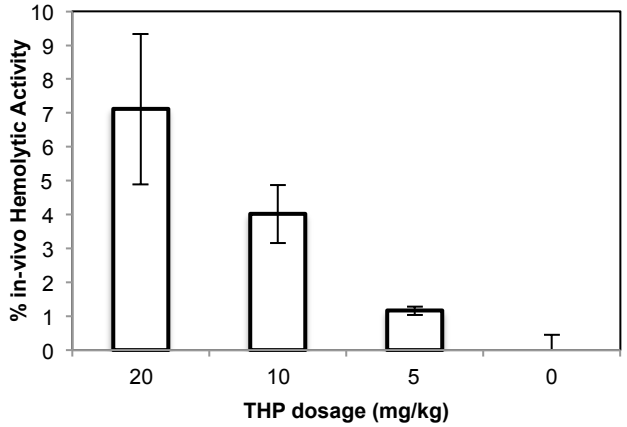

Figure 6.5. *in vivo* hemolytic activity of EAR8-II-THP and 4% BSA.

6.3.4 *In vitro* Complement Activation

We evaluated complement activation in human serum containing peptide-drug complexes in the presence and absence of BSA, by using ELISA to measure the generation of C5b-9 complexes, as a final product of the complement cascade. All EAR8-II-THP complexes with or without BSA induced the formation of C5b-9 to some extent in pooled human serum. The results suggested that the presence of BSA in the complex solution did not have a direct effect on C5b-9 formation. Most of the complexes are considered to cause complement activation that is likely inconsequential in a biological context, since the C5b-9 concentrations were only 10-60% higher than control serum samples (as a baseline) without NP incubation [239]. It is worth noting that the serum samples treated with Zymosan (i.e., positive control) showed more than 1000% increase in C5b-9 concentrations which is substantially higher than in any of the NP treated trials. However, samples with very high concentrations of THP (160 μM) and lower concentrations (10-20 μM) showed statistically significant difference from the baseline ($p < 0.05$). One reason may be differences in the size and nanostructures with diluted NPs. Even though particle size distribution results did not show a clear difference between various concentrations of the NPs, the nanostructure of the particles may undergo changes upon dilution.

In addition, similar to hemolysis results, it was observed that C5b-9 formation is independent of NP pre-incubation with BSA. The relative change in C5b-9 concentration to the baseline is about 30-60%, which is biologically insignificant. Table 6.3, presents the concentrations (μg/ml) of C5b-9 formed by serum due to NPs incubation, and Figure 6.6 illustrates the relative percentage of C5b-9 formation in respect to untreated serum control. These observations suggested that THP concentration in the complex played an important role in complement activation, as moderate THP concentration in NPs, either with or without BSA showed the least-significant activation of the complement. Consequently, we can claim that BSA existence in NP formation does not trigger immune response in the form of C5b-9 complement formation.

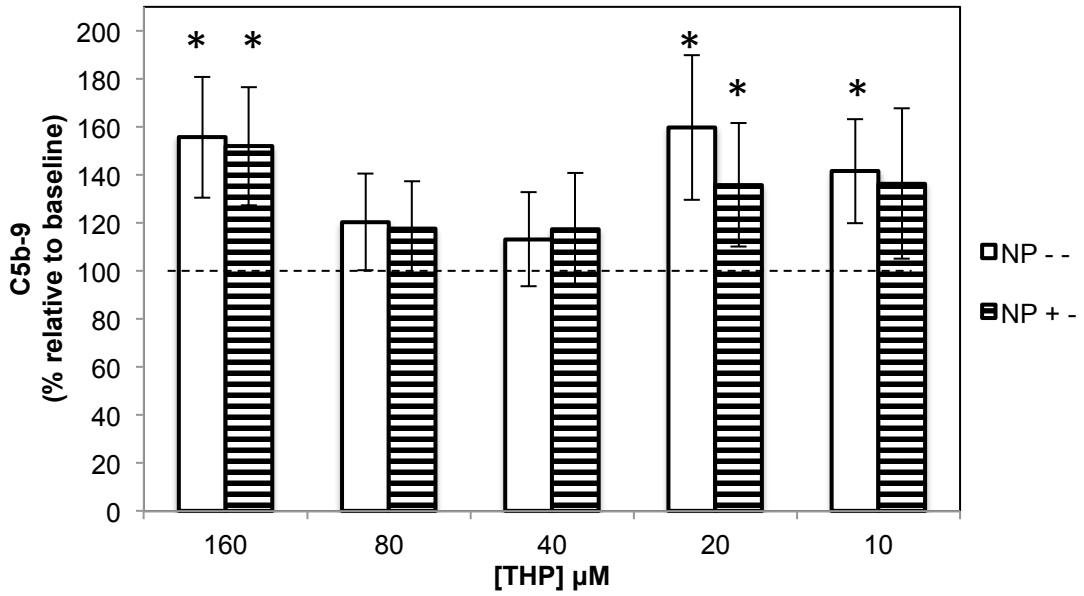

Figure 6.6. Effect of BSA binding on complement activation. Final BSA concentration was 64µM in serum, and results are expressed as percentage of respective control baseline. * = Significant rise of C5b-9 formation compared to the untreated serum control ($p < 0.05$). Zymosan (10 mg/ml) was used as positive control, and the relative percentage of C5b-9 formation by Zymosan was observed as 1230% (not shown).

6.4 Conclusions

The effect of protein binding was shown to be significant in the biological and immunological interactions of peptide-drug complexes, including macrophage toxicity and uptake as well as cytokine expression at the mRNA level, hemolysis, and complement activation. Strong protein binding between our unique amphiphilic peptide-drug (NP) complex is hypothesized to be through hydrophobic interactions between tryptophan residues in BSA and hydrophobic THP molecules, and EAR8-II. Macrophages are more sensitive to larger sizes and cationic particles due to their negatively charged plasma membrane. When the peptide-drug complexes were bound to serum albumin, their particle sizes decreased considerably, thus circumventing possible aggregation and avoiding macrophage uptake. In addition, the negative surface charge of the particles in the presence of albumin provided repulsion between the particles and macrophages to further decrease uptake. However, unprotected NPs and NPs combined with IgG had significantly larger particle sizes and positively charged surfaces, facilitating their uptake by macrophages. Cytokine expression results also suggested a considerably lower induction of cytokines by the cells treated with protected NPs

compared to those treated with peptide-drug complexes alone. Further biocompatibility studies revealed the positive effect of BSA binding to the complex in reducing hemolytic activities and producing insignificant amounts of complement complex C5b-9. All these results verified the significant effect of albumin binding on reducing the side effects of the peptide-based drug delivery system, especially towards macrophages and red blood cells, without causing other incompatibilities. The albumin binding strategy shows promising potential as a basis for peptide-based drug delivery formulations with clinical application in cancer therapy.

Table 6.3. Effect of BSA in haemolytic activity of the EAR8-II-THP complex

Samples (uM)		**Hemolysis %**			**C5b-9 (**μg/ml)
THP	BSA	Mean± Margin Error[+]	Evaluation <15%	%Hemolysis Reduction[++]	Mean± Margin Error[+]
160	0	38.46 ± 0.42	Fail	-	7.12 ± 0.05[*]
0	64	2.08 ± 0.75	Pass	-	6.13 ± 0.70[*]
80	0	8.19 ± 0.46	Fail	-	5.51 ± 0.43
40	0	6.40 ± 0.34	Fail	-	5.18 ± 0.49
20	0	4.74 ± 0.17	Pass	-	7.31 ± 0.92[*]
10	0	3.88 ± 0.08	Pass	-	6.48 ± 0.11[*]
80	64	5.16 ± 0.33	Fail	37.08	5.39 ± 0.42
40	64	2.86 ± 0.16	Pass	55.25	5.38 ± 0.78
20	64	2.44 ± 0.09	Pass	48.55	6.22 ± 0.79[*]
10	64	1.70 ± 0.13	Pass	56.09	6.24 ± 1.21
80	12.8	3.55 ± 1.05	Pass	56.63	7.16 ± 0.51[*]
80	25.6	3.25 ± 0.99	Pass	60.29	6.50 ± 0.64[*]
80	51.2	4.82 ± 0.40	Pass	41.12	6.21 ± 0.64[*]
80	102.4	4.39 ± 0.19	Pass	46.29	6.24 ± 0.60[*]
Zymosan	-	-	-	-	56.28 ± 2.30[*]

[+]Margin error was calculated with critical value for 95% confidence interval.

[++]Hemolysis reduction percentage was calculated relative to the corresponding THP concentration treatment in the absence of BSA.

[*]Baseline C5b-9 level (Control) was 4.57±0.79 μg/ml. Significant differences with respect to the baseline: [*]$p < 0.05$

Chapter 7

Albumin-Bound Peptide-based Drug Delivery System Promotes Target-ability through SPARC Inhibition

7.1 Introduction

One of the most important functionalities of albumin is the transcytosis of bound ligands such as hormones, peptides, and fatty acids through receptor-mediated processes. Transcytosis is the process of delivering molecules across the vascular endothelial cells for nutritional purposes [240]. Schnitzer *et al.,* demonstrated specific binding between albumin and 60-kDa microvascular endothelial glycoprotein (gp60) and secreted protein, acidic and rich in cysteine (SPARC), that initiates the endothelial transcytosis [241,242]. SPARC is an extracellular matrix glycoprotein that has been shown to bind albumin with high affinity. SPARC is overexpressed in a number of tumors, including breast, lung, melanoma, prostate, and plays a key role in tumor metastasis through de-adhesion, migration and angiogenesis [15]. SPARC expression is suggested to facilitate drug distribution in tumors and enhance clinical effectiveness of albumin-associated nanoparticles because of SPARC-albumin binding affinity [243]. To exploit albumin transcytosis' properties and its high affinity to SPARC receptors, many albumin-based drug delivery systems (e.g., *nab* technology) have been developed and have shown greater drug accumulation in tumor cells than in normal tissues [16].

Previously, I focused on the effect of albumin in delivering peptide-drug complexes with low immunogenicity and increased biocompatibility. The results suggested that albumin has a key role in safe delivery of the peptide-based hydrophobic anticancer drug delivery system *in vitro* because of the following properties: the high affinity of albumin to the hydrophobic drug pirarubicin through hydrophobic interactions and shielding of the peptide-drug complex against macrophages and red blood cells leading to lower phagocytosis, cytokine expression, and hemolytic activities. The third feature of albumin, which is tumor accumulation through SPARC binding affinity, is explored in the current study.

EAR8-II, a model amino acid pairing ionic-complementary peptide, has so far shown great promise for encapsulating the hydrophobic drug Pirarubicin (THP) and inducing excellent anticancer activities

against various cancer cells *in vitro* [186]. In addition, binding affinity with serum albumin utilized the drug delivery system with the properties that induce less inflammatory responses. Since albumin binding has shown positive effects on enhancing the biocompatibility of the complex, this study focuses on the anticancer activity of the albumin-bound peptide-drug complexes. A549, is a type of human non-small cell lung carcinoma (NSCLC), is used here to evaluate the anticancer activity of the complex. Cell viability, uptake tests have been conducted to evaluate the therapeutic activity of the THP at the cellular level. qRT-PCR technique is employed to determine SPARC expression level at the mRNA level. A549 cells have shown overexpression of SPARC protein, which is responsible for tumor metastasis. Therefore, developing a delivery system with capability to inhibit the SPARC expression in lung cancer cells is an ultimate goal of the current research.

7.2 Experimental

7.2.1 Materials

The peptide EAR8-II, Pirarubicin (THP), and bovine serum albumin (BSA) are the main components used here and the sources are similar to those reported in previous chapters. qRT-PCR reagents are also the same materials presented in Chapter 6 (6.2.2.3).

7.2.2 Methods

7.2.2.1 Cellular-based Methods

A549 cells were cultured in 96-well plates with 10^4 cells/well for cytotoxicity and cellular uptake experiments, in 24-well plates with 4.5 10^4 cells/well for RNA extraction, and in 6-well plates with 2.4 10^5 cells/well for protein extraction. Cells were incubated in F-12 medium containing 10% FBS, overnight at 37°C, until the cell confluence reached ~ 60%. 24 hr later, the medium was replaced with serum-free F-12 containing peptide-drug complexes at various concentrations (final [THP]: 0.3-38 μM). The first group of sample treatments was the complex without pre-incubation with BSA, and the second group of treatments was the same complexes pre-incubated with BSA at a 64 uM final concentration. The third group was considered for fixed THP concentration in the complex, and BSA

concentration was varied from 0-64 uM in solution. Cells were incubated with the treatments for 6 and 24 hours to be further tested for cellular uptake and cytotoxicity. Also, a 6 hours treatment was considered for RNA extraction experiment. The cell-counting kit (CCK-8) was used for cell toxicity assay using a micro-plate reader (absorbance 450 nm). THP cellular uptake tests were conducted on treated cells by complete cell lysis with 1% SDS in Tris-EDTA and pipetting up-and-down. BioTeK Monochromator-based Multi-mode Microplate reader measured the emission fluorescence intensity of the cells. The amount of THP uptake is directly proportional to the emission intensity at 590 nm. Normalized fluorescence intensities were obtained by subtracting the values from the intensities of untreated cells.

7.2.2.2 SPARC Inhibition Analysis by Quantitative Reverse Transcription Polymerase Chain Reaction (qRT-PCR)

The total RNA was extracted from A549 cell samples with Trizol reagent (Sigma-Aldrich, Canada), and the single stranded complementary DNA was synthesized from 500 ng of total RNA using qScript SuperMix from Quanta Biosciences (Gaithersburg, MD, USA). The cDNA for human β-actin as a housekeeping gene and human SPARC were amplified by PCR using Agilent Technologies (Paq5000). Briefly, 2 µl of each cDNA sample after 10-times dilution was amplified in a 20 µl PCR reaction containing 10 µl of PerfeCta SYBER Green Fast Mix, Low ROX from Quanta Biosciences and 0.75 µl of 10 µM primers (reverse and forward). The primers were synthesized by Sigma-Aldrich (Oakville, ON, Canada). The forward and reverse primers for human β-actin are: 5' GGCGACGAGGCCCAGA 3', and 5' CGATTTCCCGCTCGGC 3' [244], and for human SPARC primers are 5′ AAGATCCATGAGAATGAGAAG 3' and 5′ AAAAGCGGGTGGTGCAATG 3' [243], respectively. Samples were amplified under the following temperature profile: initial denaturation 1 min at 95°C, 45 cycles of 10 sec at 95°C and 30 sec in 60°C. Data are collected at the end of melt curve. Relative transcript levels were calculated using relative standard curve method [215,216].

7.3 Results and Discussion

In this study the effect of albumin binding on anticancer activity of the peptide-drug complex (EAR8-II-THP) was assessed.

7.3.1 Cellular Toxicity and Uptake

EAR8-II-THP complexes have shown a significant anticancer activity against the A549 cell line. A549 cells after 24 hr incubation with the 5-to-1 mass ratio peptide-drug complexes at various concentrations of THP (0.3 -37 μM) was tested for cellular toxicity assay (CCK8). The results revealed high cellular toxicity particularly at higher THP concentration in the absence of serum. The IC_{50} was calculated at ~ 3.6 μM of THP, which is significantly lower than the previous results in chapter 4, where the complexes were applied to the A549 cells in the F-12 medium containing 10% FBS having IC_{50} of ~ 19.3 μM [186]. Already this result indicates the presence of serum proteins affecting the toxicity of the complex. Here, complexes were pre-incubated with only serum albumin before being introduced to the A549 cells in order to isolate the effect of BSA. The IC_{50} for albumin-bound complexes was calculated at [THP]~ 5 μM, which is slightly higher that the one calculated for unbound complexes. This effect can be explained by delaying the THP release in the presence of BSA and cause cell death at higher THP concentrations showing stealth property of BSA for NPs (Figure 7.1A).

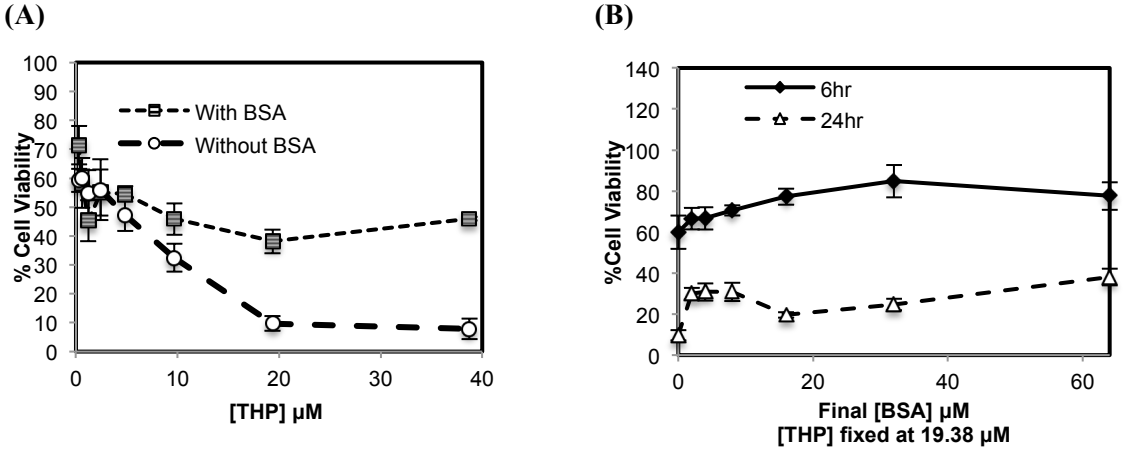

Figure 7.1. Percentage viability of the A549 cells when treated with **(A)** the EAR8-II-THP complexes at various THP concentrations with and without BSA (64μM) pre-incubation. Incubation duration was 24 hr, **(B)** the fixed complex concentration and varied BSA concentration for 6hr and 24 hr incubation time.

In order to find the influence of BSA concentration in A549 cellular toxicity, a fixed complex concentration at [THP] of 19.38 μM was incubated with varied BSA concentrations (0-64 μM). As shown in Figure 7.1B, the percentage of cell toxicity is independent of BSA concentration, indicating the passive property of BSA in the complex's cytotoxicity effect on A549 cells.

In addition to cytotoxicity testing, uptake of THP by A549 cells was evaluated by exploiting the intrinsic fluorescence property of THP through a microplate reader. When the THP concentration in the complex was increased, the emission intensity observed in lysed cells increased proportionally. Longer incubation times also led to higher THP uptake, illustrating the higher efficiency of the complex over time (Figure 7.2A).

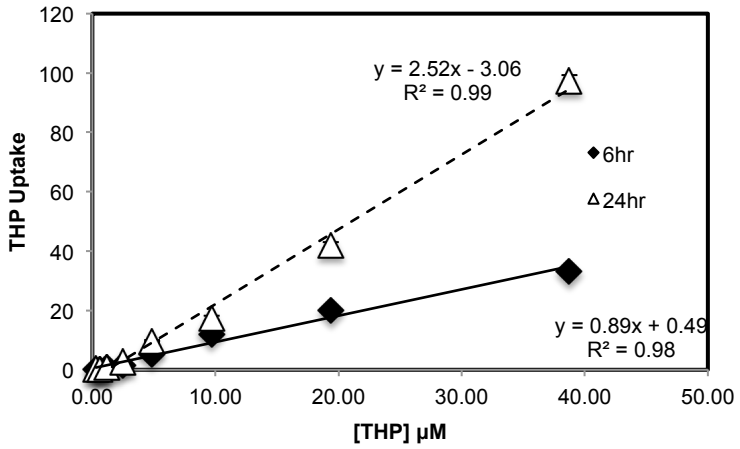

Figure 7.2. Normalized fluorescence emission intensity of THP uptake by the A549 cells treated by the various concentration of EA8-II-THP complexes

7.3.2 Inhibition of Endogenous SPARC Expression at the mRNA Level

First, the endogenous expression of SPARC in non-small cell lung carcinoma (A549 cell line) was evaluated by qRT-PCR method showing prevalent SPARC expression at mRNA and protein level normalized by β-actin as a housekeeping gene. To study the respond of A549 cells toward albumin-bound complexes, the SPARC expression level was evaluated for cells treated with the EAR8-II-THP complex bound with BSA at different concentrations (0-512 μM). Cells were incubated with the

treatments for 6 hr. This step was done because the cell viability results showed relative high cell viability in a 6 hr incubation time. However, if the cells were tested for 24 hr, the cell viability would be too low to be able to extract enough RNA for qRT-PCR experiments.

A literature review suggested that if the SPARC expression in a specimen is 75% or more relative to the expression of the housekeeping gene (i.e., β-actin), the specimen should be considered SPARC positive. Specimens are considered SPARC negative when SPARC expression is less than 25% to the expression of β-actin. A level between 25-75% is considered a moderate SPARC level [243]. In the current study, SPARC expression levels reduced significantly when the cells were treated with the complex, and this drop was more significant when the complex was bound with albumin. The normalized SPARC level in respect to β-actin expression levels for untreated cells and cells treated solely with the peptide-drug complex were more than 100%, indicating the SPARC positive cells, in which the expression of SPARC is even higher than of the housekeeping gene. However, specimens treated with albumin-bound complexes showed a significantly lower SPARC level of 52-65%, which is considered SPARC intermediate. In addition, normalized SPARC expression levels were also present relative to the expression level from untreated cells, revealing that increasing the concentration of BSA led to SPARC expression levels from up 65% (Figure 7.3). The pair t-test results between each treatment and untreated specimen represented a statistically significant reduction of SPARC expression for BSA-containing complex treatments ($p < 0.05$). SPARC proteins facilitate the uptake of albumin-bound molecules to the tumor cells. In the current study, endogenous SPARC expression was inhibited at the mRNA level by albumin-bound peptide-drug complex that can be further considered as one of the action mechanism of this system against cancer cells.

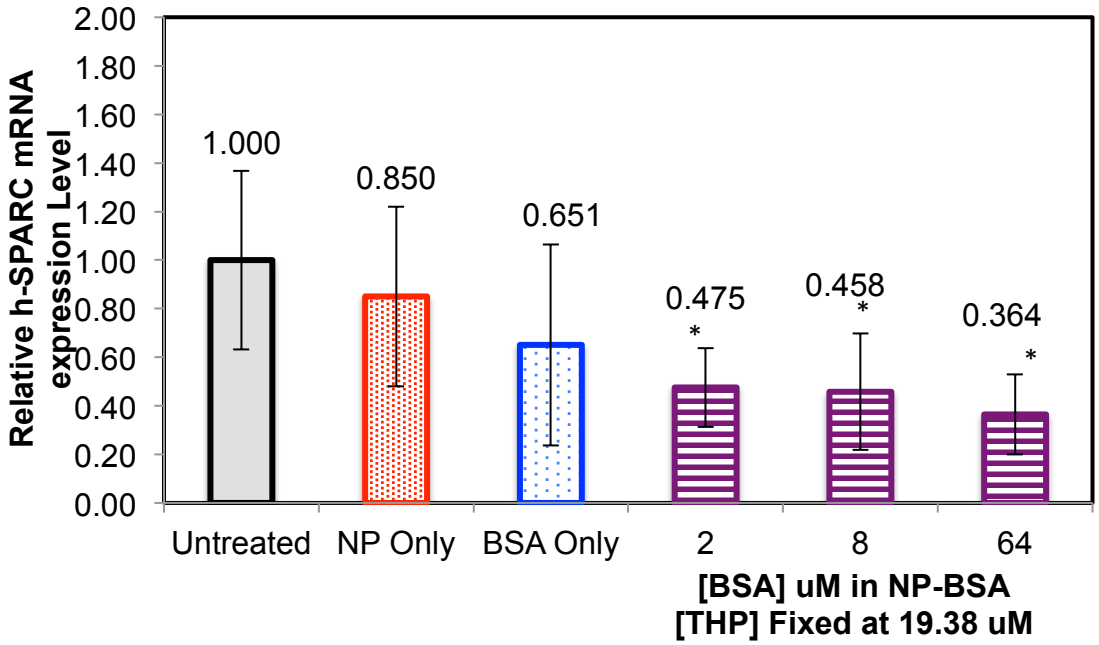

Figure 7.3. Relative SPARC expression in A549 cell line treated with EAR8-II-THP complexes (at THP final concentration of 19.38 μM and EAR8-II at 68.4 μM) and BSA concentration varied from 16 -512 μM. Error bars are relative standard deviations. * $p < 0.05$ compared with untreated cells.

7.4 Conclusions

The current study focused on albumin-bound peptide-drug complexes and their effect on non-small cell lung carcinoma (A549 cell line) through inhibition of SPARC expression at the mRNA level. It has been shown that SPARC expression facilitates the transport of albumin-bound delivery systems. The EAR8-II-THP complex was used as a drug delivery model for showing the binding affinity to albumin molecules. The effect of the presence of BSA in the complex solution on the cytotoxicity of the complex did not differ significantly to the absence of BSA. However, the target-ability of the complex increased considerably with SPARC inhibition through albumin's binding affinity to SPARC specifically. SPARC suppression is suggested as one of the uptake mechanisms by the albumin-bound peptide-based delivery system that can be further explored for more comprehensive conclusion.

Chapter 8

Conclusions and Recommendations

8.1 Original Contribution to Research

This thesis represents new findings in the inter-disciplinary fields of nanotechnology, biochemistry, thermodynamics, molecular biology, immunology, and chemical engineering. Amino acid pairing peptides present a great potential to encapsulate hydrophobic anticancer drugs and induce high *in vitro* anticancer activities. However, they have a tendency to aggregate in physiological environments, which limits their *in vivo* applications. Therefore, this research has mainly focused on overcoming the delivery limitations. Polymer conjugation and protein-binding strategies were originally investigated in this thesis to modify the self/co-assembling peptide-based drug delivery systems for longevity and target-ability applications. The major objectives and their respective outcomes of the research are summarized in the following section.

8.2 Principle Objectives and their Respective Outcomes

Characterize the physiochemical properties of amino acids pairing peptide (AAP8) functionalized with diethylene glycol (DEG)

The first objective of this research was to avoid uncontrollable aggregation of amino acid pairing peptide (AAP8) by diethylene glycol conjugation in either one or both terminals. These modifications contributed to modulating the fiber self-assembly through creating more aligned and uniform nanostructures due to increasing solubility, stability, and β-sheet content in secondary structure in the peptide. In addition, the DEG-modification led to lower toxicity of the AAP8 towards macrophages, indicating shielding properties of diethylene glycol for the peptide. The DEG modification also had advantages in hydrophobic drug stabilization in aqueous solution, consequently inducing more cytotoxicity towards lung carcinoma cells over a relatively long time, compared to the non-functionalized AAP8. As a conclusion, these DEG modifications can potentially be useful in the design and development of long circulating self-assembling peptide biomaterials for advanced drug delivery systems.

Evaluate self/co-assembly properties of an ionic-complementary peptide EAR8-II and its potential in *in vitro* delivery of the hydrophobic drug Pirarubicin (THP)

The second goal of this research project was to present a model self/co-assembling peptide EAR8-II that inherits advantages over EAK16-II and AAP8 in hydrophobic anticancer drug delivery. EAR8-II showed lower aggregation properties than AAP8 due to the replacement of phenylalanine with alanine residues providing moderate hydrophobic interactions between peptide molecules. EAR8-II showed a great potential in encapsulating the hydrophobic drug Pirarubicin (THP) in a peptide-to-drug ratio dependent manner. The complex at the peptide-to-drug mass ratio of 5:1 provided a stable solution, uniform nanostructure, and highly effective anticancer activity against various cancer cell lines.

Explore the binding affinity between serum proteins (i.e., BSA and IgG) and the EAR8-II-THP complex

Evaluating the binding affinity with serum proteins and the drug delivery system was the third objective of the current research. Results illustrate the high affinity with serum albumin, whereas the IgG showed relatively weak interaction with the EAR8-II-THP complex. EAR8-II-THP complexes form spherical and more uniform nanostructures (~ 20 nm) when bound with BSA and form larger aggregates when in contact with IgG, indicating more stability of the complex in an albumin solution. In addition, the binding affinity in the presence of salt showed no significant change compared to in a salt-free environment showing that ionic interaction is not the major driving force between serum albumin and the complex. Since the thermodynamic values showed spontaneous, exothermic, and enthalpy driven binding between BSA and the peptide-drug complex, it is determined that this binding is through hydrogen bonding and Van der Waals forces.

Study the effect of serum albumin binding to the EAR8-II-THP complex on immune responses

The main goal of the albumin binding strategy was making the peptide-based delivery system invisible to the immune system during long circulation. To show the positive effect of albumin binding on the delivery system, a series of immune response experiments were performed and resulted the significant reduction in immunogenicity of the complexes in the absence of serum albumin. The THP uptake rate and cytotoxicity of macrophages dropped considerably when the

complexes were pre-incubated with BSA. The cytokines responsible for inflammatory responses expressed relatively lower when the cells were treated with albumin-bound EAR8-II-THP complexes. Furthermore, the percentage of hemolytic activity also reduced more than half in the existence of serum albumin. All these findings indicate the shielding feature of serum albumin for the nanoparticles in physiological conditions.

Determine target-ability of the albumin-bound peptide-based drug delivery system

The last objective of the current research was exploring the target-ability of the albumin-bound peptide-based drug delivery system. Albumin has a high affinity to SPARC (secreted protein acidic and rich in cysteine), which is overexpressed in many cancer cells. When the peptide-based drug delivery system (EAR8-II-THP) was pre-incubated with serum albumin, the cellular toxicity and the uptake of THP showed no a significant difference to when the complex was applied to the cells without BSA pre-incubation. However, the SPARC expression level showed significantly lower values when the BSA concentration was increased.

8.3 Recommendations

Based on the outcomes of this thesis, the following recommendations are suggested:

1. Confirm DEG-conjugation advantages in inflammatory responses by performing more detailed *in vitro* and *in vivo* studies;
2. Find the optimize molecular weight of conjugated polymer in order to control the particle size of suitable for *in vivo* studies;
3. Develop a robust method to evaluate the encapsulation efficiency and loading capacity of the peptide-based delivery systems;
4. Replace the short sequence based peptides with longer sequences (e.g., 16-20 amino acids) to enhance encapsulation efficiency of the hydrophobic drug;
5. Study the binding affinity with other key circulating proteins (transferrin, fibrinogen,...);

6. Combine the polymer-conjugation and albumin binding strategies in order to evaluate the synergetic effect of the modifications on therapeutic efficiency and reduced inflammatory responses;
7. Establish the *in vivo* animal model, optimize the drug concentration (below maximum toxicity dose MTD), and perform systematic *in vivo* studies to evaluate immune responses, biodistribution, and tumor inhibition rates;
8. Self/co-assembling peptides have potential to conjugate with targeting ligands (peptides, mAb...) for targeted therapy.

References

[1] Koshkaryev A, Sawant R, Deshpande M, Torchilin V. Immunoconjugates and long circulating systems: origins, current state of the art and future directions. Adv Drug Deliv Rev 2013;65:24–35.

[2] Peer D, Karp JM, Hong S, Farokhzad OC, Margalit R, Langer R. Nanocarriers as an emerging platform for cancer therapy. Nat Nanotechnol 2007;2:751–60.

[3] Gu FX, Karnik R, Wang AZ, Alexis F, Levy-nissenbaum E, Hong S, et al. Targeted nanoparticles for Cancer Therapy. Nanotoday 2007;2:14–21.

[4] Torchilin VP. Multifunctional nanocarriers. Adv Drug Deliv Rev 2006;58:1532–55.

[5] Iyer AK, Khaled G, Fang J, Maeda H. Exploiting the enhanced permeability and retention effect for tumor targeting. Drug Discov Today 2006;11:812–8.

[6] Maeda H. SMANCS and polymer-conjugated macromolecular drugs: advantages in cancer chemotherapy. Adv Drug Deliv Rev 2001;46:169–85.

[7] Roberts MJ, Bentley MD, Harris JM. Chemistry for peptide and protein PEGylation. Adv Drug Deliv Rev 2002;54:459–76.

[8] Harris JM, Chess RB. Effect of pegylation on pharmaceuticals. Nat Rev Drug Discov 2003;2:214–21.

[9] König HM, Kilbinger AFM. Learning from nature: beta-sheet-mimicking copolymers get organized. Angew Chem Int Ed Engl 2007;46:8334–40.

[10] Zhou J, Zhang X, Li M, Wu W, Sun X, Zhang L, et al. Novel lipid hybrid albumin nanoparticle greatly lowered toxicity of pirarubicin. Mol Pharm 2013;10:3832–41.

[11] Kratz F, Elsadek B. Clinical impact of serum proteins on drug delivery. J Control Release 2012;161:429–45.

[12] Elsadek B, Kratz F. Impact of albumin on drug delivery - New applications on the horizon. J Control Release 2012;157:4–28.

[13] Garg SK. The Role of Basal Insulin and Glucagon-Like Peptide-1 Agonists in the Therapeutic Management of Type 2 Diabetes—A Comprehensive Review. Diabetes Technol Ther 2010;12:11–24.

[14] Desai N. Nab Technology-A drug Delivery Platform Utilising Endothelial gp60 Receptor-based Transport and Tumour-derived SPARC for Targeting. 2007.

[15] Gradishar WJ. Albumin-bound paclitaxel: a next-generation taxane. Expert Opin Pharmacother 2006;7:1041–53.

[16] Yardley D a. nab-Paclitaxel mechanisms of action and delivery. J Control Release 2013;170:365–72.

[17] Zhao X, Pan F, Xu H, Yaseen M, Shan H, Hauser C a E, et al. Molecular self-assembly and applications of designer peptide amphiphiles. Chem Soc Rev 2010;39:3480–98.

[18] Rudra JS, Tian YF, Jung JP, Collier JH. A self-assembling peptide acting as an immune adjuvant. Proc Natl Acad Sci U S A 2010;107:622–7.

[19] Collins L, Parker AL, Gehman JD, Eckley L, Perugini M a, Separovic F, et al. Self-assembly of peptides into spherical nanoparticles for delivery of hydrophilic moieties to the cytosol. ACS Nano 2010;4:2856–64.

[20] Torchilin VP. Cell penetrating peptide-modified pharmaceutical nanocarriers for intracellular drug and gene delivery. Biopolymers 2008;90:604–10.

[21] Aina OH, Sroka TC, Chen M-L, Lam KS. Therapeutic cancer targeting peptides. Biopolymers 2002;66:184–99.

[22] Serrano GN, Zhanel GG, Schweizer F. Antibacterial activity of ultrashort cationic lipo-beta-peptides. Antimicrob Agents Chemother 2009;53:2215–7.

[23] Valencia PM, Hanewich-Hollatz MH, Gao W, Karim F, Langer R, Karnik R, et al. Effects of ligands with different water solubilities on self-assembly and properties of targeted nanoparticles. Biomaterials 2011;32:6226–33.

[24] Fung SY, Yang H, Bhola PT, Sadatmousavi P, Muzar E, Liu M, et al. Self-Assembling Peptide as a Potential Carrier for Hydrophobic Anticancer Drug Ellipticine: Complexation, Release and In Vitro Delivery. Adv Funct Mater 2009;19:74–83.

[25] Wu Y, Sadatmousavi P, Wang R, Lu S, Yuan Y-F, Chen P. Self-assembling peptide-based nanoparticles enhance anticancer effect of ellipticine in vitro and in vivo. Int J Nanomedicine 2012;7:3221–33.

[26] Fung S-Y, Yang H, Sadatmousavi P, Sheng Y, Mamo T, Nazarian R, et al. Amino Acid Pairing for De Novo Design of Self-Assembling Peptides and Their Drug Delivery Potential. Adv Funct Mater 2011;21:2456–64.

[27] Feynman R. There's plenty of room at the bottom. Caltech Eng Sci 1960;23:22–36.

[28] Couvreur P. Nanoparticles in drug delivery: past, present and future. Adv Drug Deliv Rev 2013;65:21–3.

[29] Venditto VJ, Szoka FC. Cancer nanomedicines: so many papers and so few drugs! Adv Drug Deliv Rev 2013;65:80–8.

[30] Allen TM, Cullis PR. Drug delivery systems: entering the mainstream. Science 2004;303:1818–22.

[31] Petros R a, DeSimone JM. Strategies in the design of nanoparticles for therapeutic applications. Nat Rev Drug Discov 2010;9:615–27.

[32] Shi J, Xiao Z, Kamaly N, Farokhzad OC. Self-assembled targeted nanoparticles: evolution of technologies and bench to bedside translation. Acc Chem Res 2011;44:1123–34.

[33] Zhang Y, Chan HF, Leong KW. Advanced materials and processing for drug delivery: the past and the future. Adv Drug Deliv Rev 2013;65:104–20.

[34] Liechty WB, Kryscio DR, Slaughter B V, Peppas N a. Polymers for drug delivery systems. Annu Rev Chem Biomol Eng 2010;1:149–73.

[35] Bangham a. D, Horne RW. Negative staining of phospholipids and their structural modification by surface-active agents as observed in the electron microscope. J Mol Biol 1964;8:660–IN10.

[36] Bangham a. D, Standish MM, Watkins JC. Diffusion of univalent ions across the lamellae of swollen phospholipids. J Mol Biol 1965;13:238–IN27.

[37] Gregoriadis G. Drug Entrapment in Liposomes. FEBS Lett 1973;36:292–6.

[38] Heath T, Fraley R, Papahdjopoulos D. Antibody targeting of liposomes: cell specificity obtained by conjugation of F(ab')2 to vesicle surface. Sceince 1980;210:539–41.

[39] Leserman L, Barbet J, Kourilsky F, Weinstein J. Targeting to cells of fluorescent liposomes covalently coupled with monoclonal antibody or protein A. Nature 1980;288:602–4.

[40] US Food and Drug Administration. Drugs. US FDA website [online] 2013.

[41] Swami A, Shi J, Gadde S, Votruba AR, Kolishetti N, Farokhzad OC. Multifunctional Nanoparticles for Drug Delivery Applications 2012:9–30.

[42] Torchilin VP. Recent advances with liposomes as pharmaceutical carriers. Nat Rev Drug Discov 2005;4:145–60.

[43] Langer R, Folkman J. Polymers for the sustained release of proteins and other macromolecules. Nature 1976;263:797–800.

[44] Kattan J, Droz J, Couvreur P, Marino J, Boutan-Laroze A, Rougier P, et al. Phase I clinical trial and pharmacokinetic evaluation of Doxorubicin carried by polyisohexylcyanoacrylate nanoparticles. Invest New Drugs 1992;10:191–9.

[45] Gref R, Minamitake Y, Peracchia M, Trubetskoy V, Torchilin VP, Langer R. Biodegradable long-circulating polymeric nanospheres. Science (80-) 1994;263:1600–3.

[46] Duncan R, Vicent MJ. Polymer therapeutics-prospects for 21st century: the end of the beginning. Adv Drug Deliv Rev 2013;65:60–70.

[47] Duncan R. Polymer conjugates as anticancer nanomedicines. Nat Rev Cancer 2006;6:688–701.

[48] Ringsdorf H. Structure and properties of pharmacologically active polymers. J Polym Sci Polym Symp 1975;51:135–53.

[49] Kopecek J, Kopecková P, Minko T, Lu Z. HPMA copolymer-anticancer drug conjugates: design, activity, and mechanism of action. Eur J Pharm Biopharm 2000;50:61–81.

[50] Alconcel SNS, Baas AS, Maynard HD. FDA-approved poly(ethylene glycol)–protein conjugate drugs. Polym Chem 2011;2:1442.

[51] Canal F, Sanchis J, Vicent MJ. Polymer--drug conjugates as nano-sized medicines. Curr Opin Biotechnol 2011;22:894–900.

[52] Duncan R, Vicent MJ, Greco F, Nicholson RI. Polymer-drug conjugates: towards a novel approach for the treatment of endrocine-related cancer. Endocr Relat Cancer 2005;12 Suppl 1:S189–99.

[53] Abuchowski A, Es T Van, Palczuk NC, Davis FF. Bovine serum albumin by covalent Alteration of Immunological Properties of Bovine Serum Albumin by Covalent Attachment of Polyethylene Glycol. J Biol Chem 1977;252:3578–81.

[54] Abuchowski A, Mccoy JR, Palczuk NC, Es TVAN, Davis FF. Polyethylene glycol on immunogenicity and Effect of Covalent Attachment of Polyethylene Glycol on Immunogenicity and Circulating Life of Bovine Liver Catalase. J Biol Chem 1977;252:3582–6.

[55] Vilar G, Tulla-Puche J, Albericio F. Polymers and drug delivery systems. Curr Drug Deliv 2012;9:367–94.

[56] Birrenbach G, Speiser PP. Polymerized micelles and their use as adjuvants in immunology. J Pharm Sci 1976;65:1763–6.

[57] Bae Y, Nishiyama N, Kataoka K. In vivo antitumor activity of the folate-conjugated pH-sensitive polymeric micelle selectively releasing adriamycin in the intracellular acidic compartments. Bioconjug Chem 2007;18:1131–9.

[58] Oerlemans C, Bult W, Bos M, Storm G, Nijsen JFW, Hennink WE. Polymeric micelles in anticancer therapy: targeting, imaging and triggered release. Pharm Res 2010;27:2569–89.

[59] Lee KS, Chung HC, Im SA, Park YH, Kim CS, Kim S-B, et al. Multicenter phase II trial of Genexol-PM, a Cremophor-free, polymeric micelle formulation of paclitaxel, in patients with metastatic breast cancer. Breast Cancer Res Treat 2008;108:241–50.

[60] Malik N, Evagorou E, Duncan R. Dendrimer- platinate: a novel approach to cancer chemotherapy. Anticencer Drugs 1999;10:767–76.

[61] Medina SH, El-Sayed MEH. Dendrimers as carriers for delivery of chemotherapeutic agents. Chem Rev 2009;109:3141–57.

[62] Zhang Y, Orner BP. Self-assembly in the ferritin nano-cage protein superfamily. Int J Mol Sci 2011;12:5406–21.

[63] Maham A, Tang Z, Wu H, Wang J, Lin Y. Protein-based nanomedicine platforms for drug delivery. Small 2009;5:1706–21.

[64] Ren Y, Wong SM, Lim L-Y. Folic acid-conjugated protein cages of a plant virus: a novel delivery platform for doxorubicin. Bioconjug Chem 2007;18:836–43.

[65] Flenniken ML, Liepold LO, Crowley BE, Willits D a, Young MJ, Douglas T. Selective attachment and release of a chemotherapeutic agent from the interior of a protein cage architecture. Chem Commun (Camb) 2005;2:447–9.

[66] Chen L, Remondetto G, Rouabhia M, Subirade M. Kinetics of the breakdown of cross-linked soy protein films for drug delivery. Biomaterials 2008;29:3750–6.

[67] Gradishar WJ, Tjulandin S, Davidson N, Shaw H, Desai N, Bhar P, et al. Phase III trial of nanoparticle albumin-bound paclitaxel compared with polyethylated castor oil-based paclitaxel in women with breast cancer. J Clin Oncol 2005;23:7794–803.

[68] Desai N, Trieu V, Damascelli B, Soon-shiong P. SPARC Expression Correlates with Tumor Response to Albumin-Bound Paclitaxel in Head and Neck Cancer Patients. Transl Oncol 2009;2:59–64.

[69] Desai N, Trieu V, Yao Z, Louie L, Ci S, Yang A, et al. Increased antitumor activity, intratumor paclitaxel concentrations, and endothelial cell transport of cremophor-free, albumin-bound paclitaxel, ABI-007, compared with cremophor-based paclitaxel. Clin Cancer Res 2006;12:1317–24.

[70] Gabizon AA. Liposome circulation time and tumor targeting: implications for cancer chemotherapy. Adv Drug Deliv Rev 1995;16:285–94.

[71] Maeda H, Wu J, Sawa T, Matsumura Y, Hori K. Tumor vascular permeability and the EPR effect in macromolecular therapeutics: a review. J Control Release 2000;65:271–84.

[72] Torchilin VP, Trubetskoy VS, Whiteman KR, Caliceti P, Ferruti P, Veronese FM. New Synthetic Amphiphilic Polymers for Steric Protection of Liposomes In-Vivo. J Pharm Sci 1995;84:1049–53.

[73] Allen C, Dos Santos N, Gallagher R, Chiu GNC, Shu Y, Li WM, et al. Controlling the physical behavior and biological performance of liposome formulations through use of surface grafted poly(ethylene glycol). Biosci Rep 2002;22:225–50.

[74] Zalipsky S. Chemistry of polyethylene glycol conjugates with biologically active molecules. Adv Drug Deliv Rev 1995;16:157–82.

[75] Gunaseelan S, Pooyan S, Chen P, Samizadeh M, Palombo MS, Stein S, et al. Multimeric peptide-based PEG nanocarriers with programmable elimination properties. Biomaterials 2009;30:5649–59.

[76] Torchilin VP, Omelyanenko VG, Papisov MI, Bogdanov AA, Trubetskoy VS, Herron JN, et al. Poly (ethylene glycol) on the liposome surface : on the mechanism of polymer-coated liposome longevity. Biochim Biophys Acta 1994;1195:11–20.

[77] Graham ML. Pegaspargase: a review of clinical studies. Adv Drug Deliv Rev 2003;55:1293–302.

[78] Langer R. Drug Delivery and Targeting. Nat Rev 1998;392.

[79] Alexis F, Pridgen E, Molnar LK, Farokhzad OC. Factors affecting the clearance and biodistribution of polymeric nanoparticles. Mol Pharm 2008;5:505–15.

[80] Zhang L, Gu FX, Chan JM, Wang AZ, Langer RS, Farokhzad OC. Nanoparticles in Medicine : Therapeutic Applications and Developments. Clin Pharmacol Ther 2008;83:761–9.

[81] Burkoth TS, Benzinger TLS, Jones DNM, Hallenga K, Meredith SC, Lynn DG. C-Terminal PEG Blocks the Irreversible Step in -Amyloid , the major component of plaques found in the brains of patients with Alzheimer ' s disease (AD), 1 is a 40-43 amino acid proteolytic fragment of the -amyloid precursor protein , 2 which rapidly an. Brain 1998;7863:7655–6.

[82] Lynn DG, Meredith SC. Review: model peptides and the physicochemical approach to beta-amyloids. J Struct Biol 2000;130:153–73.

[83] Pechar M, Brus J, Kostka L, Konák C, Urbanová M, Slouf M. Thermoresponsive self-assembly of short elastin-like polypentapeptides and their poly(ethylene glycol) derivatives. Macromol Biosci 2007;7:56–69.

[84] Hamley IW, Ansari I a, Castelletto V, Nuhn H, Rösler a, Klok H. Solution self-assembly of hybrid block copolymers containing poly(ethylene glycol) and amphiphilic beta-strand peptide sequences. Biomacromolecules 2005;6:1310–5.

[85] Collier JH, Messersmith PB. Self-Assembling Polymer–Peptide Conjugates: Nanostructural Tailoring. Adv Mater 2004;16:907–10.

[86] Filpula D, Zhao H. Releasable PEGylation of proteins with customized linkers. Adv Drug Deliv Rev 2008;60:29–49.

[87] Mahmoudi M, Lynch I, Ejtehadi MR, Monopoli MP, Bombelli FB, Laurent S. Protein-nanoparticle interactions: opportunities and challenges. Chem Rev 2011;111:5610–37.

[88] Lundqvist M, Stigler J, Elia G, Lynch I, Cedervall T, Dawson K a. Nanoparticle size and surface properties determine the protein corona with possible implications for biological impacts. Proc Natl Acad Sci U S A 2008;105:14265–70.

[89] Lartigue L, Wilhelm C, Servais J, Factor C, Dencausse A, Bacri J-C, et al. Nanomagnetic sensing of blood plasma protein interactions with iron oxide nanoparticles: impact on macrophage uptake. ACS Nano 2012;6:2665–78.

[90] De M, Miranda OR, Rana S, Rotello VM. Size and geometry dependent protein-nanoparticle self-assembly. Chem Commun (Camb) 2009:2157–9.

[91] Monopoli MP, Aberg C, Salvati A, Dawson K a. Biomolecular coronas provide the biological identity of nanosized materials. Nat Nanotechnol 2012;7:779–86.

[92] Kratz F. Albumin as a drug carrier: design of prodrugs, drug conjugates and nanoparticles. J Control Release 2008;132:171–83.

[93] Subramanian GM, Fiscella M, Lamousé-Smith A, Zeuzem S, McHutchison JG. Albinterferon alpha-2b: a genetic fusion protein for the treatment of chronic hepatitis C. Nat Biotechnol 2007;25:1411–9.

[94] Kremer P, Wunder A, Sinn H, Haase T, Rheinwald M, Zillmann U, et al. Laser-induced fluorescence detection of malignant gliomas using fluorescein-labeled serum albumin: experimental and preliminary clinical results. Neurol Res 2000;22:481–9.

[95] Ding R, Frei E, Fardanesh M, Schrenk H-H, Kremer P, Haefeli WE. Pharmacokinetics of 5-aminofluorescein-albumin, a novel fluorescence marker of brain tumors during surgery. J Clin Pharmacol 2011;51:672–8.

[96] McDonagh CF, Huhalov A, Harms BD, Adams S, Paragas V, Oyama S, et al. Antitumor activity of a novel bispecific antibody that targets the ErbB2/ErbB3 oncogenic unit and inhibits heregulin-induced activation of ErbB3. Mol Cancer Ther 2012;11:582–93.

[97] Stoddart C a, Nault G, Galkina S a, Thibaudeau K, Bakis P, Bousquet-Gagnon N, et al. Albumin-conjugated C34 peptide HIV-1 fusion inhibitor: equipotent to C34 and T-20 in vitro with sustained activity in SCID-hu Thy/Liv mice. J Biol Chem 2008;283:34045–52.

[98] Kendall M, Ding P, Kendall K. Particle and nanoparticle interactions with fibrinogen: the importance of aggregation in nanotoxicology. Nanotoxicology 2011;5:55–65.

[99] Cedervall T, Lynch I, Lindman S, Berggård T, Thulin E, Nilsson H, et al. Understanding the nanoparticle-protein corona using methods to quantify exchange rates and affinities of proteins for nanoparticles. Proc Natl Acad Sci U S A 2007;104:2050–5.

[100] Linse S, Cabaleiro-Lago C, Xue W-F, Lynch I, Lindman S, Thulin E, et al. Nucleation of protein fibrillation by nanoparticles. Proc Natl Acad Sci U S A 2007;104:8691–6.

[101] Colvin VL, Kulinowski KM. Nanoparticles as catalysts for protein fibrillation. Proc Natl Acad Sci U S A 2007;104:8679–80.

[102] Nie S, Xing Y, Kim GJ, Simons JW. Nanotechnology applications in cancer. Annu Rev Biomed Eng 2007;9:257–88.

[103] Weiner LM, Adams GP. New approaches to antibody therapy. Oncogene 2000;19:6144–51.

[104] Gabizon a a. Pegylated liposomal doxorubicin: metamorphosis of an old drug into a new form of chemotherapy. Cancer Invest 2001;19:424–36.

[105] Von Mehren M, Adams GP, Weiner LM. Monoclonal antibody therapy for cancer. Annu Rev Med 2003;54:343–69.

[106] Zettlitz K a, Seitter J, Müller D, Kontermann RE. Humanization of a mouse monoclonal antibody directed against a cell surface-exposed epitope of membrane-associated heat shock protein 70 (Hsp70). Mol Biotechnol 2010;46:265–78.

[107] Dhar S, Gu FX, Langer R, Farokhzad OC, Lippard SJ. Targeted delivery of cisplatin to prostate cancer cells by aptamer functionalized Pt(IV) prodrug-PLGA-PEG nanoparticles. Proc Natl Acad Sci U S A 2008;105:17356–61.

[108] Essler M, Ruoslahti E. Molecular specialization of breast vasculature: a breast-homing phage-displayed peptide binds to aminopeptidase P in breast vasculature. Proc Natl Acad Sci U S A 2002;99:2252–7.

[109] Kannagi R, Izawa M, Koike T, Miyazaki K, Kimura N. Carbohydrate-mediated cell adhesion in cancer metastasis and angiogenesis. Cancer Sci 2004;95:377–84.

[110] Juliano RL, Alam R, Dixit V, Kang M. Cell-targeting and cell-penetrating peptides for delivery of therapeutic and imaging agents. Nanomedicine and Nanobiotechnology 2009;1:324–35.

[111] Wu XL, Kim JH, Koo H, Bae SM, Shin H, Kim MS, et al. Tumor-targeting peptide conjugated pH-responsive micelles as a potential drug carrier for cancer therapy. Bioconjug Chem 2010;21:208–13.

[112] Ellerby HM, Arap W, Ellerby LM, Kain R, Andrusiak R, Rio GD, et al. Anti-cancer activity of targeted pro-apoptotic peptides. Nat Med 1999;5:1032–8.

[113] Burg M a, Pasqualini R, Arap W, Ruoslahti E, Stallcup WB. NG2 proteoglycan-binding peptides target tumor neovasculature. Cancer Res 1999;59:2869–74.

[114] Dubey PK, Mishra V, Jain S, Mahor S, Vyas SP. Liposomes modified with cyclic RGD peptide for tumor targeting. J Drug Target 2004;12:257–64.

[115] Xiong X-B, Huang Y, Lu W-L, Zhang X, Zhang H, Nagai T, et al. Intracellular delivery of doxorubicin with RGD-modified sterically stabilized liposomes for an improved antitumor efficacy: in vitro and in vivo. J Pharm Sci 2005;94:1782–93.

[116] Kunath K, Merdan T, Hegener O, Häberlein H, Kissel T. Integrin targeting using RGD-PEI conjugates for in vitro gene transfer. J Gene Med 2003;5:588–99.

[117] Mitra A, Coleman T, Borgman M, Nan A, Ghandehari H, Line BR. Polymeric conjugates of mono- and bi-cyclic alphaVbeta3 binding peptides for tumor targeting. J Control Release 2006;114:175–83.

[118] Kim WJ, Yockman JW, Jeong JH, Christensen L V, Lee M, Kim Y-H, et al. Anti-angiogenic inhibition of tumor growth by systemic delivery of PEI-g-PEG-RGD/pCMV-sFlt-1 complexes in tumor-bearing mice. J Control Release 2006;114:381–8.

[119] Temming K, Lacombe M, van der Hoeven P, Prakash J, Gonzalo T, Dijkers ECF, et al. Delivery of the p38 MAPkinase inhibitor SB202190 to angiogenic endothelial cells: development of novel RGD-equipped and PEGylated drug-albumin conjugates using platinum(II)-based drug linker technology. Bioconjug Chem 2006;17:1246–55.

[120] Torchilin V. Multifunctional and stimuli-sensitive pharmaceutical nanocarriers. Eur J Pharm Biopharm 2009;71:431–44.

[121] Fundueanu G, Constantin M, Stanciu C, Theodoridis G, Ascenzi P. pH- and temperature-sensitive polymeric microspheres for drug delivery: the dissolution of copolymers modulates drug release. J Mater Sci Mater Med 2009;20:2465–75.

[122] Meyer DE, Shin BC, Kong G a, Dewhirst MW, Chilkoti a. Drug targeting using thermally responsive polymers and local hyperthermia. J Control Release 2001;74:213–24.

[123] Sershen SR, Westcott SL, Halas NJ, West JL. Temperature-sensitive polymer – nanoshell composites for photothermally modulated drug delivery. J Biomed Mater Res A 2000;51:293–8.

[124] Alexiou C, Arnold W, Klein RJ, Parak FG, Hulin P, Bergemann C, et al. Locoregional cancer treatment with magnetic drug targeting. Cancer Res 2000;60:6641–8.

[125] Zhang S. Emerging biological materials through molecular. Biotechnol Adv 2002;20:321–39.

[126] Zhang S, Holmes T, Lockshin C, Rich A. Spontaneous Assembly of a Self-complementary Oligopeptide to Form a Stable Macroscopic Membrane. Proc Natl Acad Sci United States 1993;90:3334–8.

[127] Zhang S, Lockshin C, Cook R, Rich A. Unusually Stable b-sheet Formation in an Ionic Self-Compelemtarty Oligopeptide. Biopolymers 1994;34:663–72.

[128] Altman M, Lee P, Rich a, Zhang S. Conformational behavior of ionic self-complementary peptides. Protein Sci 2000;9:1095–105.

[129] Zhang S, Holmes TC, DiPesrsio M, Hynes RO, Su X, Rich A. Self-complementary oligopeptide matrices support mammalian cell attachment. Biomaterials 1995;16:1385–93.

[130] Holmes TC, de Lacalle S, Su X, Liu G, Rich a, Zhang S. Extensive neurite outgrowth and active synapse formation on self-assembling peptide scaffolds. Proc Natl Acad Sci U S A 2000;97:6728–33.

[131] Zhang S, Altman M. Peptide self-assembly in functional polymer science and engineering. React Funct Polym 1999;41:91–102.

[132] Keyes-Baig C, Duhamel J, Fung S-Y, Bezaire J, Chen P. Self-assembling peptide as a potential carrier of hydrophobic compounds. J Am Chem Soc 2004;126:7522–32.

[133] Nagai Y, Unsworth LD, Koutsopoulos S, Zhang S. Slow release of molecules in self-assembling peptide nanofiber scaffold. J Control Release 2006;115:18–25.

[134] Song H, Zhang L, Zhao X. Hemostatic Efficacy of Biological Self-Assembling Peptide Nanofibers in a Rat Kidney Model. Macromol Biosci 2010;10:33–9.

[135] Cigognini D, Satta A, Colleoni B, Silva D, Donegà M, Antonini S, et al. Evaluation of early and late effects into the acute spinal cord injury of an injectable functionalized self-assembling scaffold. PLoS One 2011;6:e19782.

[136] Guo H, Cui G, Yang J, Wang C, Zhu J, Zhang L, et al. Sustained delivery of VEGF from designer self-assembling peptides improves cardiac function after myocardial infarction. Biochem Biophys Res Commun 2012;424:105–11.

[137] Li X, Katsanevakis E, Liu X, Zhang N, Wen X. Engineering neural stem cell fates with hydrogel design for central nervous system regeneration. Prog Polym Sci 2012;37:1105–29.

[138] Zhang S, Yan L, Altman M, Lässle M, Nugent H, Frankel F, et al. Biological surface engineering: a simple system for cell pattern formation. Biomaterials 1999;20:1213–20.

[139] Santoso SS, Vauthey S, Zhang S. Structures, function and applications of amphiphilic peptides. Curr Opin Colloid Interface Sci 2002;7:262–6.

[140] Santoso S, Hwang W, Hartman H, Zhang S. Self-assembly of Surfactant-like Peptides with Variable Glycine Tails to Form Nanotubes and Nanovesicles. Nano Lett 2002;2:687–91.

[141] Hartgerink JD, Beniash E, Stupp SI. Self-assembly and mineralization of peptide-amphiphile nanofibers. Science 2001;294:1684–8.

[142] Schwartz JJ, Zhang S. Peptide-mediated cellular delivery. Curr Opin Mol Ther 2000;2:162–7.

[143] Lindsay M a. Peptide-mediated cell delivery: application in protein target validation. Curr Opin Pharmacol 2002;2:587–94.

[144] Zhang S. Building from the bottom up. Mater Today 2003:20–7.

[145] Yanlian Y, Ulung K, Xiumei W, Horii A, Yokoi H, Shuguang Z. Designer self-assembling peptide nanomaterials. Nano Today 2009;4:193–210.

[146] Fung SY, Yang H, Chen P. Formation of colloidal suspension of hydrophobic compounds with an amphiphilic self-assembling peptide. Colloids Surf B Biointerfaces 2007;55:200–11.

[147] Fung SY, Yang H, Chen P. Sequence effect of self-assembling peptides on the complexation and in vitro delivery of the hydrophobic anticancer drug ellipticine. PLoS One 2008;3:e1956.

[148] Fung SY, Keyes C, Duhamel J, Chen P. Concentration effect on the aggregation of a self-assembling oligopeptide. Biophys J 2003;85:537–48.

[149] Yang H, Fung S-Y, Pritzker M, Chen P. Surface-assisted assembly of an ionic-complementary peptide: controllable growth of nanofibers. J Am Chem Soc 2007;129:12200–10.

[150] Haldar D, Banerjee A, Drew MGB, Das K, Cambridge R, March UK, et al. First crystallographic signature of an acyclic peptide nanorod : molecular mechanism of nanorod formation by a self-assembled tetrapeptide † A terminally protected acyclic tetrapeptide Boc-Aib-Val- crystals and further self-assembly of this supramolecular. R Soc Chem 2003:1406–7.

[151] Matsui H, Gologan B, Pan S, Jr GED. Controlled immobilization of peptide nanotube-templated. Eur Phys J D 2001;16:403–6.

[152] Hong Y, Legge RL, Zhang S, Chen P. Effect of amino acid sequence and pH on nanofiber formation of self-assembling peptides EAK16-II and EAK16-IV. Biomacromolecules 2003;4:1433–42.

[153] Mart RJ, Osborne RD, Stevens MM, Ulijn R V. Peptide-based stimuli-responsive biomaterials. Soft Matter 2006;2:822.

[154] Fung S-Y, Oyaizu T, Yang H, Yuan Y, Han B, Keshavjee S, et al. The potential of nanoscale combinations of self-assembling peptides and amino acids of the Src tyrosine kinase inhibitor in acute lung injury therapy. Biomaterials 2011;32:4000–8.

[155] Chen P, Yang H, Fung S-Y. Amino acid pairing-based self-assembling peptides and methods, 2009.

[156] Fung S, Yang H, Sadatmousavi P, Sheng Y, Mamo T, Nazarian R, et al. Supporting Information for " Amino Acid Pairing for De Novo Design of Self-Assembling Peptides and their Drug Delivery Potentials " 2011.

[157] Owens DE, Peppas N a. Opsonization, biodistribution, and pharmacokinetics of polymeric nanoparticles. Int J Pharm 2006;307:93–102.

[158] Liu D, Wu W, Ling J, Wen S, Gu N, Zhang X. Effective PEGylation of Iron Oxide Nanoparticles for High Performance In Vivo Cancer Imaging. Adv Funct Mater 2011:n/a–n/a.

[159] Fukushima Y. Association of Poly (ethylene glycol) Modified with Peptide Strands with a High Propensity to Form a NL -Sheet Conformation. J Polym Sci Part A Polym Chem 2001;39:742–5.

[160] Tian E, Landowski TH, Stephens OW, Yaccoby S, Barlogie B, Shaughnessy JD. Ellipticine derivative NSC 338258 represents a potential new antineoplastic agent for the treatment of multiple myeloma. Mol Cancer Ther 2008;7:500–9.

[161] Cavalcanti LP, Torriani IL. Thermotropic phase behavior of DPPC liposome systems in the presence of the anti-cancer agent "Ellipticine". Eur Biophys J 2006;36:67–71.

[162] Peracchia MT, Vauthier C, Desmaele D, Gulik A, Dedieu J-C, Demoy M, et al. Pegylated Nanoparticles from a Novel Methoxypolyethylene Glycol Cyanoacrylate Amphiphilic Copolymer. Pharm Res 1998;15:550–6.

[163] Fant K, Esbjo EK, Jenkins A, Grossel MC, Lincoln P, Norde B. articles Effects of PEGylation and Acetylation of PAMAM Dendrimers on DNA Binding , Cytotoxicity and in Vitro Transfection Efficiency. Mol Pharm 2010;17.

[164] Lomakin a, Chung DS, Benedek GB, Kirschner D a, Teplow DB. On the nucleation and growth of amyloid beta-protein fibrils: detection of nuclei and quantitation of rate constants. Proc Natl Acad Sci U S A 1996;93:1125–9.

[165] Sonoki T, Matsuzaki H, Nagasaki a, Hata H, Yoshida M, Matsuoka M, et al. Detection of inducible nitric oxide synthase (iNOS) mRNA by RT-PCR in ATL patients and HTLV-I infected cell lines: clinical features and apoptosis by NOS inhibitor. Leuk Off J Leuk Soc Am Leuk Res Fund, UK 1999;13:713–8.

[166] Macmicking J, Xie Q, Nathan C. Nitric Oxide and Macrophage Function. Annu Rev Immunol 1997;15:323–50.

[167] Sadatmousavi P. Peptide-Mediated Anticancer Drug Delivery. University of Waterloo, 2009.

[168] Sadatmousavi P, Mamo T, Chen P. Diethylene glycol functionalized self-assembling peptide nanofibers and their hydrophobic drug delivery potential. Acta Biomater 2012;8:3241–50.

[169] Greish K, Nagamitsu A, Fang J, Maeda H, Hospital H. Copoly(styrene-maleic acid)-Pirarubicin Micelles: High Tumor-Targeting Efficiency with Little Toxicity1. Bioconjug Chem 2005;16:230–6.

[170] Daruwalla J, Greish K, Nikfarjam M, Millar I, Malcontenti-Wilson C, Iyer AK, et al. Evaluation of the effect of SMA-pirarubicin micelles on colorectal cancer liver metastases and of hyperbaric oxygen in CBA mice. J Drug Target 2007;15:487–95.

[171] Daruwalla J, Nikfarjam M, Greish K, Malcontenti-Wilson C, Muralidharan V, Christophi C, et al. In vitro and in vivo evaluation of tumor targeting styrene-maleic acid copolymer-pirarubicin micelles: Survival improvement and inhibition of liver metastases. Cancer Sci 2010;101:1866–74.

[172] Robert J, Monnier A, Poutignat N, Hrait P, Saint-gents D, Cedex F-B, et al. A Pharmacokinetic and pharmacodynamic study of the new anthracycline pirarubicin in breast cancer pateins. Cancer Chemother Pharmacol 1991;29:75–9.

[173] Takamatsu Y, Suzumiya J, Utsunomiya A, Maeda K, Matsuoka H, Suzushima H, et al. THP-COP regimen for the treatment of peripheral T-cell lymphoma and adult T-cell leukemia/lymphoma: a multicenter phase II study. Eur J Haematol 2010;84:391–7.

[174] Tsurumi H, Hara T, Goto N, Kanemura N, Kasahara S, Sawada M, et al. A phase II study of a THP-COP regimen for the treatment of elderly patients aged 70 years or older with diffuse large B-cell lymphoma. Hematol Oncol 2007;25:107–14.

[175] Greish K, Sawa T, Fang J, Akaike T, Maeda H. SMA – doxorubicin , a new polymeric micellar drug for effective targeting to solid tumours. J Control Release 2004;97:219–30.

[176] Choiprasert W, Dechsupa N, Kothan S, Garrigos M, Mankhetkorn S. Quercetin , Quercetrin Except Rutin Potentially Increased Pirarubicin Cytotoxicity by Non-Competitively Inhibiting the P-Glycoprotein-and MRP1 Function in Living K562 / adr and GLC4 / adr Cells Laboratory of Physical Chemistry , Molecular and Cellular Bio. Am J Pharmacol Toxicol 2010;5:24–33.

[177] Thumshirn G, Hersel U, Goodman SL, Kessler H. Multimeric cyclic RGD peptides as potential tools for tumor targeting: solid-phase peptide synthesis and chemoselective oxime ligation. Chemistry 2003;9:2717–25.

[178] Bawa R, Fung S-Y, Shiozaki A, Yang H, Zheng G, Keshavjee S, et al. Self-assembling peptide-based nanoparticles enhance cellular delivery of the hydrophobic anticancer drug ellipticine through caveolae-dependent endocytosis. Nanomedicine 2012;8:647–54.

[179] Goldenberg NM, Steinberg BE. Surface charge: a key determinant of protein localization and function. Cancer Res 2010;70:1277–80.

[180] Au JL-S, Jang SH, Wientjes MG. Clinical aspects of drug delivery to tumors. J Control Release 2002;78:81–95.

[181] Cheng Y-C, Prusoff W. Relationship between the inhibition constant (KI) and the concentration of inhibitor which causes 50 per cent inhibition (I50) of an enzymatic reaction. Biochem Pharmacol 1973;22:3099–108.

[182] Kim S-S, Garg H, Joshi A, Manjunath N. Strategies for targeted nonviral delivery of siRNAs in vivo. Trends Mol Med 2009;15:491–500.

[183] Oh Y-K, Park TG. siRNA delivery systems for cancer treatment. Adv Drug Deliv Rev 2009;61:850–62.

[184] Faraji AH, Wipf P. Nanoparticles in cellular drug delivery. Bioorg Med Chem 2009;17:2950–62.

[185] Dennis MS, Zhang M, Meng YG, Kadkhodayan M, Kirchhofer D, Combs D, et al. Albumin binding as a general strategy for improving the pharmacokinetics of proteins. J Biol Chem 2002;277:35035–43.

[186] Sadatmousavi P, Chen P. Self/Co-Assembling Peptide, EAR8-II, as a Potential Carrier for a Hydrophobic Anticancer Drug Pirarubicin (THP)-Characterization and in-vitro Delivery. Int J Mol Sci 2013;14:23315–29.

[187] Deng ZJ, Liang M, Toth I, Monteiro MJ, Minchin RF. Molecular interaction of poly(acrylic acid) gold nanoparticles with human fibrinogen. ACS Nano 2012;6:8962–9.

[188] Roser M, Fischer D, Kissel T. Surface-modified biodegradable albumin nano- and microspheres . II : effect of surface charges on in vitro phagocytosis and biodistribution in rats 1998;46:255–63.

[189] Deng ZJ, Liang M, Monteiro M, Toth I, Minchin RF. Nanoparticle-induced unfolding of fibrinogen promotes Mac-1 receptor activation and inflammation. Nat Nanotechnol 2011;6:39–44.

[190] Mahmoudi M, Lohse SE, Murphy CJ, Fathizadeh A, Montazeri A, Suslick KS. Variation of protein corona composition of gold nanoparticles following plasmonic heating. Nano Lett 2014;14:6–12.

[191] Mahmoudi M, Abdelmonem AM, Behzadi S, Clement JH, Dutz S, Ejtehadi MR, et al. Temperature: the "ignored" factor at the NanoBio interface. ACS Nano 2013;7:6555–62.

[192] Kratz F, Elsadek B. Clinical impact of serum proteins on drug delivery. J Control Release 2012;161:429–45.

[193] Gordon DL, Centre FM. Opsonin-dependent and independent surface phagocytosis of S . aureus proceeds independently of complement and complement receptors. Immunology 1988;64:709–14.

[194] Hallgren R, Stalenheim G. Opsonins in human serum for the phagocytosis of complexes between IgG and protein A of Staphylococcus aureus. Immunology 1978;35:13–20.

[195] Lakowicz JR. Principles of Fluorescence Spectroscopy. 3rd Editio. Springer; 1999.

[196] Shang L, Wang Y, Jiang J, Dong S. pH-dependent protein conformational changes in albumin:gold nanoparticle bioconjugates: a spectroscopic study. Langmuir 2007;23:2714–21.

[197] Maruyama T, Katoh S, Nakajima M, Nabetani H, Abbott TP, Shono A, et al. FT-IR analysis of BSA fouled on ultrafiltration and microfiltration membranes. J Memb Sci 2001;192:201–7.

[198] Fu K, Griebenow K, Hsieh L, Klibanov a M, LangerR. FTIR characterization of the secondary structure of proteins encapsulated within PLGA microspheres. J Control Release 1999;58:357–66.

[199] Agudelo D, Bourassa P, Bruneau J, Bérubé G, Asselin E, Tajmir-Riahi H-A. Probing the Binding Sites of Antibiotic Drugs Doxorubicin and N-(trifluoroacetyl) Doxorubicin with Human and Bovine Serum Albumins. PLoS One 2012;7:e43814.

[200] Cui F-L, Qin L-X, Zhang G-S, Yao X-J, Du J. Binding of daunorubicin to human serum albumin using molecular modeling and its analytical application. Int J Biol Macromol 2008;42:221–8.

[201] Guo X, Han X, Tong J, Guo C, Yang W, Zhu J, et al. The investigation of the interaction between piracetam and bovine serum albumin by spectroscopic methods. J Mol Struct 2010;966:129–35.

[202] Chen W, Huang H, Lin C, Lin F, Chan Y. Effect of Temperature on Hydrophobic Interaction between Proteins and Hydrophobic Adsorbents : Studies by Isothermal Titration Calorimetry and the van ' t Hoff Equation. Langmuir 2003;19:9395–403.

[203] De M, You C, Srivastava S, Rotello VM. Biomimetic Interactions of Proteins with Functionalized Nanoparticles : A Thermodynamic Study Isothermal Titration Calorimetry . While differential scan-. J Am Chem Soc 2007;129:10747–53.

[204] Frazier R a, Papadopoulou A, Green RJ. Isothermal titration calorimetry study of epicatechin binding to serum albumin. J Pharm Biomed Anal 2006;41:1602–5.

[205] Brancaleon L, Moseley H. Effects of photoproducts on the binding properties of protoporphyrin IX to proteins. Biophys Chem 2002;96:77–87.

[206] Brancaleon L, Magennis SW, Samuel IDW, Namdas E, Lesar A, Moseley H. Characterization of the photoproducts of protoporphyrin IX bound to human serum albumin and immunoglobulin G. Biophys Chem 2004;109:351–60.

[207] Monopoli MP, Bombelli FB, Dawson K a. Nanobiotechnology: Nanoparticle coronas take shape. Nat Nanotechnol 2011;6:11–2.

[208] Moghimi SM, Hunter a C, Murray JC. Long-circulating and target-specific nanoparticles: theory to practice. Pharmacol Rev 2001;53:283–318.

[209] Doorley GW, Payne CK. Nanoparticles act as protein carriers during cellular internalization. Chem Commun (Camb) 2012;48:2961–3.

[210] James AE, Driskell JD. Monitoring gold nanoparticle conjugation and analysis of biomolecular binding with nanoparticle tracking analysis (NTA) and dynamic light scattering (DLS). Analyst 2013;138:1212–8.

[211] Faulk W, Taylor C, Yeh C, McIntyre J. Preliminary clinical study of transferrin-adriamycin conjugate for drug delivery to acute leukemia patients. Mol Biother 1990;2:57–60.

[212] Yao Y-C, Zhan X-Y, Zhang J, Zou X-H, Wang Z-H, Xiong Y-C, et al. A specific drug targeting system based on polyhydroxyalkanoate granule binding protein PhaP fused with targeted cell ligands. Biomaterials 2008;29:4823–30.

[213] Gumpen S, Hegg PO, Martens H. Thermal stability of fatty acid-serum albumin complexes studied by differential scanning calorimetry. Biochim Biophys Acta 1979;574:189–96.

[214] Lin PM, Wright JR. Surfactant protein A binds to IgG and enhances phagocytosis of IgG-opsonized erythrocytes. Am J Physiol Lung Cell Mol Physiol 2006;291:L1199–206.

[215] Bonanomi A, Kojic D, Giger B, Rickenbach Z, Jean-Richard-Dit-Bressel L, Berger C, et al. Quantitative cytokine gene expression in human tonsils at excision and during histoculture assessed by standardized and calibrated real-time PCR and novel data processing. J Immunol Methods 2003;283:27–43.

[216] Guide to Performing Relative Quantitation of Gene Expression Using Real-Time Quantitative PCR. Appl Biosyst 2008.

[217] Immordino ML, Dosio F, Cattel L. Stealth liposomes: review of the basic science, rationale, and clinical applications, existing and potential. Int J Nanomedicine 2006;1:297–315.

[218] Hillaireau H, Couvreur P. Nanocarriers' entry into the cell: relevance to drug delivery. Cell Mol Life Sci 2009;66:2873–96.

[219] Olbrich C, Schöler N, Tabatt K, Kayser O, Müller RH. Cytotoxicity studies of Dynasan 114 solid lipid nanoparticles (SLN) on RAW 264.7 macrophages-impact of phagocytosis on viability and cytokine production. J Pharm Pharmacol 2004;56:883–91.

[220] Zou H-Y, Wu H-L, Zhang Y, Li S-F, Nie J-F, Fu H-Y, et al. Studying the interaction of pirarubicin with DNA and determining pirarubicin in human urine samples: combining excitation-emission fluorescence matrices with second-order calibration methods. J Fluoresc 2009;19:955–66.

[221] Bahmani B, Gupta S, Upadhyayula S, Vullev VI, Anvari B. Effect of polyethylene glycol coatings on uptake of indocyanine green loaded nanocapsules by human spleen macrophages in vitro. J Biomed Opt 2011;16:051303.

[222] Meerasa A, Huang JG, Gu FX. CH 50 : A Revisited Hemolytic Complement Consumption Assay for Evalua- tion of Nanoparticles and Blood Plasma Protein Interaction. Curr Drug Deliv 2011;8:290–8.

[223] Mutsaers E, Papadimitriou M. Charge of Macrophages and Their Charged Particles Interaction With Charged Particles. J Leukoc Biol 1988;44:17–26.

[224] Santos A, De Souza W. Surface charge and ultrastructure of the cell surface of resident and thioglycolate-elicited mouse peritoneal macrophages. J Submicrosc Cytol 1983;15:897–911.

[225] Agbanoma G, Li C, Ennis D, Palfreeman AC, Williams LM, Brennan FM. Production of TNF-α in macrophages activated by T cells, compared with lipopolysaccharide, uses distinct IL-10-dependent regulatory mechanism. J Immunol 2012;188:1307–17.

[226] Rader CP, Sterner T, Jakob F, Schiitze N, Eulert J. Cytokine Response of Human Macrophage-like Cells After Contact With Polyetlylene and Pure Titanium Particles Cytokine Response and Polyethylene and Pure Titanium Particles 1999;14:840–8.

[227] Hruby Z, Beck KF. Cytotoxic effect of autocrine and macrophage-derived nitric oxide on cultured rat mesangial cells. Clin Exp Immunol 1997;107:76–82.

[228] Caivano M, Cohen P. Role of Mitogen-Activated Protein Kinase Cascades in Mediating Lipopolysaccharide-Stimulated Induction of Cyclooxygenase-2 and IL-1b in RAW264 Macrophages. J Immunol 2000.

[229] Dubois RN, Abramson SB, Crofford L, Gupta R a, Simon LS, Van De Putte LB, et al. Cyclooxygenase in biology and disease. FASEB J 1998;12:1063–73.

[230] Eliopoulos AG, Dumitru CD, Wang C-C, Cho J, Tsichlis PN. Induction of COX-2 by LPS in macrophages is regulated by Tpl2-dependent CREB activation signals. EMBO J 2002;21:4831–40.

[231] Howard K a, Paludan SR, Behlke M a, Besenbacher F, Deleuran B, Kjems J. Chitosan/siRNA nanoparticle-mediated TNF-alpha knockdown in peritoneal macrophages for anti-inflammatory treatment in a murine arthritis model. Mol Ther 2009;17:162–8.

[232] Lo C-J, Lo EJ. Angiotensin II inhibits interleukin-6 mRNA expression of LPS-stimulated macrophages through down-regulating calcium signaling. J Surg Res 2013;181:287–92.

[233] Giulietti a, Overbergh L, Valckx D, Decallonne B, Bouillon R, Mathieu C. An overview of real-time quantitative PCR: applications to quantify cytokine gene expression. Methods 2001;25:386–401.

[234] Sukumari-Ramesh S, Laird MD, Singh N, Vender JR, Alleyne Jr CH, Dhandapani K. Astrocyte-Derived Glutathion Attenuates Hemin-Induced Apoptosis in Cerebral Microvascular Cells. NIH 2011;58:1858–70.

[235] Pang M, Ma L, Gong R, Tolbert E, Mao H, Ponnusamy M, et al. A novel STAT3 inhibitor, S3I-201, attenuates renal interstitial fibroblast activation and interstitial fibrosis in obstructive nephropathy. Kidney Int 2010;78:257–68.

[236] Aziz M, Jacob A, Matsuda A, Wu R, Zhou M, Dong W, et al. Pre-treatment of recombinant mouse MFG-E8 downregulates LPS-induced TNF-α production in macrophages via STAT3-mediated SOCS3 activation. PLoS One 2011;6:e27685.

[237] Wu RP, Youngblood DS, Hassinger JN, Lovejoy CE, Nelson MH, Iversen PL, et al. Cell-penetrating peptides as transporters for morpholino oligomers: effects of amino acid composition on intracellular delivery and cytotoxicity. Nucleic Acids Res 2007;35:5182–91.

[238] ASTM. Standard Practice for Assessment of Hemolytic Properties of Materials 2013.

[239] Van den Hoven JM, Nemes R, Metselaar JM, Nuijen B, Beijnen JH, Storm G, et al. Complement activation by PEGylated liposomes containing prednisolone. Eur J Pharm Sci 2013;49:265–71.

[240] Tiruppathi C, Finnegan A, Malik AB. Isolation and characterization of a cell surface albumin-binding protein from vascular endothelial cells. Proc Natl Acad Sci U S A 1996;93:250–4.

[241] Schnitzer JE, Carley WW, Palade GE. Albumin interacts specifically with a 60-kDa microvascular endothelial glycoprotein. Proc Natl Acad Sci U S A 1988;85:6773–7.

[242] Schnitzer JE, Oh P, Pinney E, Allard J. Filipin-sensitive caveolae-mediated transport in endothelium: reduced transcytosis, scavenger endocytosis, and capillary permeability of select macromolecules. J Cell Biol 1994;127:1217–32.

[243] Shao H, Tang H, Salavaggione OE, Yu C, Hylander B, Tan W, et al. Improved response to nab-paclitaxel compared with cremophor-solubilized paclitaxel is independent of secreted protein acidic and rich in cysteine expression in non-small cell lung cancer. J Thorac Oncol 2011;6:998–1005.

[244] Maina EN, Morris MR, Zatyka M, Raval RR, Banks RE, Richards FM, et al. Identification of novel VHL target genes and relationship to hypoxic response pathways. Oncogene 2005;24:4549–58.